

**REACTOR INPUT MANIPULATION FOR
DEVELOPING MODELS FOR
CATALYTIC REACTIONS**

by

Brent Howard Shanks

In Partial Fulfillment of the Requirements
for the Degree of
Doctor of Philosophy

Department of Chemical Engineering
California Institute of Technology
Pasadena, California USA

1988

(Submitted April 22, 1988)

ACKNOWLEDGEMENTS

I would like to thank Professor James Bailey for the support that he has given to this work. A large number of fellow graduate students have contributed in various ways to my research at Caltech. While there is not enough room to thank them individually, I fully understand the important impact that each has had directly or indirectly on my work. I wish to acknowledge the National Science Foundation and the General Electric Corporation for financial support of my graduate tenure.

Finally, I would like to thank Jackie, for without her encouragement and support there would be no dissertation.

ABSTRACT

A variety of phenomenological experimental methods are employed to construct and validate kinetic models for heterogeneous catalytic reaction systems. Both static input and stimulus–response experiments are performed with particular emphasis placed on the novel feedback–induced bifurcation method. These techniques are applied to CO oxidation on Rh/Al₂O₃ and Ag/Al₂O₃ to identify kinetic models that are able to reproduce transient as well as steady–state experimental data.

Static input experiments for CO oxidation on supported Rh, reduced at 170°C, reveal oscillatory responses for some inlet conditions. Two adsorbed CO species, linear and dicarbonyl forms, are observed with the linearly adsorbed CO shown from step–response experiments to be more reactive than CO adsorbed in the dicarbonyl form. The oscillations seem to be driven by surface temperature fluctuations rather than by interconversion between the adsorbed CO species.

Steady–state and step–response experiments at 147°C are used to estimate and to bound parameters in two reaction models that were previously postulated for CO oxidation on supported Ag. Data from feedback–induced steady–state bifurcation experiments are reproduced well by both models but neither reaction model is able to reproduce closed–loop Hopf bifurcation data. Also, long–time–scale transients observed in some step–response experiments are not accurately simulated by either model. A new model is proposed for CO oxidation on Ag/Al₂O₃, which incorporates a slow reversible step that forms an adsorbed oxygen species that blocks reaction sites. This model is able to reproduce the long–time–scale dynamics and a variety of cycled feedstream experiments.

The feedback–induced bifurcation method is also applied to the CO oxidation reaction on supported Rh. After reducing the Rh/Al₂O₃ catalyst at 500°C, only linearly adsorbed CO is observed. Measurements of the fractional coverage of CO

and the gas-phase CO are used for feedback control. The closed-loop bifurcation data are used to discriminate between two reaction models for CO oxidation on supported Rh, which are determined from steady-state experiments. Higher order dynamics resulting from closed-loop operation are also observed. The usefulness of various types of experimental feedback-induced bifurcations, as applied to model development, is discussed.

Finally, the feedback-induced bifurcation method is used to generate basis oscillations that are subjected to forced periodic operation. This provides a process in which entrainment behavior can be systematically examined. Experimental and simulated entrainment responses are compared and are found to be in close agreement.

TABLE OF CONTENTS

	Page
Acknowledgements	ii
Abstract	iii
Chapter 1: Introduction	1
References	8
Chapter 2: Autonomous Oscillations in Carbon Monoxide Oxidation over Supported Rhodium	14
Introduction	15
Experimental System	16
Results and Discussion	17
References	22
Figure Captions	25
Chapter 3: Experimental Investigations using Feedback-Induced Bifurcations: Carbon Monoxide Oxidation over Supported Silver	34
Introduction	35
Postulated Kinetic Models	37
Experimental System	40
Parameter Estimation	41
Feedback-Induced Bifurcation	45

Discussion	53
Conclusions	56
Notation	57
References	59
Tables	63
Figure Captions	64
Chapter 4: Modeling of Slow Dynamics in the Oxidation of Carbon Monoxide over Supported Silver	72
Introduction	73
Experimental System	74
Reaction Model	75
Results	78
Discussion	81
Conclusions	83
Notation	84
References	85
Table	87
Figure Captions	88
Chapter 5: Application of the Feedback-Induced Bifurcation Method to a Catalytic Reaction System	96

Introduction	97
Experimental System	98
Model Development	100
Bifurcation Results	104
Discussion and Conclusions	117
Notation	120
References	123
Table	126
Figure Captions	127
Chapter 6: Experimental Investigation of Entrainment Phenomena in a Periodically Forced, Autonomously Oscillating Process	138
Introduction	139
Experimental Method	141
Entrainment Diagram	143
Results	143
Conclusions	145
Notation	145
References	147
Figure Captions	149
Chapter 7: Conclusions	154

- 1 -

CHAPTER 1

INTRODUCTION

While most heterogeneous catalytic reaction systems are designed to operate at a fixed steady-state condition, the practical realization of this is difficult and, in some instances, is not the optimal operating strategy. Reactor dynamics can be introduced through a variety of stimuli and can be characterized by small time scale events (*e.g.*, reactor input perturbation) or long time scale events (*e.g.*, catalyst deactivation). Although some perturbed systems are capable of relaxing back to the desired steady-state condition, others, because of a limited stability domain around a given steady state, will not return to the original steady state. In the most extreme case, perturbations can lead to reactor runaway. Conversely, the operation of a chemical system near an unstable steady state may be desirable (Bruns and Bailey, 1975; Cinar *et al.*, 1987). Some chemical reactors will yield enhanced conversion and/or selectivity by incorporating periodic operation (*e.g.*, Bailey, 1973; Abdul-Kareem *et al.*, 1980; Barshad and Gulari, 1986; Thullie *et al.*, 1986). In general, a rate expression based upon steady-state data will not accurately describe these dynamic phenomena and, therefore, a more detailed model is necessary.

A fundamental problem in the characterization and modeling of heterogeneous catalytic reactions is the limited number of reactant and reaction intermediate species that can be quantified experimentally. With limited observations, the existence and form of some reaction steps in an overall reaction sequence can only be inferred. The goal, then, becomes to design experiments that provide sensitive information about the reaction kinetics even under the constraint of limited observables. As a secondary goal, it is preferable to perform experiments that yield the most information with a minimum of experimental difficulty and experimental repetition. Phenomenological experimental methods that have been employed to characterize heterogeneous catalytic reactions can be divided into two basic classifications. These are stimulus-response experiments in which the behavior of a reaction system is examined under dynamic input conditions and

static input experiments in which a hierarchy of reaction system responses such as steady-state multiplicity and oscillations may be observed.

The simplest stimulus-response experiment is performed by changing a reactor input in a stepwise manner and monitoring the time trajectory of the reaction system (Kobayashi and Kobayashi, 1974; Bennett, 1976). Data obtained from step-response experiments have been used for parameter estimation (Savatsky and Bell, 1982), model discrimination (Kobayashi, 1982b), and characterization of complex reaction sequences (Muller and Hofmann, 1987b). Muller and Hofmann (1987a) suggest that a carefully planned set of step-response experiments can be used for constructing a kinetic sequence corresponding to a complex reaction network by systematically stimulating individual reaction steps. The idea of developing a kinetic mechanism from step-response experiments was also proposed by Kobayashi (1982a) where an attempt was made to correlate qualitatively modes of response to reactor input step changes with underlying mechanistic features. A drawback of the step-response method can be the insensitivity of the experimental method to the underlying reaction mechanism. For example, Kobayashi (1982b) found four different parameter sets that were able to reproduce experimental step-response data for the reaction of CO and N₂O on silver. Simulations by Lyberatos *et al.* (1984) also showed step-response information to be insensitive to mechanistic differences in rival models for N₂O decomposition.

Step-response experiments tend to stimulate a single characteristic time scale of a reaction system, which can possibly obscure salient kinetic features. This problem is particularly acute in heterogeneous catalytic reactions, where surface reactions frequently occur more rapidly than adsorption and desorption of reaction species. By cycling reactor inputs rather than using a single step-change in the reactor input, multiple reaction time scales can be resolved (Bailey, 1973). For example, in an experimental application, Cutlip *et al.* (1983) exploited the multi-time scale information obtained from cycling feedstreams to discriminate between

rival models for CO oxidation on supported Pt.

For most reaction systems, introducing a static input will cause the system to yield a steady-state response. The steady state corresponding to this input may not be globally stable. If more than one steady-state condition can result from the same reactor input, the system is said to have steady-state multiplicity. Experimentally observed multiplicities have been reviewed by Hlavacek and Votruba (1978) and Hlavacek and Van Rompay (1981). As with step-response data, steady-state multiplicity data have been used for model discrimination (Herskowitz and Kenney, 1983; Graham and Lynch, 1987) and parameter estimation (Conrad and Treguer-Seguda, 1984; Harold and Luss, 1987a,1987b). Each of these applications of steady-state multiplicity data to model development requires postulating *a priori* a reaction mechanism, but Harold *et al.* (1987a,1987b) and Sheintuch (1987) depart from this approach by introducing a methodology in which multiplicity data are used to characterize functional features of intrinsic kinetic expressions.

Autonomous oscillations may also be observed in chemical systems (Ray, 1976; Sheintuch and Schmitz, 1977; Slin'ko and Slin'ko, 1978; Razon and Schmitz, 1986; Chang, 1986) and range from harmonic limit cycles to chaotic oscillations. While the oscillatory behavior of some reaction systems can be attributed to an interaction of reaction kinetics with heat and mass transfer effects (e.g., Kaul and Wolf, 1985), other experimental studies under well defined reaction conditions suggest that oscillations can be driven purely by reaction kinetics (e.g., Ertl *et al.*, 1982; Lindstrom and Tsotsis, 1986). Uppal *et al.* (1976) have shown that autonomous oscillations are possible for a system as simple as a CSTR with an exothermic reaction that has first-order, irreversible kinetics. In addition, a wide variety of kinetic mechanisms have been postulated that will also admit oscillatory responses, including surface coverage dependent parameters (Ivanov *et al.*, 1980), adsorbate interactions (Kevrekidis *et al.*, 1984a), dual adsorption sites (Patnaik,

1984), heterogeneity of the catalyst surface (Pikios and Luss, 1977; Jensen and Ray, 1986), adsorbate phase transition (Lynch *et al.*, 1986), slow adsorption of an inert species (Eigenberger, 1978), thermal fluctuations on the catalyst surface (Dagonnier and Nuyts, 1976; Lagos *et al.*, 1979), and oxidation-reduction of the catalyst (Sales *et al.*, 1982). It is clear that many kinetic models will produce oscillatory behavior under appropriate parametric values, so the experimental observation of oscillations cannot, in general, be used to construct a kinetic model for the reaction system. However, several studies (Sheintuch, 1985; Sheintuch and Luss, 1987a,1987b) have attempted to classify the oscillatory behavior of an experimental reaction system in order to develop qualitative reaction models.

Although steady-state multiplicity and autonomous oscillation data are a rich source of kinetic information, this bifurcation data can be obtained only for a limited number of reaction systems at normal operating conditions. Methods of analysis of reaction models for parametric values leading to the existence of multiplicities (Balakotaiah and Luss, 1986) and oscillations (Halbe and Poore, 1981; Doedel and Heinemann, 1983; Chang, 1986; Seydel and Hlavacek, 1987) are well developed. However, the search for regions of experimental operation in which bifurcations will occur for a given reaction system can be tedious and futile.

The use of feedback-induced bifurcations for model identification was proposed by Kuszta and Bailey (1982) as a novel synthesis of the stimulus-response and autonomous bifurcation experiments. The method consists of operating a process in a closed-loop configuration so that manipulation of controller gain values can be used to stimulate bifurcations. By using feedback to induce instabilities in a reaction system, bifurcation information can be readily obtained for systems that do not bifurcate naturally. Unlike autonomous bifurcation experiments, the bifurcation diagram for a reaction system under closed-loop operation can be systematically evaluated, since the instabilities are stimulated only by adjustment of the controller gain values. The application of the feedback-induced

bifurcation method to chemical reaction systems has been extensively developed in several numerical studies (Lyberatos *et al.*, 1984,1985; Lyberatos and Tsiligianis, 1987), but few studies involving the experimental application of the method to chemical reactions have been reported. Using feedback-induced Hopf bifurcation data, McDermott *et al.* (1985) estimated parameters in a dynamic model for an autothermal reactor with the water-gas shift reaction. Controller-induced instabilities were also exploited in experimental studies of ethylene hydrogenation by Prairie and Bailey (1986,1987) to discriminate between rival parameter sets and for estimation of characteristic reaction time scales.

A second method with potential for model discrimination that integrates stimulus-response experiments with systems that exhibit steady-state multiplicity and oscillations has been reviewed by Rehmus and Ross (1985). This method primarily consists of periodic forcing of an oscillating chemical reaction system, but periodic forcing of systems exhibiting steady-state multiplicities has also been considered (Sincic and Bailey, 1977). The dynamic behavior resulting from the interaction of periodic forcing with autonomous oscillations includes harmonic and subharmonic oscillations as well as quasi-periodic oscillations and chaos. Kevrekidis *et al.* (1984b,1986a,1986b) have developed an extensive theoretical framework for low-amplitude forcing of oscillating reaction systems, the qualitative features of which have been experimentally verified (Hudson *et al.*, 1986). Very few experimental studies have been performed with this method and no quantitative comparisons between experimental data and model calculations have been reported.

The main theme of the work presented here is the experimental application of the feedback-induced bifurcation method to model development in heterogeneous catalytic reaction systems. In the course of the experimental investigations, static input and stimulus-response data were used primarily for parameter estimation in the postulated reaction models, but also for use in kinetic mechanism development. The variety of experimental data provides a basis for comparing and contrasting

the information available from the different experimental techniques. Two reaction systems are studied, carbon monoxide oxidation on Ag/Al₂O₃ and on Rh/Al₂O₃.

Chapter 2 contains autonomous oscillation data for the CO oxidation reaction on Rh/Al₂O₃. Step-response experiments are used in conjunction with static input experiments in an effort to elucidate the underlying effects leading to the oscillatory response. The feedback-induced bifurcation method is applied in Chapter 3 to the discrimination between rival models for CO oxidation on Ag/Al₂O₃. Static input and step-response data are used to estimate and bound model parameters. Questions arising as to the validity of either postulated model in Chapter 3 are addressed in Chapter 4, where cycling experiments are used to develop an alternative kinetic model for CO oxidation on silver. The usefulness of the feedback-induced bifurcation method for model identification in heterogeneous catalytic reactions is more extensively examined in Chapter 5. CO oxidation on Rh/Al₂O₃ is studied with feedback control based on gas-phase and adsorbed species concentration measurements. Higher order dynamic response from closed-loop operation is also examined. Finally, feedback-stimulated limit cycles are used in Chapter 6 as a basis for systematically examining an oscillatory process subjected to periodic forcing.

REFERENCES

- Abdul-Kareem, H.K., A.K. Jain, P.L. Silveston, and R.R. Hudgins, "Harmonic Behavior of the Rate of Catalytic Oxidation of CO under Cycling Conditions," *Chem. Eng. Sci.*, **35**, 273 (1980).
- Bailey, J.E., "Periodic Operation of Chemical Reactors: A Review," *Chem. Eng. Commun.*, **1**, 111 (1973).
- Balakotaiah, V. and D. Luss, "Steady-State Multiplicity Features of Lumped-Parameter Chemically Reacting Systems," *Dynamics of Nonlinear Systems*, V. Hlavacek, Ed., Gordon and Breach, New York, 1 (1986).
- Barshad, Y. and E. Gulari, "Modification of Product Distribution Through Periodic Operation: Fischer Tropsch Synthesis over Ru/Al₂O₃," *Chem. Eng. Commun.*, **43**, 39 (1986).
- Bennett, C.O., "The Transient Response Method and Elementary Steps in Heterogeneous Catalysis," *Catal. Rev.-Sci. Engng.*, **13**, 758 (1976).
- Bruns, D.D. and J.E. Bailey, "Process Operation Near an Unstable Steady State Using Nonlinear Feedback Control," *Chem. Eng. Sci.*, **30**, 755 (1975).
- Chang, H.-C., "Recent Developments in the Dynamics of Heterogeneous Catalytic Reactions," *Dynamics of Nonlinear Systems*, V. Hlavacek, Ed., Gordon and Breach, New York, 85 (1986).
- Cinar, A., K. Rigopoulos, and X. Shu, "Vibrational Control of Chemical Reactors: Stabilization and Conversion Improvement in an Exothermic CSTR," *Chem. Eng. Commun.*, **59**, 299 (1987).
- Conrad, F. and V. Treguer-Seguda, "Parameter Estimation in Some Diffusion and Reaction Models: An Application of Bifurcation Theory," *Chem. Eng. Sci.*, **39**, 705 (1984).
- Cutlip, M.B., C.J. Hawkins, D. Mukesh, W. Morton, and C.N. Kenney, "Modelling of Forced Periodic Oscillations of Carbon Monoxide over Platinum Catalyst," *Chem. Eng. Commun.*, **68**, 329 (1983).

- Dagonnier, R. and J. Nuyts, "Oscillating CO Oxidation on a Pt Surface," *J. Chem. Phys.*, **65**, 2061 (1976).
- Doedel, E.J. and R.F. Heinemann, "Numerical Computation of Periodic Solution Branches and Oscillatory Dynamics of the Stirred Tank Reactor with $A \rightarrow B \rightarrow C$ Reactions," *Chem. Eng. Sci.*, **38**, 1493 (1983).
- Eigenberger, G., "Kinetic Instabilities in Heterogeneously Catalyzed Reactions II Oscillatory Instabilities with Langmuir-Type Kinetics," *Chem. Eng. Sci.*, **33**, 1263 (1978).
- Ertl, G., P.R. Norton, and J. Rustig, "Kinetic Oscillations in Platinum-Catalyzed Oxidation of CO," *Phys. Rev. Letters*, **49**, 177 (1982).
- Graham, W.R.C. and D.T. Lynch, "CO Oxidation on Pt: Model Discrimination Using Experimental Bifurcation Behavior," *AIChE J.*, **33**, 792 (1987).
- Halbe, D.C. and A.B. Poore, "Dynamics of the Continuous Stirred Tank Reactor with Reactions $A \rightarrow B \rightarrow C$," *Chem. Eng. J.*, **21**, 241 (1981).
- Harold, M.P. and D. Luss, "Use of Bifurcation Map for Kinetic Parameter Estimation. 1. Ethane Oxidation," *Ind. Eng. Chem. Res.*, **26**, 2092 (1987a).
- Harold, M.P. and D. Luss, "Use of Multiplicity Features for Kinetic Modeling: CO Oxidation on Pt/Al₂O₃," *Ind. Eng. Chem. Res.*, **26**, 2099 (1987b).
- Harold, M.P., M. Sheintuch, and D. Luss, "Analysis and Modeling of Multiplicity Features. 1. Nonisothermal Experiments," *Ind. Eng. Chem. Res.*, **26**, 786 (1987a).
- Harold, M.P., M. Sheintuch, and D. Luss, "Analysis and Modeling of Multiplicity Features. 2. Isothermal Experiments," *Ind. Eng. Chem. Res.*, **26**, 794 (1987b).
- Herskowitz, M. and C.N. Kenney, "CO Oxidation on Pt Supported Catalysts. Kinetics and Multiple Steady States," *Can. J. Chem. Eng.*, **61**, 194 (1983).

- Hlavacek, V. and P. Van Rompay, "Current Problems of Multiplicity, Stability and Sensitivity of States in Chemically Reacting Systems," *Chem. Eng. Sci.*, **36**, 1587 (1981).
- Hlavacek, V. and J. Votruba, "Hysteresis and Periodic Activity Behavior in Catalytic Chemical Reaction Systems," *Advan. Catal.*, **27**, 59 (1978).
- Hudson, J.L., P. Lamba, and J.C. Mankin, "Experiments on Low-Amplitude Forcing of a Chemical Oscillator," *J. Phys. Chem.*, **90**, 3430 (1986).
- Ivanov, E.A., G.A. Chumakov, M.G. Slin'ko, D.D. Bruns, and D. Luss, "Isothermal Sustained Oscillations Due to the Influence of Adsorbed Species on the Catalytic Reaction Rate," *Chem. Eng. Sci.*, **35**, 795 (1980).
- Jensen, K.F. and W.H. Ray, "The Role of Surface Structures in the Dynamic Behavior of Heterogeneous Catalytic Systems," *Dynamics of Nonlinear Systems*, V. Hlavacek, Ed., Gordon and Breach, New York, 111 (1986).
- Kaul, D.J. and E.E. Wolf, "Fourier Transform Infrared Spectroscopy Studies of Surface Reaction Dynamics II. Surface Coverage and Inhomogeneous Temperature Patterns of Self-Sustained Oscillations during CO Oxidation on Pt/SiO₂," *J. Catal.*, **91**, 216 (1985).
- Kevrekidis, I., L.D. Schmidt, and R. Aris, "Rate Multiplicity and Oscillations in Single Species Surface Reactions," *Surf. Sci.*, **137**, 151 (1984a).
- Kevrekidis, I., L.D. Schmidt, and R. Aris, "On the Dynamics of Periodically Forced Chemical Reactors," *Chem. Eng. Commun.*, **30**, 323 (1984b).
- Kevrekidis, I., L.D. Schmidt, and R. Aris, "Resonance in Periodically Forced Processes," *Chem. Eng. Sci.*, **41**, 670 (1986a).
- Kevrekidis, I., L.D. Schmidt, and R. Aris, "Some Common Features of Periodically Forced Reacting Systems," *Chem. Eng. Sci.*, **41**, 1263 (1986b).
- Kobayashi, H. and M. Kobayashi, "Transient Response Method in Heteroge-

- neous Catalysis," *Catal. Rev.-Sci. Engng.*, **10**, 139 (1974).
- Kobayashi, M., "Characterization of Transient Response Curves in Heterogeneous Catalyst I," *Chem. Eng. Sci.*, **37**, 393 (1982a).
- Kobayashi, M., "Rival Kinetic Models in the Oxidation of Carbon Monoxide over a Silver Catalysis by the Transient Response Method," *Chemical Reaction Engineering*, ACS Symp. Ser., **196**, 213 (1982b).
- Kuszta, B. and J.E. Bailey, "Nonlinear Model Identification By Analysis of Feedback-Stimulated Bifurcation," *IEEE Trans. Autom. Control*, **AC-27**, 227 (1982).
- Lagos, R.E., B.C. Sales, and H. Suhl, "Theory of Oscillatory Oxidation of Carbon Monoxide over Platinum," *Surf. Sci.*, **82**, 525 (1979).
- Lindstrom, T.H. and T.T. Tsotsis, "Reaction Rate Oscillations During CO Oxidation over Pt/ γ -Al₂O₃: Isothermal, Intermediate Pressure Conditions," *Surf. Sci.*, **171**, 349 (1986).
- Lyberatos, G., B. Kuszta, and J.E. Bailey, "Discrimination and Identification of Dynamic Models via Introduction of Feedback," *Chem. Eng. Sci.*, **39**, 739 (1984).
- Lyberatos, G., B. Kuszta, and J.E. Bailey, "Versal Families, Normal Forms, and Higher Order Bifurcations in Dynamic Chemical Systems," *Chem. Eng. Sci.*, **40**, 1177 (1985).
- Lyberatos, G. and C.A. Tsiligiannis, "Analysis of Feedback Induced Hopf Bifurcations via the Carleman Approximation," *Chem. Eng. Commun.*, **57**, 1 (1987).
- Lynch, D.T., G. Emig, and S.E. Wanke, "Oscillations during CO Oxidation over Supported Metal Catalysts III. Mathematical Modeling of the Observed Phenomena," *J. Catal.*, **97**, 456 (1986).
- McDermott, P.E., H.-C. Chang, and R.G. Rinker, "Experimental Investigation of Controller-Induced Bifurcation in a Fixed-Bed Autothermal Reactor," *Chem. Eng. Sci.*, **40**, 1355 (1985).
- Muller, E. and H. Hofmann, "Dynamic Modelling of Heterogeneous Catalytic Reactions-I. Theoretical Considerations," *Chem. Eng. Sci.*, **42**,

1695 (1987a).

- Muller, E. and H. Hofmann, "Dynamic Modelling of Heterogeneous Catalytic Reactions—I. Experimental Results Oxydehydrogenation of Isobutyric Aldehyde to Methacrolein," *Chem. Eng. Sci.*, **42**, 1705 (1987b).
- Patnaik, P.R., "The Effect of Surface Heterogeneity on Kinetic Oscillations in the Methanation of CO," *Chem. Eng. Commun.*, **25**, 31 (1984).
- Pikios, C.A. and D. Luss, "Isothermal Concentration Oscillations on Catalytic Surfaces," *Chem. Eng. Sci.*, **32**, 191 (1977).
- Prairie, M.R. and J.E. Bailey, "Application of Feedback-Induced Bifurcation for Evaluating Steady-State and Transient Heterogeneous Catalysis Kinetic Models," *Chem. Eng. Sci.*, **41**, 937 (1986).
- Prairie, M.R. and J.E. Bailey, "Experimental and Modeling Investigations of Steady-State and Dynamic Characteristics of Ethylene Hydrogenation on Pt/Al₂O₃," *Chem. Eng. Sci.*, **42**, 2085 (1987).
- Ray, W.H., "Bifurcation Phenomena in Chemically Reacting Systems," *Applications of Bifurcation Theory*, P.H. Rabinowitz, Ed., Academic Press, New York, 285 (1976).
- Razon, L.F. and R.A. Schmitz, "Intrinsically Unstable Behavior during the Oxidation of Carbon Monoxide on Platinum," *Catal. Rev.-Sci. Eng.*, **28**, 89 (1986).
- Rehmus, P. and J. Ross, "Periodically Perturbed Chemical Systems," *Oscillations and Traveling Waves in Chemical Systems*, R.J. Field and M. Burger, Eds., John Wiley and Sons, New York, 287 (1985).
- Sales, B.C., J.E. Turner, and M.B. Maple, "Oscillatory Oxidation of CO over Pt, Pd and Ir Catalysts: Theory," *Surf. Sci.*, **114**, 381 (1982).
- Savatsky, B.J. and A.T. Bell, "Nitric Oxide Reduction by Hydrogen over Rhodium Using Transient Response Techniques," *Catalysis Under Transient Conditions*, A.T. Bell and L.L. Hegedus, Eds., ACS Symp. Ser., **178**, 105 (1982).
- Seydel, R. and V. Hlavacek, "Strategy of Calculation of Periodic Solutions,"

Chem. Eng. Sci., **42**, 2927 (1987).

Sheintuch, M., "Nonlinear Kinetics in Catalytic Oxidation Reactions: Periodic and Aperiodic Behavior and Structure Sensitivity," *J. Catal.*, **96**, 326 (1985).

Sheintuch, M., "The Determination of Global Solutions from Local Ones in Catalytic Systems Showing Steady-State Multiplicity," *Chem. Eng. Sci.*, **42**, 2103 (1987).

Sheintuch, M. and D. Luss, "Identification of Observed Dynamic Bifurcations and Development of Qualitative Models," *Chem. Eng. Sci.*, **42**, 41 (1987a).

Sheintuch, M. and D. Luss, "Identification of Observed Dynamic Centers for Analysis of Experimental Data," *Chem. Eng. Sci.*, **42**, 233 (1987b).

Sheintuch, M. and R.A. Schmitz, "Oscillations in Catalytic Reactions," *Catal. Rev.-Sci. Eng.*, **15**, 107 (1977).

Sincic, D. and J.E. Bailey, "Pathological Dynamic Behavior of Forced Periodic Chemical Processes," *Chem. Eng. Sci.*, **32**, 281 (1977).

Slin'ko, M.G. and M.M. Slin'ko, "Self-Oscillations of Heterogeneous Catalytic Reaction Rates," *Catal. Rev.-Sci. Eng.*, **17**, 119 (1978).

Thullie, J., L. Chiao, and R.G. Rinker, "Analysis of Concentration Forcing in Heterogeneous Catalysis," *Chem. Eng. Commun.*, **48**, 191 (1986).

Uppal, A., W.H. Ray, and A.B. Poore, "The Classification of the Dynamic Behavior of Continuous Stirred Tank Reactors- Influence of Reactor Residence Time," *Chem. Eng. Sci.*, **31**, 205 (1977).

CHAPTER 2

AUTONOMOUS OSCILLATIONS IN CARBON MONOXIDE

OXIDATION OVER SUPPORTED RHODIUM

INTRODUCTION

Autonomous oscillatory states have been observed in many heterogeneous catalytic reaction systems (Chang, 1986) with carbon monoxide oxidation over platinum receiving the most attention (Razon and Schmitz, 1986). In order to elucidate the underlying sources of the oscillatory responses to time invariant inputs, several studies have been performed with reactions over supported catalysts in which transmission infrared spectroscopy was incorporated to measure IR active surface species. Particularly noteworthy are the findings presented by Kaul and Wolf (1984,1985,1986) and Lindstrom and Tsotsis (1985,1986a,1986b) for CO oxidation on supported Pt. Kaul and Wolf postulate the oscillations to be manifestations of surface non-uniformities and wave propagation of high reaction rate fronts, while Lindstrom and Tsotsis attribute mechanistic causes, specifically, oxidation and reduction of the Pt.

Few studies have reported oscillatory behavior in the reaction of CO with oxygen on rhodium (Franck *et al.*, 1983; Tufan and Lintz, 1983; Prairie *et al.*, 1988a). The aperiodic oscillations in CO₂ production reported by Franck *et al.* (1983) coincided with large temperature fluctuations in the gas phase. Using a transmission IR reactor with a thin wafer of supported Rh, Prairie *et al.* (1988a) observed fluctuations in gas-phase and surface species, which were not periodic. The purpose of the present work is to show oscillatory behavior observed for CO oxidation on Rh/Al₂O₃, which is quite different from that reported previously for this reaction. A transmission IR reactor was used so that oscillations in the surface species as well as gas-phase species could be observed simultaneously. Therefore, the contribution of different adsorbed CO species to the overall dynamic behavior could be ascertained.

EXPERIMENTAL SYSTEM

Gas flow rates of helium (99.995%), oxygen (99.5%), hydrogen (99.9995%), and carbon monoxide (99.99%) into the reactor utilized a feed system described in detail by Prairie *et al.* (1988b). The reactor is based on a transmission IR cell design of Oh and Hegedus (1982) and has been described elsewhere (Prairie, 1987). Mounted in the reactor is an exposed-tip thermocouple bent to within 0.1 mm of the catalyst surface. The effluent concentration of either CO or CO₂ was measured with a Wilkes Miran I infrared analyzer operating at 4.6 μm or 4.2 μm , respectively. At 155°C and 100 sccm total flow rate, the reactor was found to yield an ideal CSTR response to a step change in the inlet concentration with a time constant of 3.8 s.

Transmission infrared spectra were obtained with a Beckman IR-8 infrared spectrophotometer modified to use a high-speed HgCdTe detector (Santa Barbara Research, Model 40742). In order to incorporate the HgCdTe detector, a high-speed chopper (Laser Precision, Model CTX-534) is placed in the sample beam, and a lock-in amplifier (Princeton Applied Research) is coupled with the detector and chopper. This arrangement allowed for data to be taken only in single-beam mode. A monochromator slit width of 0.2 mm and a chopping speed of 400 Hz were used for all of the transmission IR spectra. An HP9825 data acquisition system was used to store the effluent and surface IR data.

5 wt % Rh/Al₂O₃ catalyst was prepared from Alon fumed alumina and RhCl₃ using the aqueous incipient wetness technique. The catalyst powder was dried overnight and calcined for five hours in flowing air at 500°C. Catalyst wafers were made by pressing the powder at 500 psi in a 20 mm diameter die. Two catalyst wafers were used in the present study: one was 35 mg and 0.10 mm thick and the other was 22 mg and 0.07 mm thick. Prior to use, the wafers were each reduced *in situ* with 20% H₂ in He at 175°C for 10 hours. Following hydrogen reduction, the reactor was cooled to 155°C while flowing He through the cell. Before introducing

any carbon monoxide to the system, a baseline spectrum was obtained.

RESULTS AND DISCUSSION

Figure 1(a) shows the spectrum resulting from introducing CO to the reduced catalyst at 155°C. The spectrum has been corrected for the baseline. Three absorbance bands were observed that have been previously assigned to adsorbed CO species on supported Rh (Yang and Garland, 1957; Yates *et al.*, 1979). The doublet at 2090 cm⁻¹ and 2025 cm⁻¹ corresponds to the symmetric and asymmetric stretching modes, respectively, of CO adsorbed in a dicarbonyl form. The band at 2070 cm⁻¹ is assigned to linearly adsorbed CO. No clear band was seen that could be attributed to a CO species adsorbed in bridged form.

To resolve the large amount of overlap between the absorbance bands, transient experiments were performed to determine the relative reactivity of the CO surface species. A transient was induced by a step-change in the feed concentration from 4% CO in He to 5% O₂ in He at 155°C. Figure 2(a) shows the response of the effluent CO mole fraction to the step-change. Also, shown in Figures 2(b) and 3 are the time trajectories of the intensities of the 2070 cm⁻¹ and 2025 cm⁻¹ bands, respectively. The 2070 cm⁻¹ band intensity decreases to zero stepwise concurrently with the concentration of CO in the reactor approaching zero. The 2025 cm⁻¹ band displays a sharp decrease in intensity followed by a slower decline. The early rapid decrease in the 2025 cm⁻¹ band occurs simultaneously with the disappearance of the 2070 cm⁻¹. Consequently, this behavior at 2025 cm⁻¹ can be attributed to overlap between the absorbance bands. This effect on the full spectrum is illustrated in Figure 1 where spectrum (b) was started 1 minute after the switch, with a scan time of 20 seconds and spectrum (c) was taken 30 minutes later. All three of the spectra in Figure 1 are shown after subtracting out the same baseline. As can be seen, the band corresponding to linearly adsorbed CO disappears within one minute. Also, a shoulder at 2125 cm⁻¹ becomes apparent.

This band was previously assigned to CO and an oxygen atom bonded to the same Rh atom (Yang and Garland, 1957; Rice *et al.*, 1981). Figures 2(b) and 3 demonstrate that linearly adsorbed CO is more reactive than dicarbonyl CO at 155°C which agrees with a previous report by Yang and Garland (1957) at a comparable temperature.

The response of the system containing the 35 mg catalyst wafer to a steady 100 sccm feed of 5% CO, 20% O₂ in He is shown in Figure 4. Measurements of the intensity of the 2070 cm⁻¹ band and of the effluent CO₂ mole fraction were performed simultaneously (Figure 4(a) and (b)). Following this measurement, the CO effluent concentration was monitored along with the 2070 cm⁻¹ band. Although the effluent mole fractions of CO and CO₂ could not be measured simultaneously, these responses were inphase, with high conversion corresponding to low linear CO coverage, because each was synchronized with the oscillations in the 2070 cm⁻¹ band. During the oscillations, no temperature fluctuation was indicated by the thermocouple, although this in the gas phase measurement may not be sensitive to temperature excursions of the catalyst. The shape of the oscillations are very similar to those reported by Plichta and Schmitz (1979) for CO oxidation on Pt foil. The instantaneous conversion of CO varied between 96% and 30% during the cycles, corresponding to reaction rates from 3.6 to 1.1 μmol/s. Based on observed quantities, the Thiele modulus (Aris, 1975) is approximately 0.55 and 0.01 for the high and low instantaneous reaction rates, respectively, based on quasi-steady state estimates.

Oscillations inphase with the effluent CO measured response were observed while monitoring the absorbance at 2025 cm⁻¹. The absorbance at 2070 cm⁻¹ decreased to nearly zero during the high reaction rate portion of the oscillations, indicating no linear CO on the surface. The absorbance at 2025 cm⁻¹ remained substantial even during high conversion. Although the absorbances at the two wavenumbers could not be monitored simultaneously, the response of the 2025

cm^{-1} band during the oscillations was very similar to that of the 2070 cm^{-1} band. These observations coupled with the reactivity results shown in Figures 2(b) and 3 indicate that the primary cause of the oscillations measured at 2025 cm^{-1} is the overlap of the absorbance band for linear CO with the dicarbonyl band. A comparison between the time scale for removal of dicarbonyl by reaction with oxygen (Figure 3) and the oscillation period shows that the contribution of the dicarbonyl species to the intensity at 2025 cm^{-1} remains essentially constant during the oscillations. Therefore, the oscillations cannot be attributed primarily to an interchange between linear CO and dicarbonyl species on the catalyst surface.

The effect of varying the inlet O_2 concentration is presented in Figure 5. Shown is the adsorbance at 2070 cm^{-1} for steady feeds of 2% CO and four O_2 concentrations: 20%, 15%, 12%, and 10%. Each of the feed configurations that result in oscillations has a nearly equivalent high conversion level in a cycle but differs markedly in the maximum absorbance during a cycle and in the cycle period. Decreasing the inlet O_2 concentration causes the absorbance to stay at a relatively high value for a longer portion of the cycle, until, as shown in Figure 5(d), the oscillations cease and the surface reaches saturation coverage.

The oscillatory behavior of the system with the 22 mg wafer is shown in Figures 6 and 7 for two different reaction temperatures, 155°C and 164°C . Plotted is the percent conversion of CO for various inlet CO mole fractions and a fixed O_2 inlet mole fraction of 0.20. The solid circles represent stable steady states, and the ends of the bands give the maximum and minimum instantaneous conversions during an oscillation. Because of limitations in the mass flow controllers, the minimum CO concentration that could be obtained accurately in the feed stream was 0.5%. At 155°C (Figure 6), decreasing the inlet CO mole fraction from a stable steady state (solid circles) with low conversion caused the system to bifurcate to a large amplitude limit cycle. No hysteresis effect was observed as

increasing the CO mole fraction from 0.03 to 0.035 caused the system to return to the low conversion state. In contrast, increasing the inlet CO concentration from the large amplitude oscillatory regime at 164°C forced the system to an oscillatory state of small amplitude and high conversion. Again, no hysteresis was observed switching between the large and small amplitude oscillations. Figure 8 shows the oscillations in the effluent CO mole fraction resulting from a feed of 5% CO, 20% O₂ at 164°C. The oscillations are not periodic as were observed for the large amplitude oscillations but were still correlated between the effluent CO mole fraction and the absorbance at 2070 cm⁻¹.

Figures 6 and 7 provide insight into a possible contributing factor to the large amplitude oscillations. While increasing the CO mole fraction at 155°C caused the oscillations to quench to a low conversion state, the system moved to a high conversion value at 164°C. If the catalyst surface is being locally heated by chemical reaction, but this heating is undetected by the thermocouple, then ignition and extinction may be occurring between the low and high conversion states as the crystallites heat and cool. The pebbly surface model proposed by Jensen and Ray (1986) could be used to explain the complex behavior shown in Figure 8, but the long-time scale oscillations in Figure 4 are difficult to reconcile with this model. Oscillations with periods of approximately 7 minutes were reported by Lynch and Wanke (1984) for CO oxidation on Pt-Pd/Al₂O₃, which were postulated to coincide with surface temperature fluctuations rather than with independent crystallite vacillations.

Although the precise oscillatory mechanism has not been isolated, it is apparent that neither interchange between linear CO and dicarbonyl species nor a change in the fractional coverage of CO adsorbed in the dicarbonyl form occurs during the oscillations. Rice *et al.* (1981) have presented data indicating that dicarbonyl species occur on Rh in a +1 oxidation state, while linearly adsorbed CO corresponds to Rh in a zero oxidation state. Using the interpretation of Rice

et al., the oscillatory data here does not confirm a change in the oxidation state of the rhodium during the oscillations. The data presented in this work do suggest that temperature fluctuations appear to be a likely contributor to the oscillatory behavior observed in this reaction system.

REFERENCES

- Aris, R., *The Mathematical Theory of Diffusion and Reaction in Permeable Catalysts, Vol. 1*, Oxford University Press, London (1975).
- Chang, H.-C., "Recent Developments in the Dynamics of Heterogeneous Catalytic Reactions," *Dynamics of Nonlinear Systems*, V. Hlavacek, Ed., Gordon and Breach, New York, 85 (1986).
- Franck, K.R., H.-G. Lintz and G. Tufan, "Oscillatory Instabilities in the Oxidation of Carbon Monoxide on Rhodium," *J. Catal.*, **79**, 466 (1983).
- Jensen, K.F. and W.H. Ray, "The Role of Surface Structures in the Dynamic Behavior of Heterogeneous Catalytic Systems," *Dynamics of Nonlinear Systems*, V. Hlavacek, Ed., Gordon and Breach, New York, 111 (1986).
- Kaul, D.J. and E.E. Wolf, "FTIR Studies of Surface Reaction Dynamics I. Temperature and Concentration Programming during CO Oxidation on Pt/SiO₂," *J. Catal.*, **89**, 348 (1984).
- Kaul, D.J. and E.E. Wolf, "Fourier Transform Infrared Spectroscopy Studies of Surface Reaction Dynamics II. Surface Coverage and Inhomogeneous Temperature Patterns of Self-Sustained Oscillations during CO Oxidation on Pt/SiO₂," *J. Catal.*, **91**, 216 (1985).
- Kaul, D.J. and E.E. Wolf, "Transient FTIR Studies of Multiplicities, Oscillations, and Reaction Non-Uniformities during CO and Ethylene Oxidation on Supported Pt and Pd Catalysts," *Chem. Eng. Sci.*, **41**, 1101 (1986).
- Lindstrom, T.H. and T.T. Tsotsis, "Reaction Rate Oscillations during CO Oxidation over Pt/ γ -Al₂O₃; Experimental Observations and Mechanistic Causes," *Surf. Sci.*, **150**, 487 (1985).
- Lindstrom, T.H. and T.T. Tsotsis, "Reaction Rate Oscillations during CO Oxidation over Pt/ γ -Al₂O₃; The Issue of Propagating Waves," *Surf. Sci.*, **167**, L194 (1986a).
- Lindstrom, T.H. and T.T. Tsotsis, "Reaction Rate Oscillations during CO Oxidation over Pt/ γ -Al₂O₃; Isothermal Intermediate Pressure Conditions," *Surf. Sci.*, **171**, 349 (1986b).

- Lynch, D.T. and S.E. Wanke, "Oscillations during CO Oxidation over Supported Metal Catalysts II. Effects of Reactor Operating Conditions on Oscillatory Behavior for a (Pt-Pd)/Al₂O₃ Catalyst," *J. Catal.*, **17**, 345 (1984).
- Oh, S.H. and L.L. Hegedus, "Dynamics of High-Temperature Carbon Monoxide Chemisorption on Platinum-Alumina by Fast-Response IR Spectroscopy," *Catalysis Under Transient Conditions*, A.T. Bell and L.L. Hegedus, Eds., ACS Symp. Ser., **178**, 79 (1982).
- Plichta, R.T. and R.A. Schmitz, "Oscillations in the Oxidation of Carbon Monoxide on a Platinum Foil," *Chem. Eng. Commun.*, **3**, 387 (1979).
- Prairie, M.R., "Steady-State and Transient Methods for Modeling Chemical Reactions on Supported Catalysts," Doctoral dissertation, California Institute of Technology (1987).
- Prairie, M.R., S.H. Oh, B.K. Cho, E.J. Shinouskis, and J.E. Bailey, "Steady-State and Transient Studies of CO Oxidation on Alumina Supported Rhodium via Transmission IR Spectroscopy," submitted (1988a).
- Prairie, M.R., B.H. Shanks, and J.E. Bailey, "Intentional Manipulation of Closed-Loop Time Delay for Model Validation Using Feedback-Induced Bifurcation Experiments," *Chem. Eng. Sci.* in press (1988b).
- Razon, L.F. and R.A. Schmitz, "Intrinsically Unstable Behavior during the Oxidation of Carbon Monoxide on Platinum," *Catal. Rev.-Sci. Engng.*, **28**, 89 (1986).
- Rice, C.A., S.D. Worley, C.W. Curtis, J.A. Guin, and A.R. Tarrer, "The Oxidation State of Dispersed Rh on Al₂O₃," *J. Chem. Phys.*, **74**, 6487 (1981).
- Tufan, G. and H.-G. Lintz, "Oxidation of Carbon Monoxide over a Supported Rhodium Catalyst," *Proc. 5th Intern. Sym. Heterogeneous Catalysis*, Varna, part II, 79 (1983).
- Yang, A.C. and C.W. Garland, "Infrared Studies of Carbon Monoxide Chemi-

sorbed on Rhodium," *J. Phys. Chem.*, **61**, 1504 (1957).

Yates, J.T., T.M. Duncan, S.D. Worley, and R.W. Vaughan, "Infrared Spectra of Chemisorbed CO on Rh," *J. Phys. Chem.*, **70**, 1219 (1979).

FIGURE CAPTIONS

- Figure 1: IR spectra of CO on Rh/Al₂O₃ at 155°C; (a) saturated coverage, (b) one minute after switch from CO to O₂, (c) 30 minutes after spectrum (b).
- Figure 2: Step change from 4% CO in He to 5% O₂ in He; (a) trajectory of the effluent CO mole fraction, (b) trajectory of the absorbance at 2070 cm⁻¹.
- Figure 3: Absorbance trajectory at 2025 cm⁻¹ for switch from 4% CO to 5% O₂.
- Figure 4: Oscillations at 155°C for a steady feed of 5% CO, 20% O₂; (a) absorbance at 2070 cm⁻¹, (b) effluent CO₂ mole fraction, (c) effluent CO mole fraction.
- Figure 5: Response of the adsorbance at 2070 cm⁻¹ for a feed composition of 2% CO and (a) 20% O₂, (b) 15% O₂, (c) 12% O₂, (d) 10% O₂.
- Figure 6: Oscillatory behavior of the reaction at 155°C. Bands denote oscillation amplitudes, and solid circles denote stable steady states.
- Figure 7: Oscillatory behavior of the reaction at 164°C. Bands indicate the magnitude and maximum and minimum values of the oscillation.
- Figure 8: Small amplitude oscillations in the effluent CO mole fraction at 164°C with feed composition of 5% CO, 20% O₂.

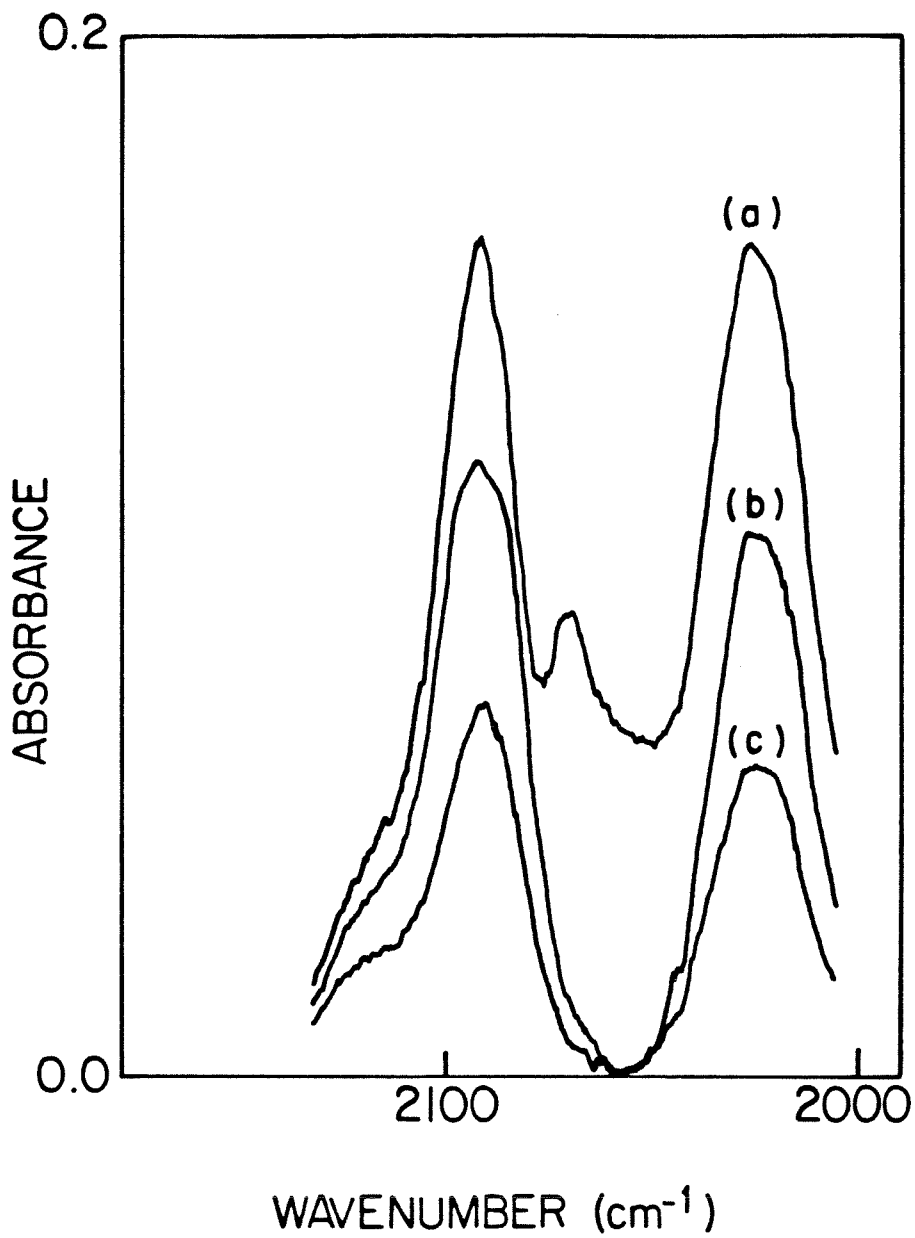


Figure 1

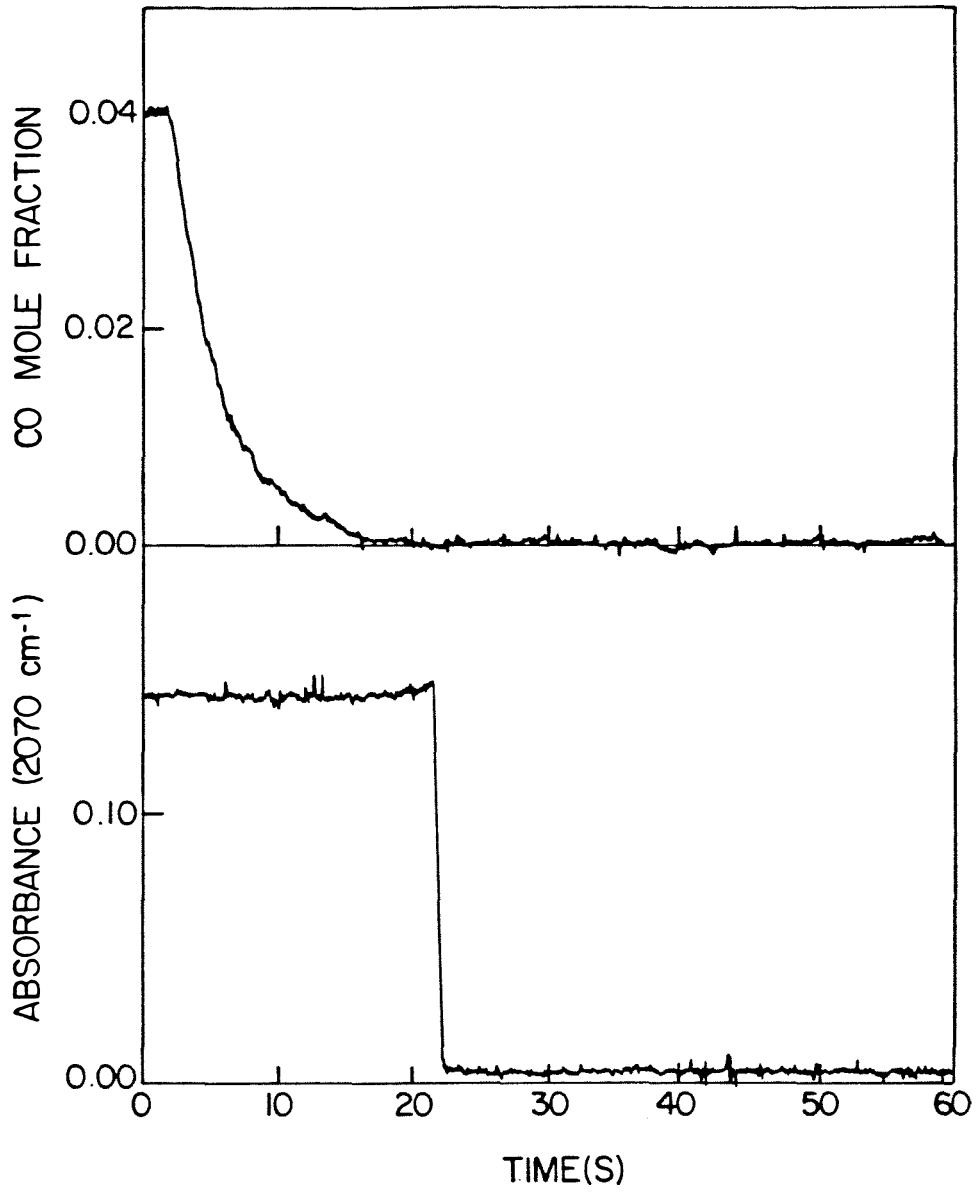


Figure 2

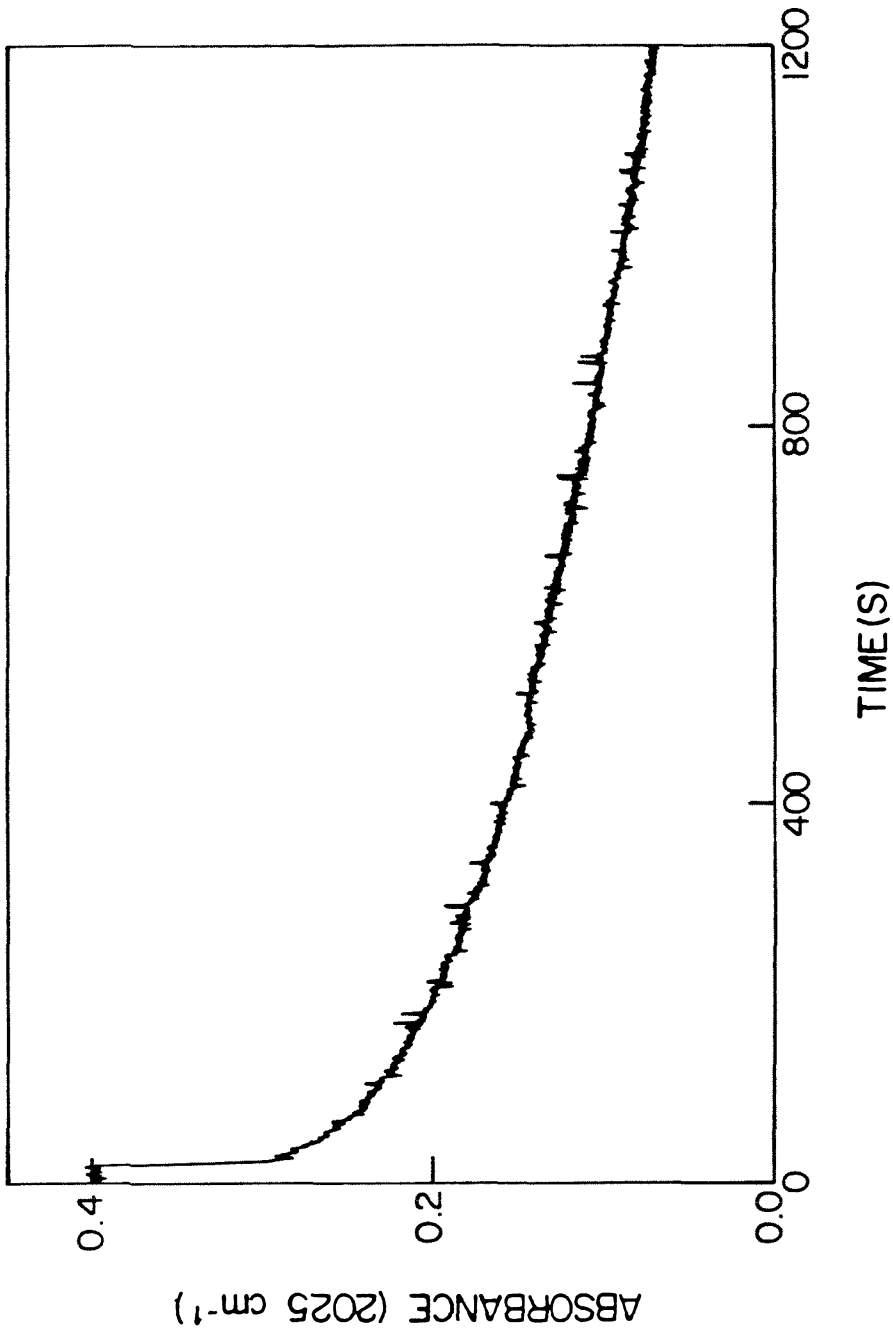


Figure 3

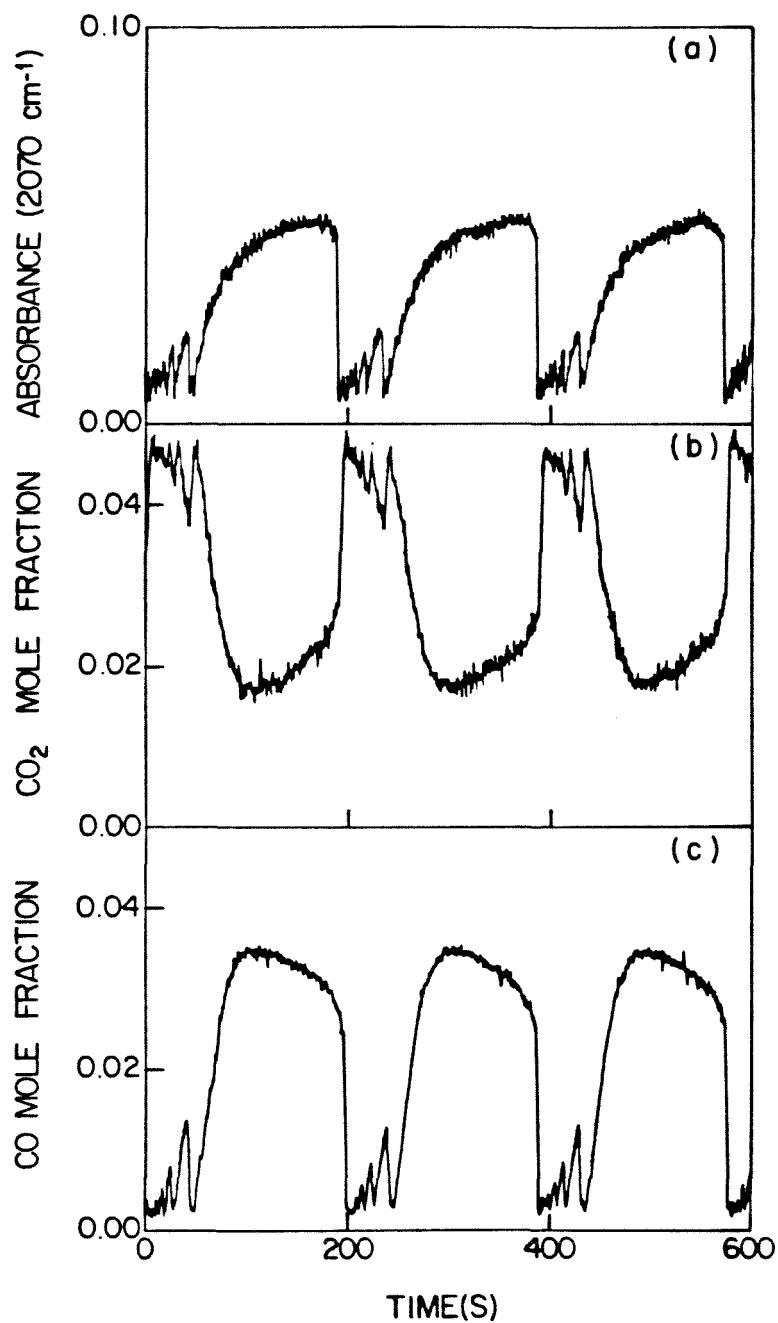


Figure 4

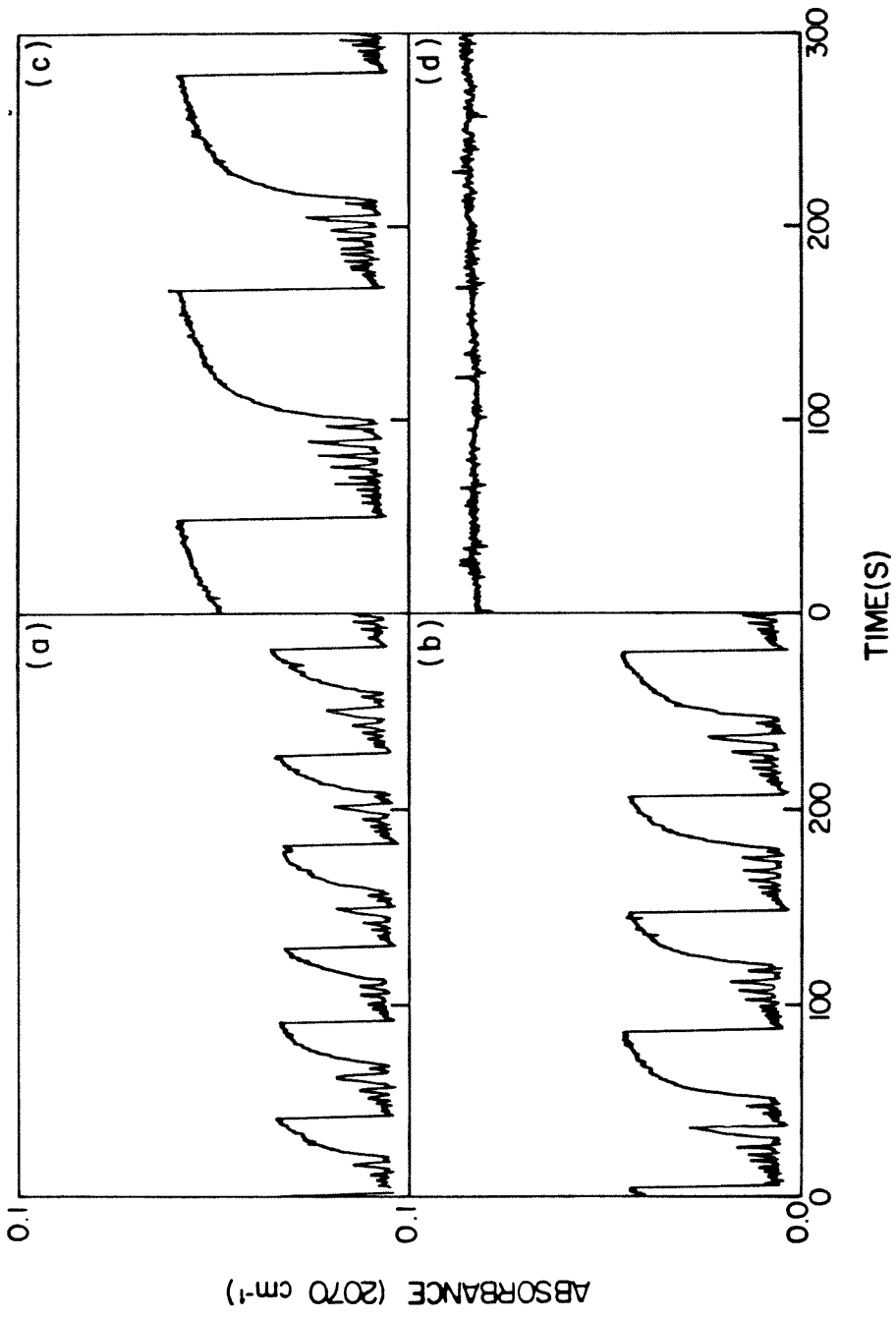


Figure 5

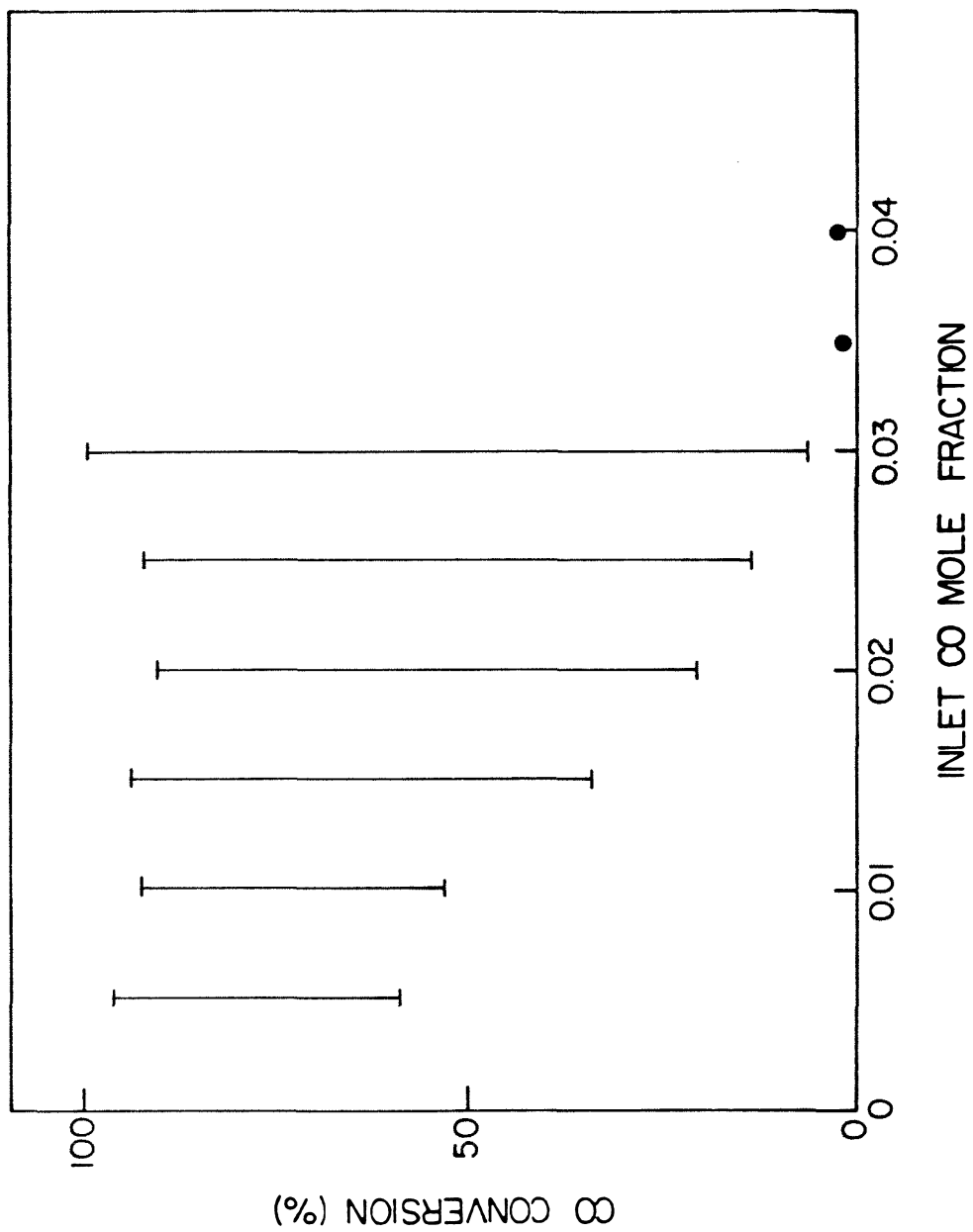


Figure 6

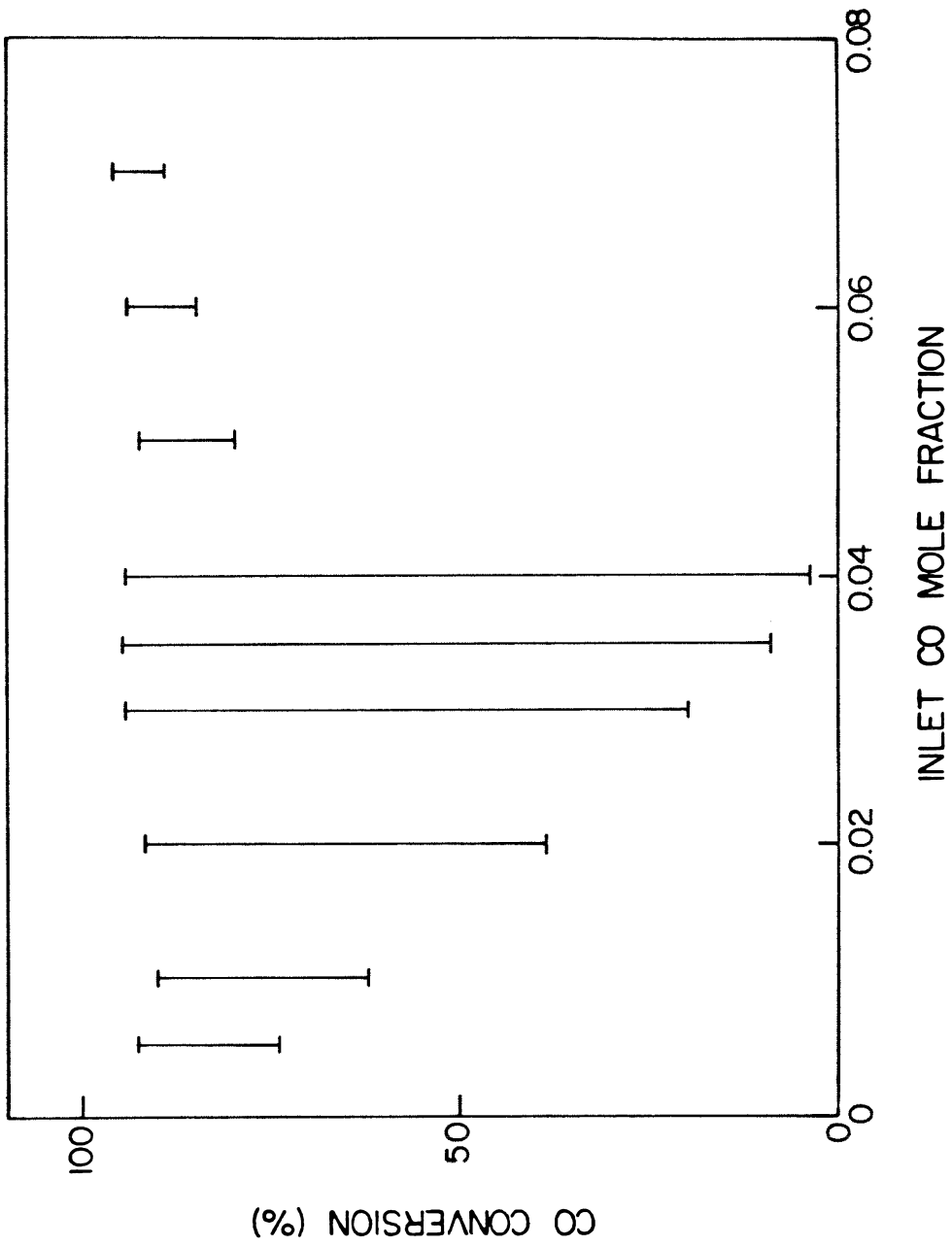


Figure 7

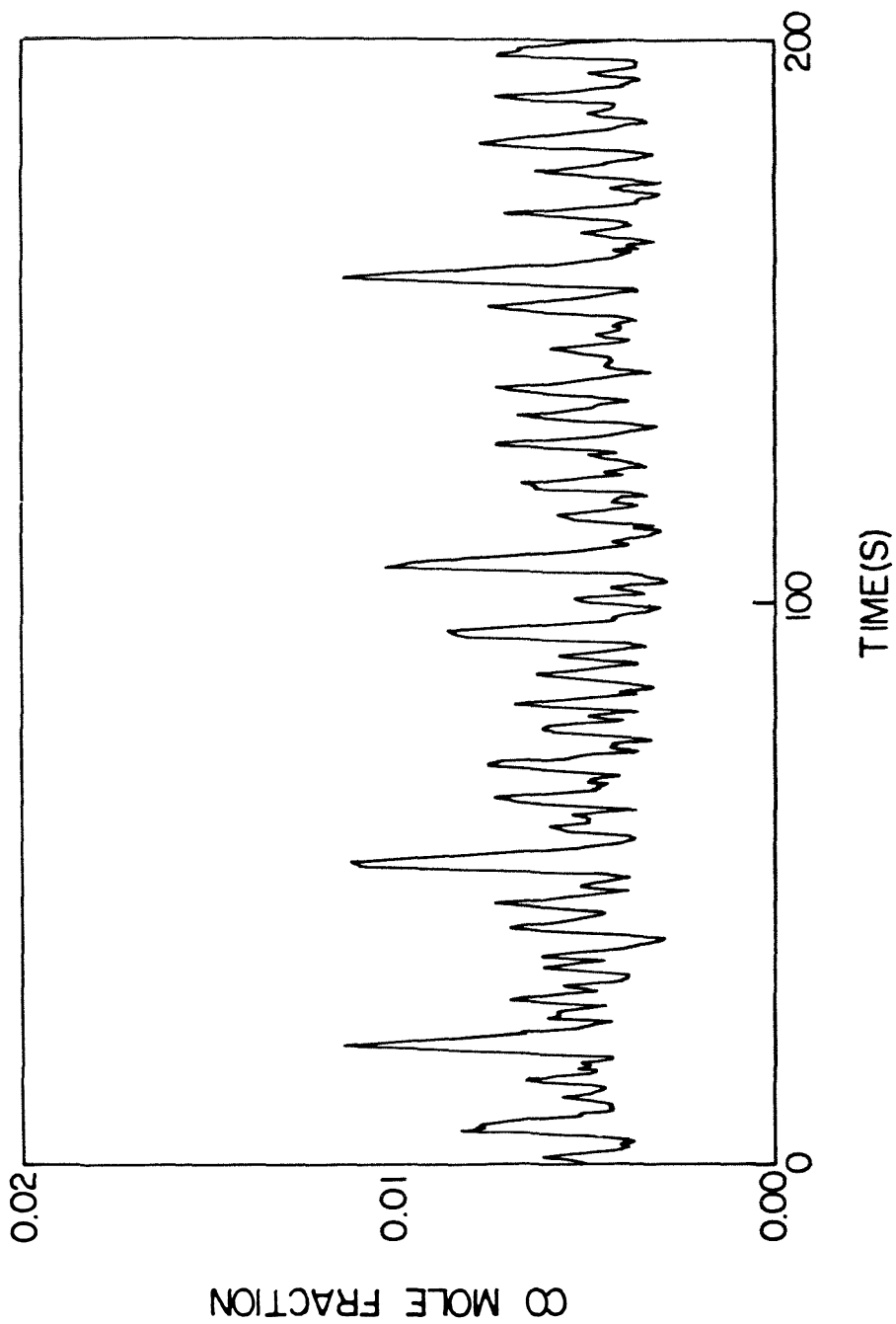


Figure 8

CHAPTER 3

EXPERIMENTAL INVESTIGATIONS USING FEEDBACK-INDUCED

BIFURCATIONS: CARBON MONOXIDE OXIDATION

OVER SUPPORTED SILVER

INTRODUCTION

Steady-state experiments in which gas phase species are monitored have been shown in some cases to be inadequate in discriminating between rival heterogeneous catalytic models. Therefore, a different vantage has become necessary for investigating catalytic kinetic models. Two general approaches utilizing gas phase measurement have been applied to this problem: variation of a reaction input with time and operation of a reaction at or near a point of instability.

Time dependent inputs have been primarily applied using the transient response method, reviewed by Kobayashi and Kobayashi (1974) and Bennett (1976), in which a reaction is subjected to a perturbation (e.g., a step-change in the reactant concentration or the reaction temperature). The behavior of the perturbed system as it undergoes a transition to a new steady state can be used to evaluate a kinetic model. By classifying possible characteristic features in transient response curves, Kobayashi (1982a) describes general correspondences between catalytic reaction sequences and transient experimental data. For this type of experiment, the characteristic time scale or scales of the reaction system being studied must be considered. First, the residence time of the reactor must be sufficiently small as not to obscure the dynamics of the reaction. Also, if the elementary reaction steps occur on widely different time scales, the transient that is due to a slow step may completely dominate the observed response. Multiple time scales can generally be more extensively examined by using a forced cyclic input rather than a single perturbation (Bailey and Horn, 1970). An example experimental study by Cutlip *et al.* (1983) used forced periodic oscillation data to discriminate between four rival models for CO oxidation on platinum.

Multiple steady states and autonomous oscillations have been experimentally observed for a range of reaction systems (Sheintuch and Schmitz, 1977; Hlavacek and Votruba, 1978; Slin'ko and Slin'ko, 1978). These kinetic instability data pro-

vide a powerful test of postulated reaction models by prescribing strict nonlinear behavior that the models must be able to simulate to be accepted. Sheintuch (1985) discusses general mechanistic conditions necessary in a reaction model to simulate kinetic instabilities occurring in catalytic oxidation reactions. In a more specific application, Chang and Aluko (1984) have used data on reaction oscillations to discriminate between Eley-Rideal and Langmuir-Hinshelwood mechanisms for carbon monoxide oxidation on platinum. Unfortunately, not all reactions and experimental reactor configurations have regions of instability that occur naturally at normal operating conditions, and if instabilities do occur, an extensive search of parameter space is often necessary to isolate the conditions that give rise to multiplicity or oscillations.

Kushta and Bailey (1982) have incorporated elements of each of these approaches, transient response and autonomous bifurcations, in introducing a method in which feedback is used to stimulate bifurcation. Using this method, nonlinear information, which is only available when a system is at bifurcation can be obtained even when the system does not bifurcate autonomously. In a modeling study, Lyberatos *et al.* (1984) used feedback-induced bifurcation to discriminate between two rival kinetic models for the catalytic decomposition of N_2O . The technique was also applied to ethylene hydrogenation by Prairie and Bailey (1986,1987). In their work, experimental bifurcation data were used to differentiate between two parameter sets and to estimate parameters for a postulated model.

The idea of feedback-induced bifurcation is applied in the present work to CO oxidation on alumina-supported silver. Using kinetic models presented in the literature for this reaction, the kinetic parameters are estimated from conventional steady-state and transient step-response experiments. Then the experimental bifurcation results will be compared with the simulated bifurcation behavior of the rival kinetic models. The sensitivity of the reaction kinetics to open-loop ex-

periments compared to experimental determination of bifurcations resulting from closed-loop operation will be examined to determine if the bifurcation experiments provide new information relative to the open-loop experiments.

POSTULATED KINETIC MODELS

Because of its unique ability to catalyze alkene epoxidation, particularly the oxidation of ethylene, silver catalysts have been studied extensively under a variety of reaction conditions. Most controversial has been the characterization of the adsorbed states of oxygen on the silver catalyst. While at least two adsorbed oxygen species are accepted as being present on silver, no general agreement as to the exact forms (i.e., monatomic, diatomic, and/or oxide) has been reached (Sachtler, 1970; Verykios *et al.*, 1980; Sachtler *et al.*, 1981). In order better to understand the interaction between oxygen and silver, the CO oxidation reaction on silver has been studied. Several studies have shown that neither CO or CO₂ will adsorb on silver without preadsorption of oxygen (Lawson, 1968; Keulks and Ravi, 1970; Keulks and Chang 1970), although Force and Bell (1975) assign a band to weakly chemisorbed CO₂ on silver in transmission IR experiments.

Two alternative models have been presented in the literature for the CO-O₂ reaction on a silver catalyst. The first mechanism that was considered for the CO oxidation reaction on silver (Model 1) was postulated by Keulks and Chang (1970). They based the model on static isotopic exchange experiments performed at 100°C and 200 Torr using isotopic ¹⁸O₂ with C¹⁶O in a recirculation reactor containing powdered silver catalyst. The model is expressed by the following equations:





where the adsorbed form of oxygen is described by the authors as being either monatomic or diatomic. For the simulations in this work, the sequence given by Equations (1A-D) will be taken as elementary steps, and O^* will be assumed monatomic. The assumption of dynamic equilibrium in Equation (1C) will be addressed later in this work. The resulting differential equations for Model 1 in an isothermal CSTR are

$$n \frac{dx_1}{dt} = F_{CO} - x_1 F_o - k_2 x_1 \theta_1 \quad (1)$$

$$n \frac{dx_2}{dt} = F_{O_2} - x_2 F_o - k_1 x_2 \theta_v^2 \quad (2)$$

$$n \frac{dx_3}{dt} = -x_3 F_o + k_2 x_1 \theta_1 - k_{-4} x_3 \theta_1 + k_4 \theta_3 \quad (3)$$

$$n_s \frac{d\theta_1}{dt} = 2k_1 x_2 \theta_v^2 - k_2 x_1 \theta_1 - k_{-4} x_3 \theta_1 + k_4 \theta_3 \quad (4)$$

$$n_s \frac{d\theta_3}{dt} = k_{-4} x_3 \theta_1 - k_4 \theta_3. \quad (5)$$

Using the transient response method, Kobayashi (1982b) proposed an alternative reaction sequence (Model 2):



The postulated model was fit to experimental transients in the effluent CO_2 concentration resulting from step-changes of the inlet reactant concentrations. A differential reactor containing silver impregnated on $\alpha-Al_2O_3$ was operated at

20°C in all of Kobayashi's experiments. The set of equations describing Model 2 in the isothermal CSTR used in the present simulations are

$$n \frac{dx_1}{dt} = F_{CO} - x_1 F_o - k_3 x_1 \theta_2 \quad (6)$$

$$n \frac{dx_2}{dt} = F_{O_2} - x_2 F_o - k_1 x_2 \theta_v \quad (7)$$

$$n \frac{dx_3}{dt} = -x_3 F_o + k_4 \theta_3 - k_{-4} x_3 \theta_1 \quad (8)$$

$$n_s \frac{d\theta_1}{dt} = 2k_2 \theta_2 \theta_v - 2k_{-2} \theta_1^2 + k_4 \theta_3 - k_{-4} x_3 \theta_1 \quad (9)$$

$$n_s \frac{d\theta_2}{dt} = k_1 x_2 \theta_v - k_2 \theta_2 \theta_v + 2k_{-2} \theta_1^2 - k_3 x_1 \theta_2 \quad (10)$$

$$n_s \frac{d\theta_3}{dt} = k_3 x_1 \theta_2 - k_4 \theta_3 + k_{-4} x_3 \theta_1. \quad (11)$$

In Equations (1-5) and (6-10), x_1 , x_2 , and x_3 are the mole fractions of CO, O₂, and CO₂, respectively, and F_{CO} and F_{O_2} are the inlet flow rates of CO and O₂. The fractional coverages of the adsorbed species are given by the θ_i 's, where θ_1 corresponds to O*, θ_2 to O₂*, θ_3 to CO₃*, and θ_4 to CO₂*. The expression for the fraction of vacant sites, θ_v , is different for the two models with $\theta_v = 1 - \theta_1 - \theta_3 - \theta_4$ for Model 1 and $\theta_v = 1 - \theta_1 - \theta_2 - \theta_3$ for Model 2. Using the dynamic equilibrium assumption in Model 1, θ_4 can be removed from θ_v with $\theta_4 = x_3(1 - \theta_1 - \theta_3)/(K_d + x_3)$.

All of the experiments conducted in this work were performed at constant temperature and pressure, so the number of moles of gas in the reactor was also constant. Therefore, a closed form of the exit molar flow rate, F_o , can be determined giving

$$F_o = F_T - k_1 x_2 \theta_v^2 - k_{-4} x_3 \theta_1 + k_4 \theta_3 \quad (12)$$

for Model 1 and

$$F_o = F_T - k_1 x_2 \theta_v - k_3 x_1 \theta_2 + k_4 \theta_3 - k_{-4} x_3 \theta_1 \quad (13)$$

for Model 2. These expressions were used to remove F_o from the model equations.

EXPERIMENTAL SYSTEM

Specific details of the experimental apparatus, including characterization of the static and dynamic behavior of the individual components in the system, have been provided elsewhere (Prairie *et al.* 1988). Briefly, the system contains four major components: mass flow controllers, reactor, infrared analyzer, and micro-computer. Carbon monoxide (99.99%), oxygen (99.5%), hydrogen (99.9995%), and helium (99.995%) are fed to the reactor through independent Tylan mass flow controllers with a maximum feed rate of 20 sccm except for the helium controller, which has a maximum rate of 200 sccm. Upstream from the CO mass flow controller, the CO passes through a carbonyl trap. A total flow rate of 100 sccm was used for all of the experiments. Wilkes Miran I infrared analyzers operating at 4.6 μm and 4.2 μm were used to monitor effluent concentrations of CO and CO₂, respectively. The time constants of the IR cells were 0.2 seconds for the flow rate used, so the mixing in the IR cells was neglected in modeling. The IR analyzers were found to have an accuracy of $\pm 1\%$ for the range of concentrations measured in the experiments. A Hewlett-Packard 9825B microcomputer was used for data acquisition from the IR analyzers and for control of the mass flow controllers. The maximum sampling rate with the control algorithm was 4 Hz, which was shown to be sufficiently fast relative to the dynamics of the system so that the sampling could be modeled as continuous (Prairie *et al.*, 1988).

The stainless steel, fixed-bed, internal recycle reactor ($\approx 10 \text{ cm}^3$ total volume) was loaded with 2.3 grams of Engelhard 1 wt% silver on α -alumina catalyst. The silver forms a thin shell on the $\frac{1}{8}$ inch cylindrical alumina core. Following the procedure presented by Seyedmonir *et al.* (1984), oxygen chemisorption experiments yielded a dispersion of 13.7% for the silver on alumina. 100 of the halved catalyst cylinders were used in the reactor with the remaining volume packed with 2 mm glass beads. For this packing and a 100 sccm flow rate, the reactor had a residence

time of 4.7 seconds. All of the experiments were performed at 147°C. The reactor temperature was monitored by two thermocouples located at different bed heights and was controlled by a Thermo Electric PI controller.

Prior to the experiments, the catalyst was treated with 10% oxygen for 2 hours at 250°C and then reduced in 20% hydrogen also at 250°C. Reactant gases, CO and O₂ in helium, were fed to the reactor until the catalyst stabilized (\approx 36 hours). This long initial transient was also observed by Nowobilski *et al.* (1986) for the ethylene epoxidation reaction over silver and was attributed to an oxidation of the silver. Also, Seyedmonir *et al.* report slow oxygen uptake on reduced Ag/Al₂O₃ in chemisorption experiments performed at 170°C.

The effect of internal diffusion on the reaction kinetics was assessed using the observable modulus, Φ_o , introduced by Weisz and Prater (1954). Within the range of experiments that were performed in the present work, the maximum steady-state reaction rate was found to be 9.5 $\mu\text{mol}/\text{cm}^3\text{s}$ corresponding to 20% CO and 20% O₂ in the feed stream. Mercury porosimetry data indicated that the silver catalyst was a bidisperse pore system, so the random-pore model (Smith, 1981) was used to determine the effective diffusivity, D_e . For the reaction conditions used, CO in helium had a $D_e = 0.0112 \text{ cm}^2/\text{s}$ and O₂ in helium a $D_e = 0.0108 \text{ cm}^2/\text{s}$. Therefore, $\Phi_o = 0.0116$ and 0.0106 for CO and O₂ respectively, indicating that internal diffusional effects can be neglected (Weisz, 1973). External mass transfer restrictions were eliminated by operating in a mixing regime in which increasing impeller velocity had no effect on the overall reaction rate.

PARAMETER ESTIMATION

In order for a catalytic model to reproduce dynamic behavior, the model must be able to fit steady-state data as a first criterion. Therefore, steady-state experiments were used to estimate kinetic parameters for each proposed model.

Parameters that were indeterminate from static experiments were then evaluated by fitting the models to step-response experiments. The type of experiment necessary to determine parametric values in each model can be illustrated by considering the nondimensionalized forms of the Equations (1-5) and (6-11). The dimensionless equations describing Model 1 are

$$\tau \frac{dx_1}{dt} = x_1^i - x_1 - \hat{k}_2 x_1 \theta_1 + \hat{k}_1 x_1 x_2 \theta_v + \frac{\tau_{s1}}{\tau_{s2}} x_1 x_3 \theta_1 - \frac{\tau_{s1}}{\tau_{s2} K_{eq}} x_1 \theta_3 \quad (14)$$

$$\tau \frac{dx_2}{dt} = x_2^i - x_2 - (1 - x_2) \hat{k}_1 x_2 \theta_v + \frac{\tau_{s1}}{\tau_{s2}} x_2 x_3 \theta_1 - \frac{\tau_{s1}}{\tau_{s2} K_{eq}} x_2 \theta_3 \quad (15)$$

$$\tau \frac{dx_3}{dt} = -x_3 - (1 - x_3) \left(\frac{\tau_{s1}}{\tau_{s2}} x_3 \theta_1 - \frac{\tau_{s1}}{\tau_{s2} K_{eq}} x_2 \theta_3 \right) + \hat{k}_2 x_1 \theta_1 + \hat{k}_1 x_2 x_3 \theta_v \quad (16)$$

$$\tau_{s1} \frac{d\theta_1}{dt} = 2\hat{k}_1 x_2 \theta_v - \hat{k}_2 x_1 \theta_1 - \frac{\tau_{s1}}{\tau_{s2}} x_3 \theta_1 - \frac{\tau_{s1}}{\tau_{s2} K_{eq}} \theta_3 \quad (17)$$

$$\tau_{s2} \frac{d\theta_3}{dt} = x_3 \theta_1 - \frac{\theta_3}{K_{eq}}, \quad (18)$$

where

$$\hat{k}_i = \frac{k_i}{F_T} \quad K_{eq} = \frac{k_{-4}}{k_4} \quad \tau_{s1} = \frac{n_s}{F_T} \quad \tau_{s2} = \frac{n_s}{k_{-4}},$$

and for Model 2 are

$$\tau \frac{dx_1}{dt} = x_1^i - x_1 - (1 - x_1) \hat{k}_3 x_1 \theta_2 + \hat{k}_1 x_1 x_2 \theta_v - \hat{k}_4 x_1 \theta_3 + \hat{k}_{-4} x_1 x_3 \theta_1 \quad (19)$$

$$\tau \frac{dx_2}{dt} = x_2^i - x_2 - (1 - x_2) \hat{k}_1 x_2 \theta_v + \hat{k}_3 x_1 x_2 \theta_2 - \hat{k}_4 x_2 \theta_3 + \hat{k}_{-4} x_2 x_3 \theta_1 \quad (20)$$

$$\tau \frac{dx_3}{dt} = -x_3 - (1 - x_3) (\hat{k}_{-4} x_3 \theta_1 - \hat{k}_4 \theta_3) + \hat{k}_3 x_1 x_3 \theta_2 + \hat{k}_1 x_2 x_3 \theta_v \quad (21)$$

$$\tau_{s1} \frac{d\theta_1}{dt} = -2\hat{k}_{-2} \theta_1 + 2\hat{k}_2 \theta_2 \theta_v + \hat{k}_4 \theta_3 - \hat{k}_{-4} x_3 \theta_1 \quad (22)$$

$$\tau_{s1} \frac{d\theta_2}{dt} = \hat{k}_1 x_2 \theta_v + \hat{k}_{-2} \theta_1^2 - \hat{k}_2 \theta_2 \theta_v - \hat{k}_3 x_1 \theta_2 \quad (23)$$

$$\tau_{s1} \frac{d\theta_3}{dt} = \hat{k}_3 x_1 \theta_2 - \hat{k}_4 \theta_3 + \hat{k}_{-4} x_3 \theta_1, \quad (24)$$

with similar dimensionless groups. The parameters, \hat{k}_i , K_d , and K_{eq} , can be determined from steady-state data, but the parameters τ_{s1} and τ_{s2} in Model 1

and τ_{s1} in Model 2 must be evaluated from dynamic experiments. For these models, τ_{s2} arises only in Model 1.

Steady-state experiments were performed for a range of feed conditions, 2-20% CO and 2-20% O₂ in helium. In all, 70 data points were obtained using different feed compositions while measuring the effluent CO concentration. The steady-state CO mole fraction was measured after spending 1 hour at a fixed inlet composition. The observed reaction rate was then calculated by knowing the amount of CO consumed for the fixed total flow rate.

The rate parameters were estimated by minimizing a sum of squares objective function for the difference between the observed and calculated reaction rates. A finite difference, Levenberg-Marquardt routine (IMSL routine ZXSSQ) was used for solving the nonlinear least squares problem. The specific forms of the calculated reaction rates

$$r_{c1} = k_2 x_1 \theta_1 \quad (25)$$

for Model 1 and

$$r_{c2} = k_3 x_1 \theta_2 \quad (26)$$

for Model 2, are also implicitly a function of the remainder of the state variables. While x_1 , x_2 , and x_3 can be determined from a mass balance on the reactor, the fractional coverages of adsorbed species must be evaluated by solving the steady-state form of the adsorbed species balances simultaneously with the least square determination of the rate parameters. Dynamic equilibrium of Equation (1C) in Model 1 was assumed because the minimization routine was insensitive to the magnitude of the forward and reverse rate parameters for this step which, therefore, could be taken as arbitrarily large. However, the ratio of the forward and reverse rate constants, K_d , always remained the same in the parameter optimization searches. Also, k_4 and k_{-4} in Model 1 could not be independently determined from static experiments because, at steady state, Equation (18) gives a relationship between θ_1 and θ_3 in terms of $K_{eq} = k_{-4}/k_4$.

The results of the steady-state parameter estimation are summarized in Table 1 for each of the models. Also given in the table are the correlation coefficients for the best-fit parameter sets. Shown in Figure 1 is a comparison of the experimental steady-state data and the two models for three fixed inlet O_2 mole fractions (0.02,0.05,0.14) and a range of CO feed concentrations. Keulks and Chang (1970) presented no parameters for their postulated model, but the dynamic equilibrium assumption for Equation (1C) agrees well with the suggestion of Force and Bell (1975), that weakly chemisorbed CO_2 can exist on the silver catalyst. A comparison between the parameters estimated for Model 2 and those given by Kobayashi (1982b), although determined at different temperatures, reveals similar relative values for the corresponding rate parameters.

Step-response experiments were used to evaluate the relative magnitude of the dynamic surface parameters in Model 1, τ_{s1} and τ_{s2} , and in Model 2, τ_{s1} . In these experiments, transients are induced in the reactor by a step-change in the inlet reactant concentrations, and the effluent responses of CO and CO_2 are monitored. Several different feed concentrations were used in the step-response experiments, but all yielded rapid monotonic approach to the steady-state condition. The exception to this behavior was a switch from pure CO feed to a CO- O_2 mixture, which created a slow overshoot in CO_2 production. The slow transient resulting from introducing O_2 to a reduced catalyst will be discussed later. The rapid transients observed from step-change in the inlet concentrations involving other feed configurations indicated that the dynamic surface parameters are small relative to the reactor time constant. Simulations of the transient response data could give only upper bounds on the values of τ_{s1} (< 0.1 s) and τ_{s2} (< 0.1 s) for each model because, the dynamics of the reactor dominated the observed responses. The step-response experiments were also used to determine the time delay in the system due to transport and measurement lag. The measured time delay, $\tau_D = 3.26$ s, will be used in the bifurcation simulations.

FEEDBACK-INDUCED BIFURCATION

Feedback to the inlet gas flow rates was introduced to the open-loop process by applying a feedback control algorithm. The reasons for choosing an arctangent control function have been presented by Prairie *et al.* (1988). For the inlet reactant flow rates, the algorithms have the form

$$F_{CO} = F_{CO}^{ref} + \frac{2w}{\pi} \text{Tan}^{-1}[u_{CO}(x_1 - x_1^{ref})] \quad (27)$$

$$F_{O_2} = F_{O_2}^{ref} + \frac{2w}{\pi} \text{Tan}^{-1}[u_{O_2}(x_1 - x_1^{ref})], \quad (28)$$

where u_{CO} and u_{O_2} are the gains to the CO and O₂ mass flow controllers, respectively. Here, feedback in both of the control algorithms is based on the effluent mole fraction of CO. The controller gains can be independently manipulated, and consequently these were used as the bifurcation parameters in the feedback experiments. Primarily, two types of bifurcations result for the closed-loop configuration given in Equations (27-28): steady-state and Hopf bifurcation. Steady-state bifurcation experiments can be simulated using the steady-state form of Equations (14-18) and (19-24) with the inlet flow rates replaced by Equations (27-28), but Hopf bifurcation simulations require the full set of dynamic equations. Therefore, analysis of the static and dynamic bifurcations can be treated separately.

Steady-State Bifurcation

The system will go through a steady-state bifurcation when changing the value of a bifurcation parameter causes the base or reference steady-state (steady-state corresponding to no feedback control), to become unstable concurrently with the emergence of two new stable steady states. In the static bifurcation experiments, a steady state resulting from 10% CO and 10% O₂ in the feed was used as the reference condition. Feedback was then added to the system with a

value of $w = 5$ sccm used for the half-width of the arctangent control function. Because of noise in the experimental system, the value of x_1^{ref} ($= 0.074$) could be determined only to an accuracy of two digits.

Using a fixed gain to the O₂ mass flow controller, the CO gain u_{CO} was increased until the system was operating on one of the bifurcation branches. The entire static bifurcation diagram was then traced by decreasing the CO gain incrementally until the system returned to its reference condition, which defines one of the two bifurcation branches. Then the CO gain was incrementally increased until the system traced the other bifurcation branch. Sometimes a perturbation to the system was necessary for the second branch to be evaluated. Figure 2 shows experimental data that were determined in this manner. Plotted is the deviation of the effluent mole fraction of CO from the reference CO mole fraction versus the CO gain for two different fixed O₂ gains, 0.0 and 400.

Using just the parameters estimated from steady-state experiments and conditions identical with those used in the steady-state bifurcation experiments, the rival models were used to simulate the static bifurcation data. The results of these simulations are shown with the corresponding data points in Figure 2. Here, the model curves were determined by simultaneously solving the steady-state equations with the inlet flow rates under feedback control. Because the precise value of x_1^{ref} is difficult to obtain with a high enough degree of accuracy, the experimental system has been perturbed from an ideal, symmetric bifurcation. Therefore, rather than displaying pitchfork bifurcation, where the stable solutions all merge at the bifurcation point, the experiments and model produce imperfect steady-state bifurcation (Iooss and Joseph, 1980). This type of bifurcation was first observed for an experimental catalytic reaction system by Prairie and Bailey (1986).

As Figure 2 shows, static bifurcation experiments cannot be used to discriminate between the rival models for CO oxidation because the simulations for each

model give excellent reproduction of the experimental data.

Hopf Bifurcation

Since steady-state bifurcation does not differentiate between the two models, the behavior of the system was studied under Hopf bifurcation conditions. When a system passes through a Hopf bifurcation, the reference steady state becomes unstable, and the system variables exhibit a limit cycle. The system was studied at or near a bifurcation point, so a local analysis was used for the simulations of model stability. A convenient form in which to do this analysis is through transfer functions. By using a frequency domain analysis, time delay that is inherent to the experimental system can be readily treated. A block diagram for the experimental system has been given by Prairie *et al.* (1988) with a corresponding overall transfer function matrix

$$\mathbf{G}_T = [\mathbf{I} + \mathbf{G}_p \mathbf{G}_{mfc} \mathbf{G}_c \mathbf{D}]^{-1} \mathbf{G}_p \mathbf{G}_{mfc} \mathbf{G}_c, \quad (29)$$

where the individual transfer function matrices are \mathbf{G}_p for the CO oxidation reaction in a CSTR, \mathbf{G}_{mfc} for the mass flow controllers, \mathbf{G}_c for the control algorithm, and \mathbf{D} for the system time delay.

The transfer functions, \mathbf{G}_{mfc} , \mathbf{G}_c , and \mathbf{D} can be determined independently and are intrinsic to the experimental system. A detailed description of the methods used to evaluate the matrices is presented elsewhere (Prairie *et al.*, 1988), so only the final matrix values will be given here. Only two elements of the \mathbf{G}_{mfc} matrix are nonzero; these are given by

$$g_{mfc,11} = 0.956 \exp(-0.31\omega) \quad (30)$$

for the CO mass flow controller, and

$$g_{mfc,22} = 0.945 \exp(-0.49\omega) \quad (31)$$

for the O₂ mass flow controller, where the pre-exponential factor gives the amplitude ratio and the exponential term gives the phase shift for the controllers. The transfer function G_c also has two elements that are nonzero,

$$g_{c,11} = -cu_{CO} \quad (32)$$

$$g_{c,21} = -cu_{O_2} \quad (33)$$

where $c = 2w/\pi F_T$. Finally, the delay matrix, D , will have two nonzero elements

$$d_{11} = d_{22} = \exp(-\tau_D s). \quad (34)$$

The process transfer function, G_p , is determined from the catalytic model Equations (14-18) and (19-24). For the local analysis, these equations are linearized about the reference steady-state condition, and deviation variables, $\bar{x} = x - x^{ref}$, can be introduced, where x is a vector of the state variables (*i.e.*, $x = (x_1, x_2, x_3, \theta_1, \theta_3)^T$ for Model 1). The time domain model can then be represented by

$$\tau \frac{d\bar{x}}{dt} = A\bar{x} + Bu \quad (35)$$

$$y = C\bar{x} \quad (36)$$

where A is the Jacobian of the model equations evaluated at $\bar{x} = 0$, u is a vector of the manipulated variables which are the dimensionless inlet CO and O₂ flow rates, and y is a vector containing the observable variables, which here consist only of the CO effluent mole fraction. G_p , then, is found by taking the Laplace transform of Equations (35-36) and removing \bar{x} , giving

$$G_p(s) = C(I\tau s - A)^{-1}B \quad (37)$$

In the simulations, the resolvent of A was determined numerically for a specific reference steady state using the QZ method (Golub and Van Loan, 1983) which can be used for unsymmetric eigenvalue problems. Because of the large disparity in the magnitude of the Jacobian matrix eigenvalues associated with both

postulated models, the resolvent of \mathbf{A} was also evaluated for a single reference steady state, using symbolic manipulation. Despite the apparent “stiffness” of the model system Jacobian, the numeric QZ algorithm gave identical results with those derived by symbolic manipulation.

The stability behavior of the model equations can be determined by solving for the zeros of

$$p(s) = \det[\mathbf{I} + \mathbf{G}_p \mathbf{G}_{mfc} \mathbf{G}_c \mathbf{D}], \quad (38)$$

which is the characteristic function associated with the overall transfer function, \mathbf{G}_T . Steady-state bifurcation will occur when a single root of the characteristic function has zero real and imaginary parts ($p(0)=0$), and the remaining roots all have a negative real component. This condition on Equation (38) gives a relationship between u_{CO} and u_{O_2} ,

$$u_{CO} = \frac{-0.945g_{p,12}(0)u_{O_2}}{0.956g_{p,11}(0)} + \frac{1}{0.956g_{p,11}(0)}, \quad (39)$$

for steady-state bifurcation. Equation (39) gives the exact theoretical point of static bifurcation, but as shown in the previous section, a small perturbation in the system will give imperfect bifurcation, making the experimental determination of an exact steady-state bifurcation point difficult. The perturbed bifurcation is the reason for using a different analysis for static bifurcation than for Hopf bifurcation.

For Hopf bifurcation to occur, the characteristic function must have a complex conjugate pair of roots with zero real part ($p(i\omega) = 0$), while the remaining roots lie in the negative half plane. At a Hopf bifurcation point, the values of the bifurcation parameters are given by

$$u_{CO} = \text{Re} \left[\frac{-1 - 0.945g_{p,12}(i\omega)u_{O_2} (\cos(\tau_D\omega - 0.49\omega) - i\sin(\tau_D\omega + 0.49\omega))}{0.956g_{p,11}(i\omega) (\cos(\tau_D\omega + 0.31\omega) - i\sin(\tau_D\omega + 0.31\omega))} \right] \quad (40)$$

$$u_{CO} = \text{Im} \left[\frac{-1 - 0.945g_{p,12}(i\omega)u_{O_2} (\cos(\tau_D\omega - 0.49\omega) - i\sin(\tau_D\omega + 0.49\omega))}{0.956g_{p,11}(i\omega) (\cos(\tau_D\omega + 0.31\omega) - i\sin(\tau_D\omega + 0.31\omega))} \right] \quad (41)$$

which are parametric in the bifurcation frequency, ω .

Shown in Figure 3 is an example of the form in which the Hopf bifurcation experimental data are obtained. The deviation of the effluent CO mole fraction from the reference condition is plotted versus time for decreasing values of the CO gain and a fixed O₂ gain. The experimental data shown resulted from a feed of 16% CO and 4% O₂. Each section shows the last 90 seconds of 600 seconds spent at the prescribed CO gain value. The value of the O₂ gain was held constant at 100 throughout the experiment. The stability of the experimental limit cycle near the bifurcation point was determined by forcing the stable system through a Hopf point and then back to the stable condition. No hysteresis in the bifurcation point was observed, indicating that the system exhibits a supercritical Hopf bifurcation (Iooss and Joseph, 1980). Because supercritical Hopf bifurcation was observed, the experimental Hopf bifurcation point was found using the method outlined by Prairie and Bailey (1987), which is based on the amplitudes of a sequential set of limit cycles near the Hopf bifurcation point. The effects of noise and of perturbation of the programmed reference steady-state value have been addressed by Prairie *et al.* (1988) and have been found to have a negligible effect on the observed Hopf bifurcation point.

The Hopf bifurcation experimental data were tabulated in the form of a bifurcation or stability diagram for a reference feed composition of 16% CO and 4% O₂. A half-width of 3 sccm was used for the arctangent control function in all of the Hopf bifurcation experiments reported in this work. A total of 17 Hopf bifurcation points were obtained by fixing the O₂ gain between -300 and 500 and by increasing the magnitude of the CO gain until the system bifurcated to a limit cycle. Oxygen gains outside the -300 to 500 range caused the oxygen mass flow controller to default fully open or closed, leading to behavior uncharacterized in the model for the mass flow controllers. Figure 4(a) shows the results of the Hopf bifurcation experiments in O₂ gain, CO gain parametric space. Shown in Figure

4(b) is the frequency of the resulting limit cycles versus the CO gain necessary to induce bifurcation. Implicit in this figure is the corresponding O₂ gain at the bifurcation point.

Using the dynamic surface parameters estimated from the transient step-response data as initial values, the two models were fit numerically to the experimental Hopf bifurcation gain and frequency data shown previously through minimization of an objective function. The objective function used, $F(\tau_{s,j})$, where $j=1,2$ for Model 1 and $j=1$ for Model 2, had the form

$$F(\tau_{s,j}) = \sum_{i=1}^{17} [\alpha(\omega_i - \omega(u_{O_2,i}))^2 + (u_{CO,i}^H - u_{CO}^H(u_{O_2,i}))^2], \quad (42)$$

where ω_i and $u_{CO,i}^H$ are the bifurcation frequency and gain observations for a specific $u_{O_2,i}$, $\omega(u_{O_2,i})$ and $u_{CO}^H(u_{O_2,i})$ are the corresponding model values, and α is a weighting factor. The results of the minimization, which are given in Table 2, were found to be independent of the value of the weighting factor. Using the result of the chemisorption experiment, a value of $\tau_{s,1} = 0.6$ s is calculated. The possible cause of the difference between the chemisorption value of $\tau_{s,1}$ and the value found from fitting the models to data obtained in dynamic experiments is considered in more detail elsewhere (Shanks and Bailey, 1987).

Figure 4(a) shows the simulations of the stability diagram under the imposed experimental conditions for both models, using the best fit values of the dynamic parameters. In this figure, the reference steady state is stable within the stability envelope and unstable elsewhere. At the bottom of the envelope, the straight line corresponds to a locus of the steady-state bifurcation points, while passing out of the envelope at any other point will lead to Hopf bifurcation. The simulated and experimental bifurcation frequencies are shown in Figure 4(b) plotted against the CO gain at bifurcation. While the two models give bifurcation diagrams of different shape, neither of the models could be said to be clearly superior for reproducing the experimental data. Model 1 fits the experimental bifurcation

frequency data extremely well, although this is somewhat misleading, since the curves shown are projections of the limit cycle frequencies onto the frequency-CO gain plane, obscuring the frequency dependence on the O₂ gain value. If the bifurcation frequency is plotted versus the oxygen gain value u_{O_2} at bifurcation, Model 1 does not fit as well as Model 2.

An example of the sensitivity of Model 1 to the values of the dynamic surface parameters is demonstrated in Figure 5. Shown are bifurcation diagrams for Model 1 using the best fit values of τ_{s1} and τ_{s2} and two other sets of the two parameters. As shown in the figure, the stability envelope calculated for the model system is sensitive to order-of-magnitude changes in these parameters.

The stability of the limit cycles near the bifurcation point for the models was investigated using the BIFOR2 program presented by Hassard *et al.* (1981). The numerical bifurcation program evaluates the leading coefficient of the asymptotic expansion for the nonzero Floquet exponent corresponding to the periodic solution. This coefficient provides the stability information. In order to apply the program, the model equations must be in time-domain form. Time delay was treated in these calculations using a memory function given by Lyberatos (1985). Time delay was approximated by a finite system of equations for the model, which in the infinite limit gives exactly the eigenvalue structure of the model with delay. Both kinetic models were checked for $u_{O_2} = 100$ and gave stable limit cycles at bifurcation, which agrees with the experimental observations.

As a second test of the models, Hopf bifurcation points were determined experimentally for a range of CO inlet mole fractions from 0.04-0.16 and a fixed O₂ mole fraction in the feed of 0.04. Here, the reference steady state is different for each case, depending on the feed CO mole fraction. Figure 6(a) shows experimental data for the CO gain necessary to induce bifurcation at a fixed O₂ gain plotted against the inlet CO mole fraction. The data presented are for O₂ gains of 150 and -150. Also shown in this figure are the results of simulations of bifurca-

tion gain and frequency using the two models. These calculations were performed using the dynamic parameters determined by best fit to the stability diagram in Figure 4; *i.e.*, the values in Table 2. Figure 6(b) gives the frequency of the Hopf bifurcations for the given CO inlet mole fraction. As can be seen, neither model appears to give an adequate reproduction of the experimental bifurcation data, although each model does give different results.

DISCUSSION

The inability of either kinetic model to reproduce the experimental Hopf bifurcation data can be attributed to several possible problems: inaccuracy in the model of the experimental apparatus or incorrect kinetic mechanism. As mentioned previously, Prairie *et al.* (1988) have carefully characterized the experimental system and have postulated a model for the apparatus that agrees closely with the experimentally observed bifurcation points and frequencies. The model, though, is least accurate for time delays of 5 seconds or less. In this region the model, while agreeing with the qualitative shape of the experimental bifurcation curve, gives larger magnitudes of the controller gain necessary to induce Hopf bifurcation than those observed experimentally. The time delay in the present work, 3.26 s, is within the region where the system apparatus model is less accurate. The direction of the offset between the simulations and the experimental data here is consistent with that seen in the reactor system model alone for small time delays. To overcome this problem, it is necessary to obtain as complete a stability envelope for a single reference steady state as is possible, subject to the limitations of the experimental apparatus, so that the qualitative shape of the envelope can be used in discriminating between rival models. The extent of the stability envelope that can be observed experimentally in Figure 4(a) was limited

by the O_2 gain values available. Consequently, to extend this work, a different or more compact stability envelope is needed.

A different stability diagram can be constructed by changing the feedback configuration so that different reaction species other than CO are monitored for control. Large O_2 gains were needed in these experiments because, as shown in the steady-state experiments, the reaction rate is relatively unaffected by the oxygen concentration in the reactor and fluctuations in the CO concentration of the size seen in the bifurcation experiments have little effect on the consumption of O_2 . The current reactor system is limited to measuring the IR active species, CO and CO_2 , so experiments were performed in which the measured effluent concentrations of both CO and CO_2 were used for feedback. Control of the CO mass flow controller around the reference feed of 10% CO was based on the gain, u_{CO} , associated with the CO deviation variable and another gain, u_{CO_2} , with the CO_2 deviation variable. During these experiments, the flow rate of O_2 was held constant so that 10% O_2 was always in the inlet feed. Large values of u_{CO_2} were necessary to induce Hopf bifurcation, so only a very small portion of the stability diagram could be determined.

The controller gains necessary to stimulate Hopf bifurcation can be decreased in magnitude by increasing the time delay between measurement and control. This behavior is displayed in Figure 7, where the stability diagram and bifurcation frequency have been simulated using Model 2 with the experimental $\tau_D = 3.26$ s and a second delay, $\tau_D = 10.0$ s. Using the larger time delay decreases the magnitude of the O_2 gain at the Hopf bifurcation points but also introduces new behavior. The locus of the gain values giving pure imaginary roots of the characteristic function ($p(i\omega) = 0.0$) winds back on itself for increasing values of the frequency parameter. Dotted in Figure 7 are the portions of the curve where the purely imaginary roots of the characteristic equation are not the roots with largest real parts. Consequently, these points do not correspond to Hopf bifurcation loci. In addition to

the F_1 and F_2 bifurcation points (Lyberatos *et al.*, 1985) seen in the small time delay simulation, the 10.0 s simulation also contains a F_3 bifurcation point. The problem with increasing the time delay can be seen in Prairie *et al.* (1988) where the bifurcation behavior of a system becomes increasingly dominated by the time delay as this parameter increases, thus obscuring the inherent nonlinear structure of the system of interest. There is a trade-off, then, between manipulating time delay to decrease controller gains, and decreasing the sensitivity of the observed bifurcation characteristics to the underlying reaction kinetics, which are the object of the experiments. More experiments need to be performed to further elucidate the effect of intentionally manipulating time delay in the experimental system.

One of the major difficulties in postulating a representative kinetic model of the CO-O₂ reaction on silver is determining the state of the silver catalyst surface during reaction. The very slow initial transient before the catalyst activity stabilizes is not described in either proposed model. However, this transient indicates that either the morphology of the supported silver is changing, an active site blockage is occurring, or the primary active site for CO oxidation and, therefore, the rate-determining kinetic step is changing. By reducing the used catalyst in hydrogen at 250°C, much of the original high activity can be recovered, which would seem to discount morphological change as the primary contributor to the slow dynamics. The blocking of active sites would most likely be due to the formation of an inactive oxide site. Other work with silver catalysts has indicated the presence of a silver oxide on the surface or subsurface (Keulks and Outlaw, 1972; Temkin, 1979; Sachtler *et al.* 1981).

The slow transient evident during activity stabilization is not expected to affect the Hopf bifurcation experiments significantly, since these oscillations occur on a much shorter time scale. The postulated models, while not reproducing the slow dynamics, could still be valid under the conditions imposed in the dynamic feedback-induced bifurcation experiments, because the slow process will remain

at quasi-steady state throughout the Hopf experiments. The changing state of the surface would have the most impact on Model 2, as this model was fit by Kobayashi (1982b) to transients imposed immediately after reduction.

The slow transients observed during step-response experiments point to the need for using multiple experimental methods to study catalytic reactions and to test proposed reaction mechanisms. Feedback-induced bifurcation experiments cannot alone provide comprehensive characterization of a kinetic mechanism for a specific catalytic reaction. For example, the bifurcation data are sensitive to small kinetic time constants that cannot be determined from open-loop experiments (Kuszta and Sinha, 1980), while the long transients observed in step-response experiments have little effect on the Hopf bifurcation behavior.

CONCLUSIONS

Bifurcation data can be readily obtained for a catalytic reaction by utilizing feedback control. Simulations of the feedback-induced bifurcation experiments indicate that the observed bifurcation behavior can be attributed to the process being studied, not solely to the experimental apparatus that is being used. While the two postulated mechanisms for the CO–O₂ reaction are indiscriminate from conventional steady-state and transient experiments, differences in the nonlinear structure of the models are exploited in the bifurcations resulting from closed-loop operation.

Both kinetic models gave excellent reproductions of the experimental steady-state bifurcation data, including the effect of perturbing the reference condition. The models, though, failed to fit adequately the Hopf bifurcation data for a single reference steady state or for multiple feed conditions. It was found that smaller magnitude gains were needed to induce dynamic bifurcation in the experimental

system than were given by the simulations of each kinetic model. However, parametric information about small time-scale processes, which was not available in open-loop experiments, was obtained by introducing a control loop.

NOTATION

A	Jacobian matrix
B	coefficient matrix of manipulated variables
<i>c</i>	scale factor for the arctangent function
C	coefficient matrix of the process observables
d_{ii}	element of the delay matrix
D	delay matrix
<i>F</i>	flow rate (mol/s)
$F(\tau_{sj})$	objective function
g_{ii}	element of transfer function matrix
G	transfer function matrix
k_i	rate parameter (mol/s)
K_d	dynamic equilibrium parameter in Model 1
K_{eq}	equilibrium parameter in Model 1
<i>n</i>	reactor capacity (mol)
n_s	active sites on the catalyst (mol)
$p(s)$	characteristic function
<i>r</i>	reaction rate (mol/s)
<i>t</i>	time (s)
<i>u</i>	controller gain
u	vector of manipulated variables
<i>w</i>	half-width of the arctangent function (sccm)
x_i	gas-phase mole fraction

\mathbf{x}	vector of the state variables
\mathbf{y}	vector of the observables
α	weighting factor
ω_i	fractional surface coverage
τ	reactor residence time (s)
τ_D	system time delay (s)
τ_{sj}	dynamic surface parameter (s)
ω	bifurcation frequency (rad/s)

subscripts

c	controller
$c1$	Model 1 calculation
$c2$	Model 2 calculation
CO	carbon monoxide
mfc	mass flow controller
o	outlet
O_2	oxygen
p	process
T	total

superscripts

H	Hopf
ref	reference condition

REFERENCES

- Bailey, J.E. and F. Horn, "Catalyst Selectivity Under Steady-State and Dynamic Operation: An Investigation of Several Kinetic Mechanisms," *Ber. Bunsenges. Phys. Chem.*, **74**, 611 (1970).
- Bennett, C.O., "The Transient Response Method and Elementary Steps in Heterogeneous Catalysis," *Catal. Rev.-Sci. Engng.*, **13**, 758 (1976).
- Chang, H.C. and M. Aluko, "Multi-Scale Analysis of Exotic Dynamics in Surface Catalyzed Reactions-I," *Chem. Eng. Sci.*, **39**, 37 (1984).
- Cutlip, M.B., C.J. Hawkins, D. Mukesh, W. Morton, and C.N. Kenney, "Modelling of Forced Periodic Oscillations of Carbon Monoxide over Platinum Catalyst," *Chem. Eng. Commun.*, **68**, 329 (1983).
- Force, E.L. and A.T. Bell, "Infrared Spectra of Adsorbed Species Present During the Oxidation of Ethylene over Silver," *J. Catal.*, **38**, 440 (1975).
- Golub, G.H. and C.F. Van Loan, *Matrix Computations*, Johns Hopkins University Press, Baltimore, Md. (1983).
- Hassard, B.D., N.D. Kazarinoff, and Y.-H. Wan, *Theory and Applications of Hopf Bifurcation*, Cambridge University Press, Cambridge (1981).
- Hlavacek, V. and J. Votruba, "Hysteresis and Periodic Activity Behavior in Catalytic Chemical Reaction Systems," *Advan. Catal.*, **27**, 59 (1978).
- Iooss, G. and D.D. Joseph, *Elementary Stability and Bifurcation Theory*, Springer-Verlag, New York (1980).
- Keulks, G.W. and Chang C.C., "The Kinetics and Mechanism of Carbon Monoxide Oxidation," *J. Phys. Chem.*, **74**, 2590 (1970).
- Keulks, G.W. and J.F. Outlaw, "A Study of the Mechanism of Carbon Monoxide Oxidation over Silver: Interactions Between Carbon Monoxide and Preadsorbed Oxygen," *Proc. 5th Int. Congr. Catal.*, **2**, 959 (1972).

- Keulks, G.W. and A. Ravi, "Infrared Spectroscopic Study of Carbon Monoxide Adsorption on Hydrogen and Oxygen Treated Silver Surfaces," *J. Phys. Chem.*, **74**, 783 (1970).
- Kobayashi, H. and M. Kobayashi, "Transient Response Method in Heterogeneous Catalysis," *Catal. Rev.-Sci. Engng.*, **10**, 139 (1974).
- Kobayashi, M., "Characterization of Transient Response Curves in Heterogeneous Catalyst I," *Chem. Eng. Sci.*, **37**, 393 (1982a).
- Kobayashi, M., "Rival Kinetic Models in the Oxidation of Carbon Monoxide over a Silver Catalysis by the Transient Response Method," *Chemical Reaction Engineering*, ACS Symp. Ser., **196**, 213 (1982b).
- Kuszta, B. and J.E. Bailey, "Nonlinear Model Identification By Analysis of Feedback-Stimulated Bifurcation," *IEEE Trans. Autom. Control*, **AC-27**, 227 (1982).
- Kuszta, B. and N.K. Sinha, "On Identification of Linear Systems with Feedback: High Gain Feedback Case," *Int. J. Systems Sci.*, **11**, 403 (1980).
- Lawson, A., "Factors Influencing the Compensation Effect during Formic Acid Decomposition on Silver," *J. Catal.*, **11**, 295 (1968).
- Lyberatos, G., "The Effect of Time Delay on the Feedback Identification of Chemical Reaction Systems," *Chem. Eng. Sci.*, **40**, 2160 (1985).
- Lyberatos, G., B. Kuszta, and J.E. Bailey, "Discrimination and Identification of Dynamic Models via Introduction of Feedback," *Chem. Eng. Sci.*, **39**, 739 (1984).
- Lyberatos, G., B. Kuszta, and J.E. Bailey, "Versal Families, Normal Forms, and Higher Order Bifurcations in Dynamic Chemical Systems," *Chem. Eng. Sci.*, **40**, 1177 (1985).
- Nowobilski, P.J., C. Takoudis, and M. Weaver, "Low Pressure Ethylene Epoxidation over Silver Catalysts," AICHE Annual Meeting, Miami Beach (1986).
- Prairie, M.R. and J.E. Bailey, "Application of Feedback-Induced Bifurcation for Evaluating Steady-State and Transient Heterogeneous Catalysis," *Chem. Eng. Sci.*, **40**, 1177 (1985).

- ysis Kinetic Models," *Chem. Eng. Sci.*, **41**, 937 (1986).
- Prairie, M.R. and J.E. Bailey, "Experimental and Modeling Investigations of Steady-State and Dynamic Characteristics of Ethylene Hydrogenation on Pt/Al₂O₃," *Chem. Eng. Sci.*, **42**, 2085 (1987).
- Prairie, M.R., B.H. Shanks, and J.E. Bailey, "Intentional Manipulation of Closed-Loop Time Delay for Model Validation Using Feedback-Induced Bifurcation Experiments," *Chem. Eng. Sci.* in press (1988).
- Sachtler, W.M.H., "The Mechanism of the Catalytic Oxidation of Some Organic Molecules," *Catal. Rev.-Sci. Eng.*, **4**, 27 (1970).
- Sachtler, W.M.H., C. Backx, and R.A. Van Santen, "On the Mechanism of Ethylene Epoxidation," *Catal. Rev.-Sci. Eng.*, **23**, 127 (1981).
- Syedmonir, S.R., D.E. Strohmayer, G.L. Geoffroy, and M.A. Vannice, "Characterization of Supported Silver Catalysts II. Adsorption Studies of Well-Dispersed Ag on η -Al₂O₃," *Adsorp. Sci. Tech.*, **1**, 253 (1984).
- Shanks, B.H. and J.E. Bailey, "Modeling of Slow Dynamics in the Oxidation of Carbon Monoxide over Supported Silver," *AIChE J.*, **33**, 1971 (1987).
- Sheintuch, M., "Nonlinear Kinetics in Catalytic Oxidation Reactions: Periodic and Aperiodic Behavior and Structure Sensitivity," *J. Catal.*, **96**, 326 (1985).
- Sheintuch, M. and R.A. Schmitz, "Oscillations in Catalytic Reactions," *Catal. Rev.-Sci. Eng.*, **15**, 107 (1977).
- Slin'ko, M.G. and M.M. Slin'ko, "Self-Oscillations of Heterogeneous Catalytic Reaction Rates," *Catal. Rev.-Sci. Eng.*, **17**, 119 (1978).
- Smith, J.M., *Chemical Engineering Kinetics*, McGraw-Hill, Inc., New York (1981).
- Temkin, M.I., "The Kinetics of Some Industrial Heterogeneous Catalytic Reactions," *Advan. Catal.*, **28**, 173 (1979).

Verykios, X.E., F.P. Stein, and R.W. Coughlin, "Oxidation of Ethylene over Silver: Adsorption, Kinetics, Catalyst," *Catal. Rev.-Sci. Eng.*, **22**, 197 (1980).

Weisz, P.B., "Diffusion and Chemical Transformation," *Science*, **179**, 433 (1973).

Weisz, P.B., and C.D. Prater, "Interpretation of Measurements in Experimental Catalysis," *Advan. Catal. Related Subj.*, **6**, 143 (1954).

TABLE 1: Parameters estimated from steady-state data.
(r^2 is the correlation coefficient for the model relative to all of the steady-state experimental data.)

Model 1		Model 2	
k_1 (mol/s)	1.23×10^{-4}	k_1 (mol/s)	9.64×10^{-4}
k_2 (mol/s)	2.59×10^{-4}	k_2 (mol/s)	1.60×10^{-4}
K_d	0.195	k_{-2} (mol/s)	2.40×10^{-6}
K_{eq}	171	k_3 (mol/s)	1.46×10^{-4}
r^2	0.93	k_4 (mol/s)	9.59×10^{-2}
		k_{-4} (mol/s)	1.83×10^{-2}
		r^2	0.98

TABLE 2: Dynamic surface parameters estimated from Hopf bifurcation data.

Model 1		Model 2	
τ_{s1} (s)	0.03	τ_{s1} (s)	0.03
τ_{s2} (s)	0.007	r_{ω}^2	0.97
r_{ω}^2	0.97	r_u^2	0.89
r_u^2	0.90		

FIGURE CAPTIONS

- Figure 1: Steady-state reaction rate data and simulations for Model 1 (dashed) and Model 2 (solid). (a) $x_2^i = 0.14$, (b) $x_2^i = 0.05$, (c) $x_2^i = 0.02$.
- Figure 2: Experimental and calculated curves for steady-state bifurcation with Model 1 (dashed) and Model 2 (solid). (a) $u_{O_2} = 0.0$, (b) $u_{O_2} = 400$.
- Figure 3: Experimental Hopf bifurcation data with $u_{O_2} = 100$.
- Figure 4: (a) Bifurcation diagram with data and best fit simulations for Model 1 (dashed) and Model 2 (solid). (b) Hopf bifurcation frequency relationship to the carbon monoxide gain.
- Figure 5: Simulated bifurcation diagrams for Model 1 with $\tau_{s1} = 0.03$ s and $\tau_{s2} = 0.007$ s (solid), $\tau_{s1} = 0.03$ s and $\tau_{s2} = 0.07$ s (dashed), and $\tau_{s1} = 0.3$ s and $\tau_{s2} = 0.007$ s (dash-dot).
- Figure 6: (a) Carbon monoxide gain necessary for Hopf bifurcation with fixed oxygen gain ($u_{O_2} = 150$:squares; $u_{O_2} = -150$:circles) for different inlet CO mole fractions with Model 1 (dashed) and Model 2 (solid). (b) Frequency of the resulting Hopf bifurcations.
- Figure 7: Simulated bifurcation diagram and bifurcation frequency using Model 2 with $\tau_D = 3.26$ s (solid) and $\tau_D = 10.0$ s (dashed). The dotted curves correspond to nonleading zeros of the characteristic equation for $\tau_D = 10.0$ s.

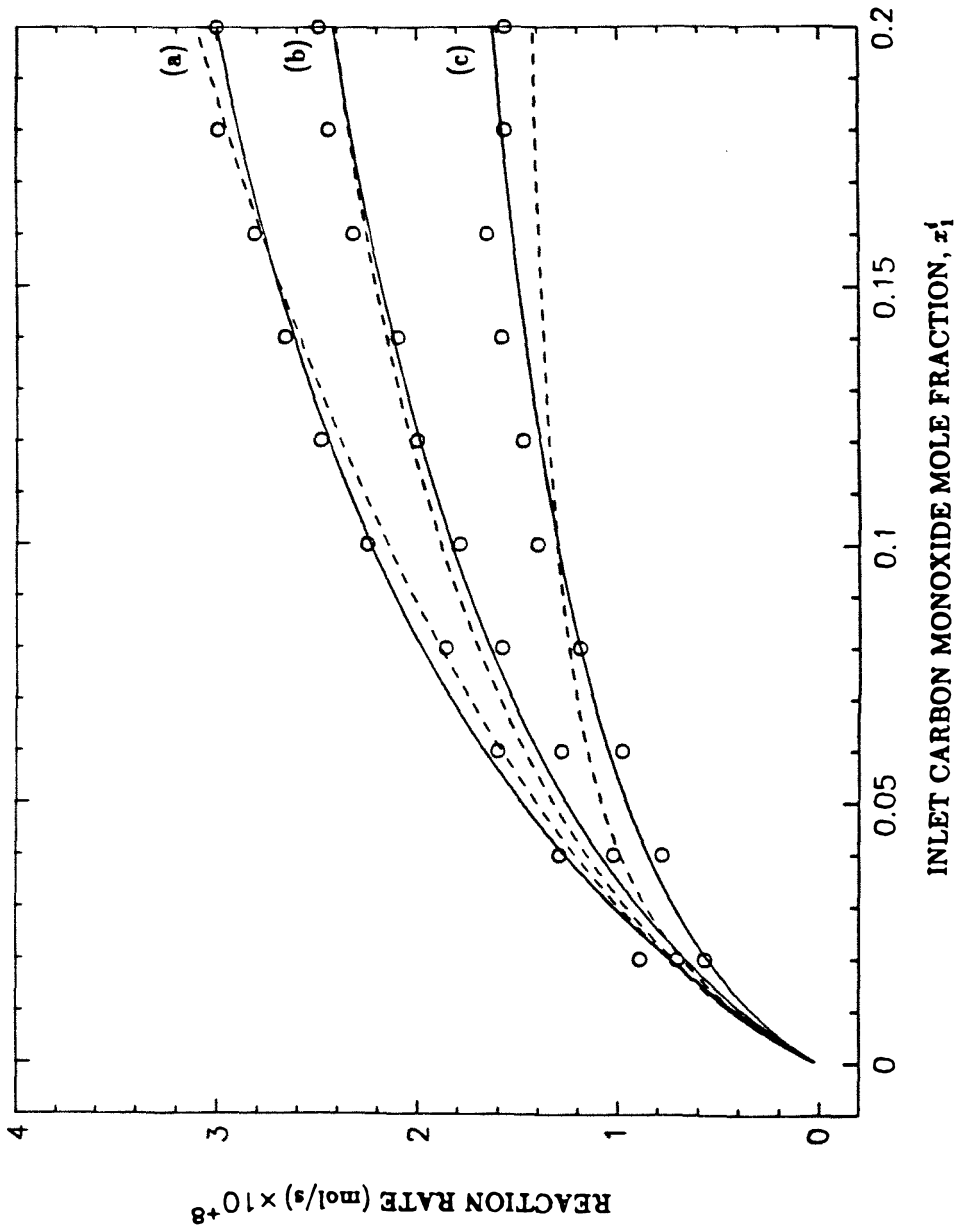


Figure 1

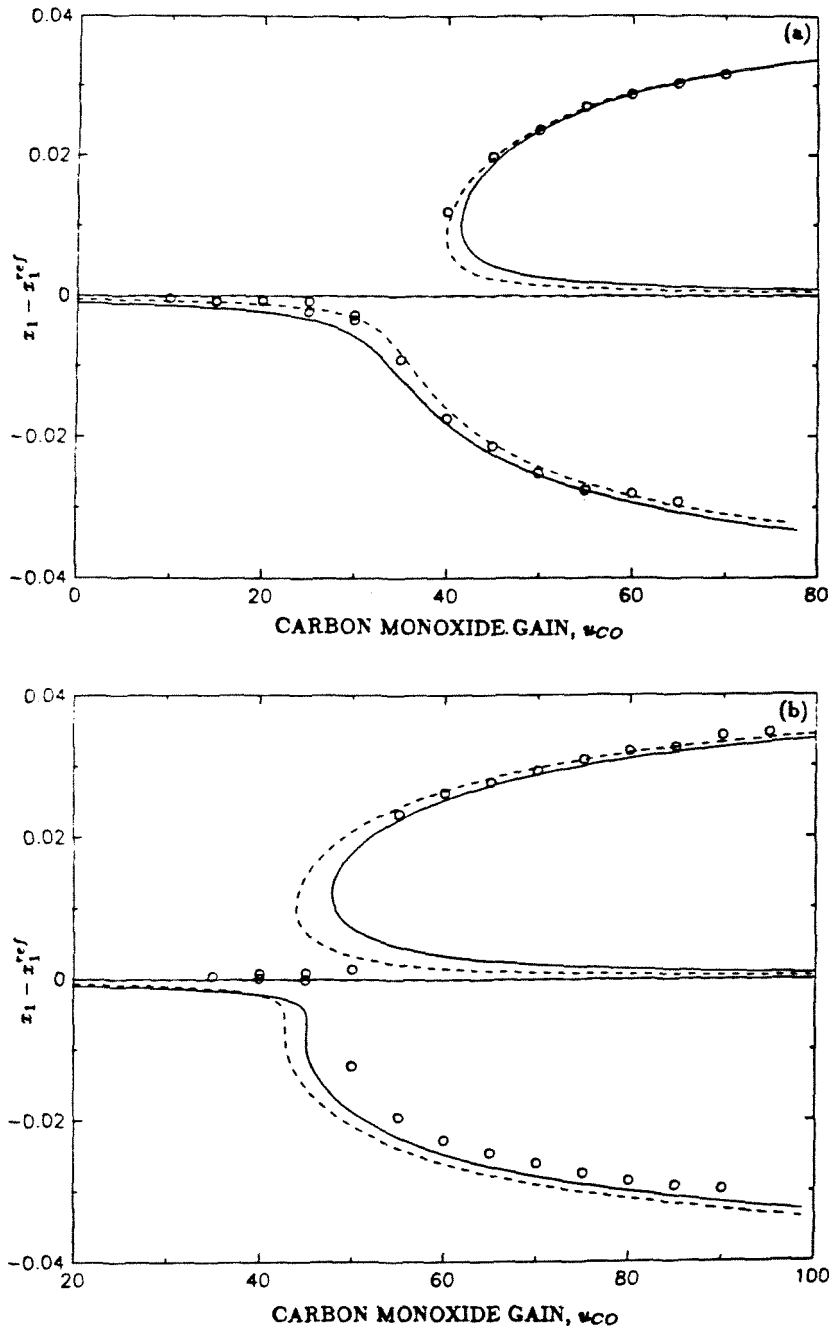


Figure 2

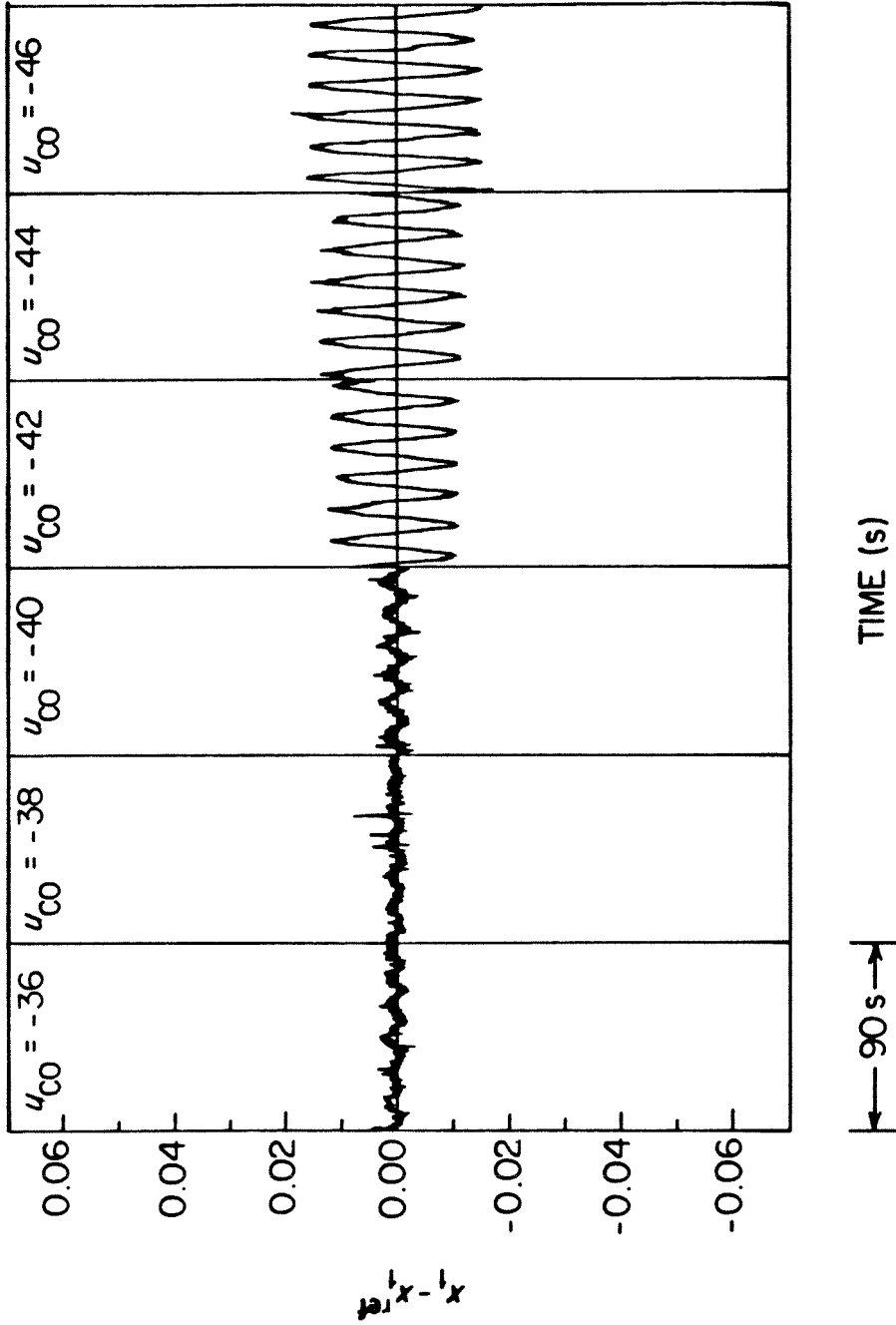


Figure 3

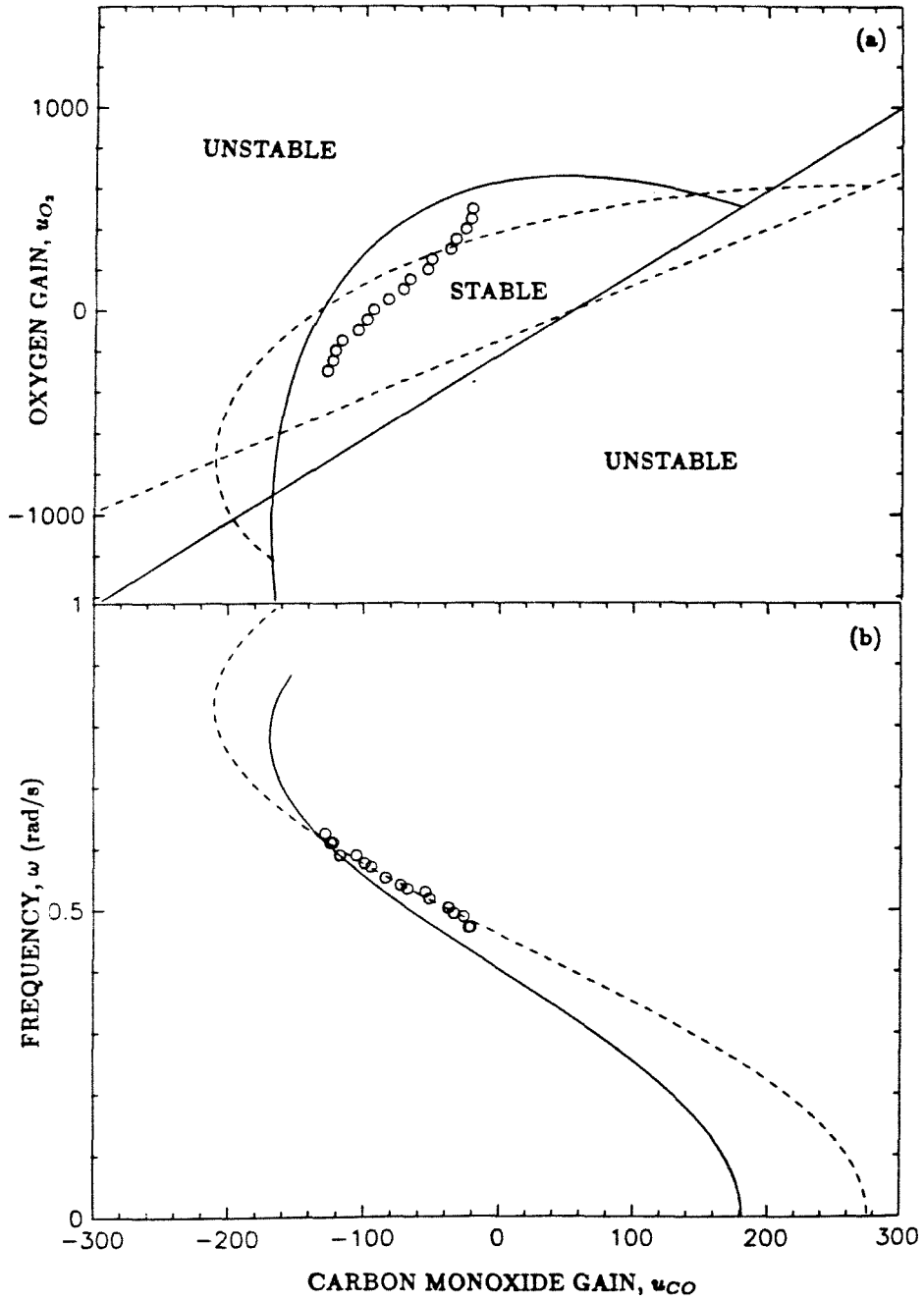


Figure 4

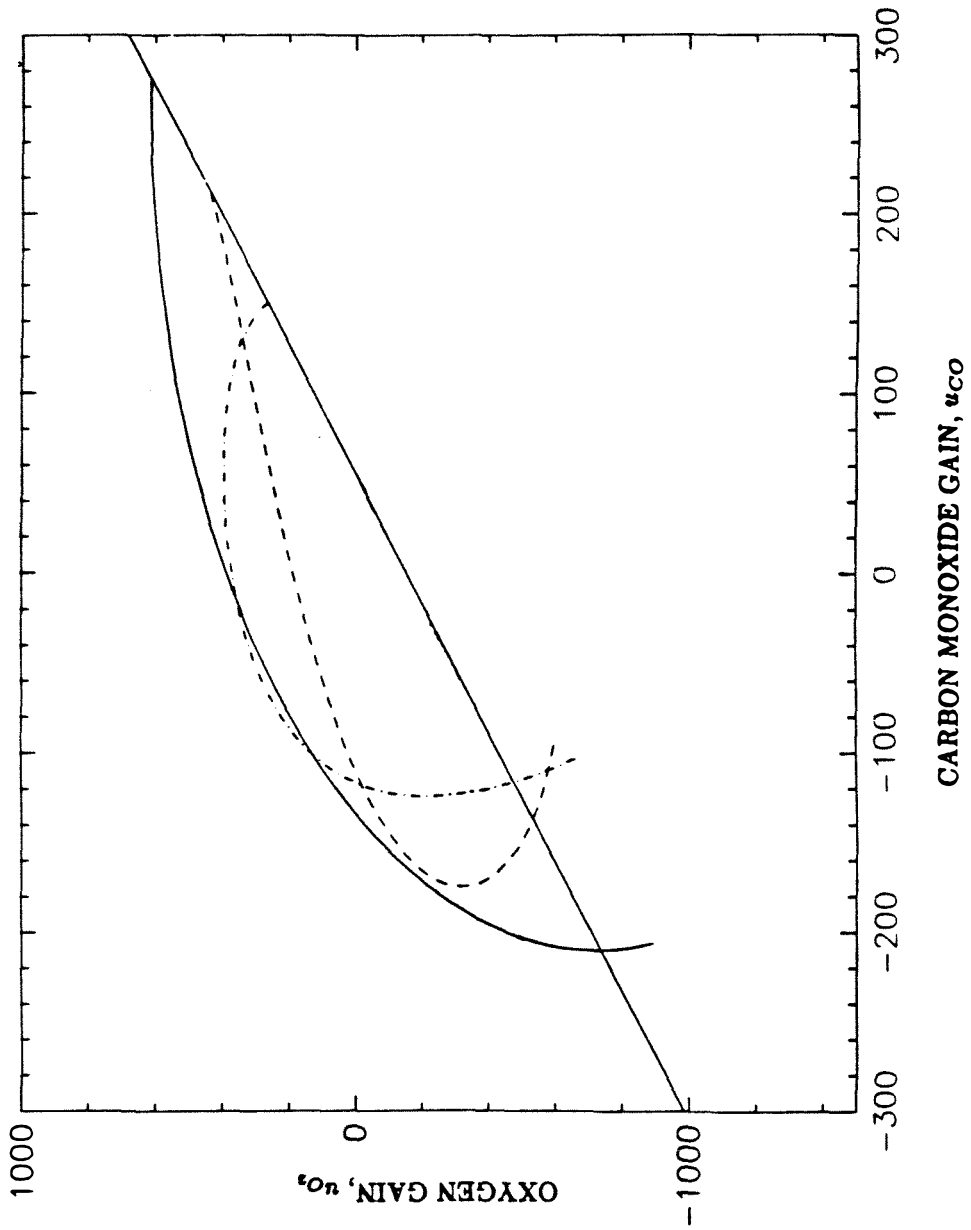


Figure 5

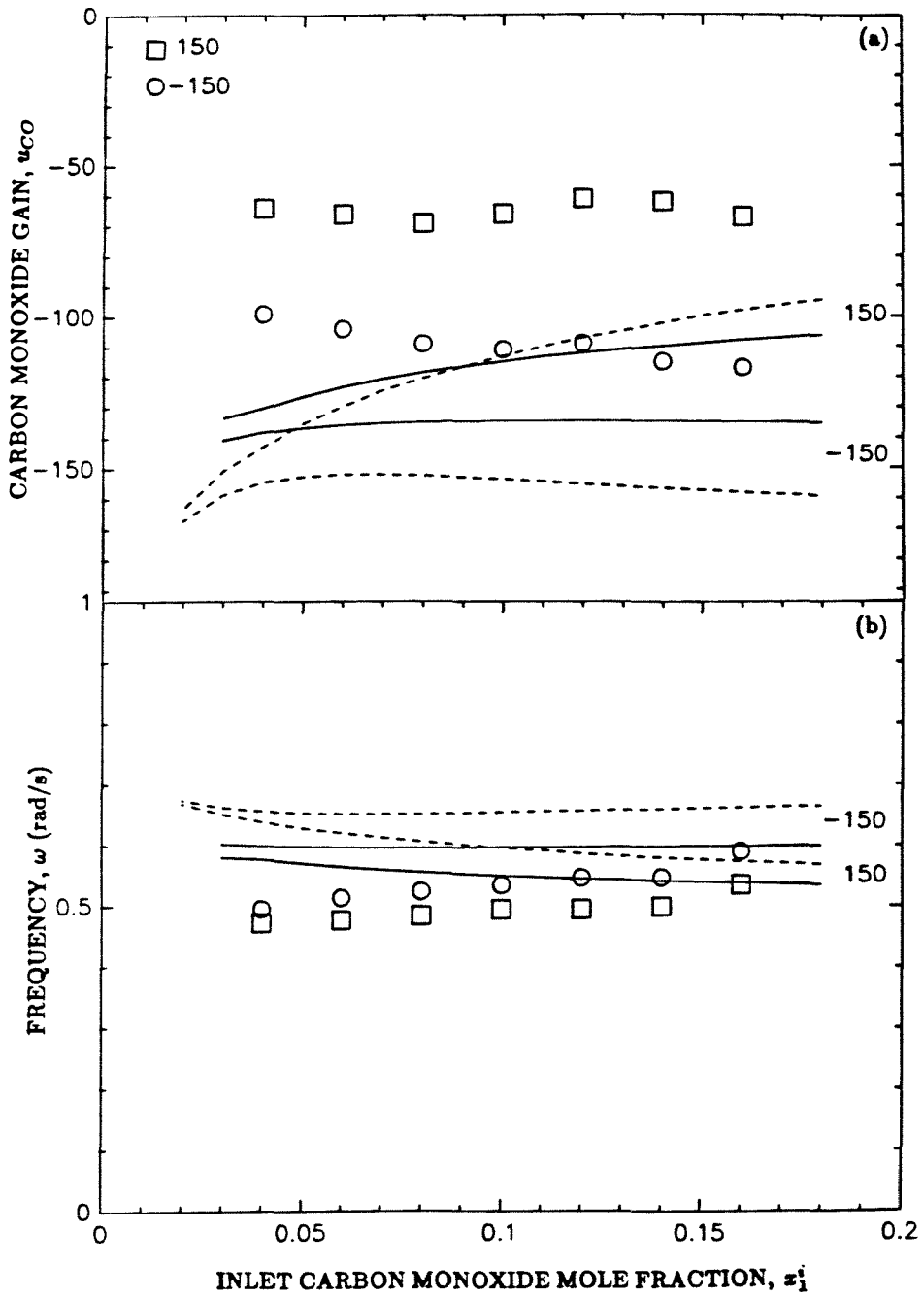


Figure 6

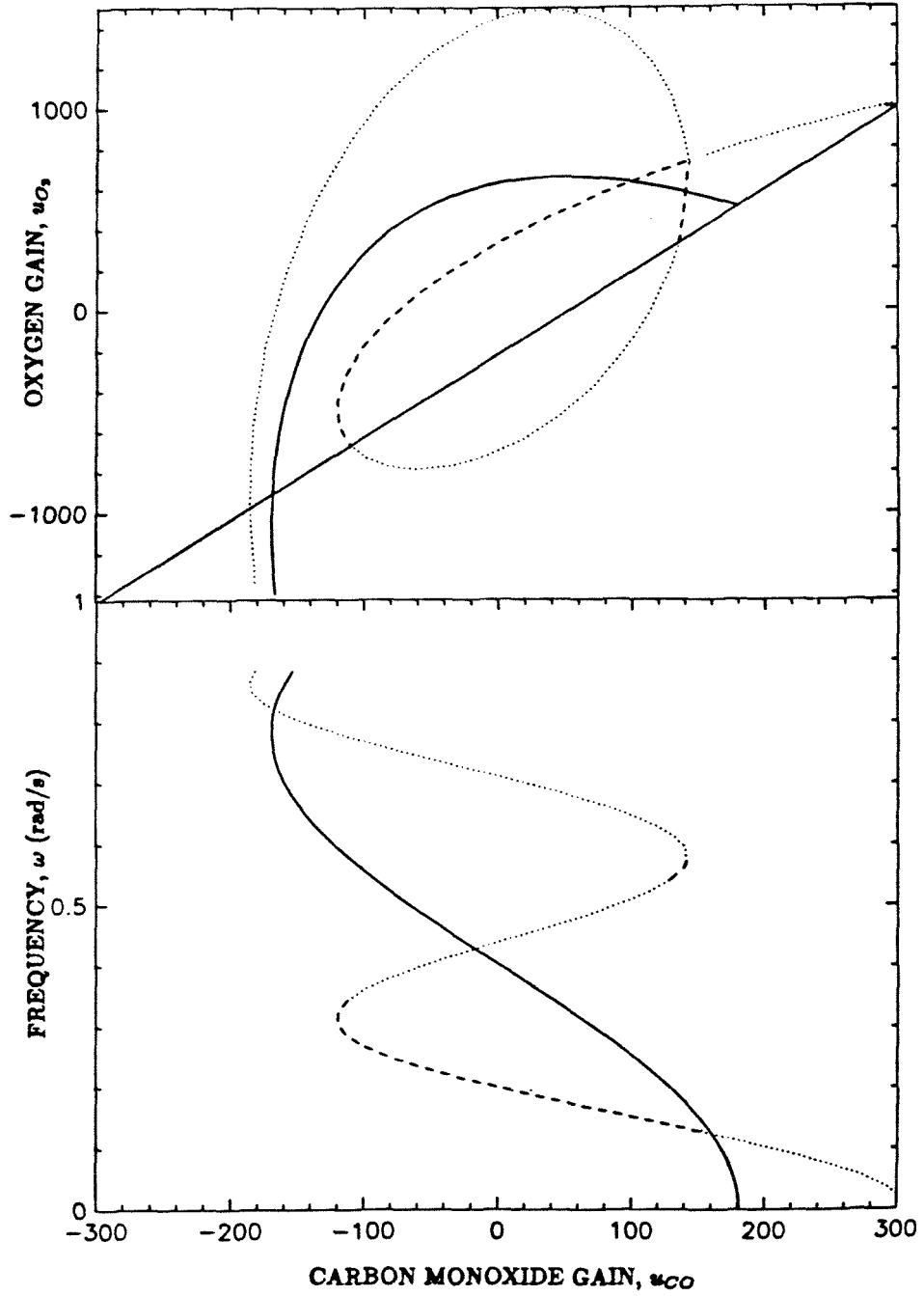


Figure 7

CHAPTER 4

**MODELING OF SLOW DYNAMICS IN THE OXIDATION OF
CARBON MONOXIDE OVER SUPPORTED SILVER**

INTRODUCTION

Silver catalysts have received a large amount of attention because of their ability to selectively catalyze ethylene epoxidation (reviewed by Sachtler, 1970; Verykios *et al.*, 1980; Sachtler *et al.*, 1981). The most elusive aspect of this reaction concerns the form or forms of adsorbed oxygen on the silver catalysts. While the existence of at least two oxygen species on silver is generally accepted, less equanimity has been reported as to the oxygen species that participate in oxidation reactions on silver. Czanderna (1964) has postulated that at temperatures of 0°C to 100°C, lower surface coverages are dominated by a monatomic oxygen form and higher coverages give predominantly a diatomic oxygen species. For higher temperatures (150-250°C), Force and Bell (1975b) suggest that any diatomic oxygen formed on the silver will readily decompose. Several studies suggest that while both diatomic and monatomic oxygen are present on silver and both are active for ethylene adsorption, one form promotes epoxidation and the other complete oxidation to CO₂ and H₂O (Sachtler *et al.*, 1981).

While oxygen adsorption on silver has been studied with a variety of techniques, the oxygen species contributing to the reaction mechanism at reaction conditions are difficult to analyze. Adding to the analysis problems is the relative complexity of the ethylene epoxidation reaction. One approach for reducing the system to a more manageable form is to use carbon monoxide oxidation as the model oxidation system on silver. Keulks and Outlaw (1972) studied CO oxidation over silver in a recirculation reactor operating at 100°C. Oxygen was preadsorbed on the silver catalyst in small quantities to maintain fractional surface coverages of less than 10% of a monolayer, and both CO and CO₂ were found to adsorb. CO and CO₂ did not adsorb without the preadsorption of O₂. Keulks and Outlaw conclude that a monatomic oxygen species is active for CO and CO₂ adsorption. Using the initial stage of adsorption of N₂O and O₂ as sources for monatomic

and diatomic oxygen species, respectively, Kobayashi and Takegami (1984) presented transient data for CO oxidation over alumina-supported silver. Differences in the observed activation energies for the CO-O₂ and CO-N₂O reactions were attributed to different rate-controlling steps. Since diatomic oxygen was assumed to be the active site for CO adsorption, the slower rate for the CO-N₂O reaction relative to the CO-O₂ reaction was postulated to be due to the slow formation of diatomic oxygen from a monatomic oxygen source.

In previous work with the CO oxidation reaction studied at 147°C, Shanks and Bailey (1987) report a slow transient when oxygen is introduced to a reduced silver catalyst. The present study uses transient experiments to examine in more detail the source of the long-time-scale dynamics. Experimental data are compared with simulation results to test the validity of a proposed reaction model for CO oxidation over Ag/Al₂O₃.

EXPERIMENTAL SYSTEM

The catalyst used in the experimental reactor was 2.3 g of 1 wt% silver on 3 mm cylindrical α -Al₂O₃ pellets (Engelhard). A dispersion of 13% for the silver catalyst was determined from oxygen chemisorption experiments based on the method of Seyedmonir *et al.* (1984). In addition to the catalyst, 2 mm glass beads were used to pack the reactor (≈ 10 cm³ total volume). For this packing and for the conditions used in all of the experiments, 100 sccm total flow rate and 147°C, the reactor behaved as an ideal CSTR with a residence time of 4.7 s.

Gas flow rates of helium (99.995%), oxygen (99.5%), hydrogen (99.9995%), and carbon monoxide (99.99%) into the reactor were set and monitored by two banks of identical mass flow controllers (Tylan). A carbonyl trap operating at 500°C was used upstream of the CO mass flow controllers. Also, the CO, O₂, and He inlet lines contained desiccant columns. Computer controlled, high-speed

solenoid valves were used to switch between the two mass flow controller banks. The effluent CO and CO₂ concentrations were measured with two infrared analyzers (Wilkes Miran I) operating at 4.6 μm and 4.2 μm , respectively. Mixing that is due to the IR cells was found to be negligible. More specific details of the experimental apparatus have been presented by Prairie *et al.* (1988).

Pretreatment of the catalyst consisted of introducing 10% oxygen in helium for 2 hours at 250°C and then reducing with 20% hydrogen also at 250°C. The catalyst activity stabilized after approximately 36 hours of exposure to a feed of 10% CO and 10% O₂ at 147°C. By reducing again with 20% hydrogen at 250°C, the unstable catalytic activity could be reproduced, which then required a similar length of time to reach a stable value. Kobayashi (1982a) and Nowobilski *et al.* (1986) also report long initial stabilization transients for their studies of the ethylene epoxidation reaction over silver catalysts. In the work by Nowobilski *et al.*, the long transient was attributed to slow oxidation of the initially reduced silver.

Internal diffusional and external mass transfer effects were found to be negligible for the operating conditions imposed in all of the experiments (Shanks and Bailey, 1987).

REACTION MODEL

Two kinetic models have been postulated previously in the literature for the CO-O₂ reaction on Ag. Keulks and Chang (1970) based their model on isotopic tracer experiments performed at 100°C in a recirculation reactor. The model contains no differentiation between various forms of adsorbed oxygen, but in later work the monatomic oxygen species is regarded as the active site for CO adsorption and reaction (Keulks and Outlaw, 1972). Using transient response experiments in a differential reactor operating at 20°C, Kobayashi (1982b) has postulated a

reaction mechanism in which diatomic oxygen is the reactive adsorbed species. In other work (Shanks and Bailey, 1987), these models were compared with dynamic experiments. Both models provided good descriptions of steady-state rate data but failed to reproduce long transients that resulted when introducing oxygen to a reduced silver catalyst.

An alternative model represented by



was used in the current work. The postulated existence of step (1D), the formation of an inert oxygen species, results from observations in the transient experiments described later. Because of the long transient that was observed during catalyst stabilization, the exact nature of the vacant site, S , is not clear. Temkin (1979) and Sachtler *et al.* (1981) suggest that this site may be silver oxide. If this site is an oxide, then successive oxygen may be adsorbing on top of the surface oxide (Keulks and Outlaw, 1972). Preadsorption of oxygen on silver has been shown in several studies to be a necessary precursor for the adsorption of either CO or CO₂ (e.g., Keulks and Ravi, 1970; Lawson, 1968). Force and Bell (1975a), in transmission IR experiments, have assigned a band to CO₂ that is weakly chemisorbed directly on silver.

The equations representing the model (1A-D) in an isothermal CSTR are

$$n \frac{dx_1}{dt} = F_{CO} - x_1 F_o - k_2 x_1 \theta_1 \quad (1)$$

$$n \frac{dx_2}{dt} = F_{O_2} - x_2 F_o - k_1 x_2 \theta_v^2 \quad (2)$$

$$n \frac{dx_3}{dt} = -x_3 F_o + k_3 \theta_2 - k_{-3} x_3 \theta_v \quad (3)$$

$$n_s \frac{d\theta_1}{dt} = 2k_1 x_2 \theta_v^2 - k_2 x_1 \theta_1 + k_4 \theta_1 - k_{-4} \theta_3 \quad (4)$$

$$n_s \frac{d\theta_2}{dt} = k_2 x_1 \theta_1 - k_3 \theta_2 + k_{-3} x_3 \theta_v \quad (5)$$

$$n_s \frac{d\theta_3}{dt} = k_4 \theta_1 - k_{-4} \theta_3, \quad (6)$$

where x_1 , x_2 , and x_3 are the mole fractions of CO, O₂, and CO₂, respectively, θ_i is the fractional coverage of an adsorbed species, and F_{CO} and F_{O_2} are the inlet molar flow rates of CO and O₂, respectively. The fractional coverages θ_1 , θ_2 , and θ_3 correspond to OS, CO₂S, and OⁱS, respectively, with the fraction of vacant sites, θ_v , given by $1 - \theta_1 - \theta_2 - \theta_3$. Experimental data were taken under isothermal (147°) and isobaric (≈ 1 atm) conditions, so the number of moles of gas in the reactor remains constant. Therefore, the exit molar flow rate, F_o , can always be determined from the equation

$$F_o = F_T - k_1 x_2 \theta_v^2 - k_2 x_1 \theta_1 + k_3 \theta_2 - k_{-3} x_3 \theta_v. \quad (7)$$

Equation (7) can be used to remove F_o from the differential equations (1-3).

Kinetic parameters were determined for the model from an estimation scheme based on steady-state rate data. Here, estimation of the parameters used a finite-difference, Levenberg-Marquardt routine in conjunction with a minimization of the sum of squares objective function based on the difference between the observed and calculated reaction rates. Using various feed compositions of 2-20% CO and 2-20% O₂, 70 steady-state reaction rates were determined. The observed rates were evaluated by monitoring the effluent CO concentration, giving the amount of CO consumed. Accordingly, the simulated reaction rate was calculated using the theoretical consumption rate of CO:

$$r = k_2 x_1 \theta_1. \quad (8)$$

From static experiments, k_4 and k_{-4} cannot be independently evaluated, so only the ratio $K_e = k_4/k_{-4}$ can be estimated from steady-state rate data. The results of the parameter estimation are summarized in Table 1.

Two parameters are left undetermined from this procedure: n_s , the total moles of catalytic active sites in the reactor and k_4 (or k_{-4}). Based on the oxygen chemisorption result, the number of sites available in the CSTR for oxygen chemisorption is 2.92×10^{-5} moles. This number is not necessarily equivalent to n_s , because it was determined on the reduced silver catalyst. At reaction conditions, n_s is probably less than the chemisorption result as evidenced by the loss in activity of the catalyst during the initial stabilization period following the introduction of CO and O₂ to the H₂ treated silver. The value of k_4 and, therefore, k_{-4} (through K_e) must be determined from dynamic experiments.

RESULTS

Transient experiments in which reactant concentrations were changed stepwise were performed while monitoring the effluent concentrations of CO and CO₂. Two characteristic time scales were observed: a rapid response when an oxygen-rich reaction environment was maintained, and a very slow response when stepping from only CO in He to O₂ and CO in He. The slow transient will be discussed later with the results from cycling experiments. The rapid response can be used to estimate a value for n_s . Figure 1 shows the transients in the CO and CO₂ effluent resulting from a step-change of 1% CO, 10% O₂ to 10% CO, 10% O₂. Also shown on this figure are simulated responses of the model for three values of n_s , between 7.5×10^{-6} and 5.0×10^{-5} . The value $n_s = 7.5 \times 10^{-6}$ moles gives the best reproduction of the experimental data. The simulated trajectories were calculated using Gear's method (IMSL routine DGEAR) to simultaneously solve equations (1-6). Because of the assumption of slow exchange for step (1D) of the reaction sequence and the undetermined value of k_4 , the fractional coverage of Oⁱ was taken to be constant at its initial steady-state value during the simulations used in estimating

a value for n_s . The conditions for this step-response experiment were chosen so that the catalyst was always exposed to an oxygen-rich environment.

The slow transient observed when the catalyst was reduced in CO at reaction temperature was characterized, using cycled reactant feed concentration experiments. Figures 2(a) and 3(a) show the experimental effluent CO (top trajectory) and CO₂ (lower trajectory) for symmetric cycling between 10% CO, 10% O₂ and 10% CO for two periods, 60 s and 1800 s, respectively. In both cases, each of the indicated feed streams was introduced into the reactor for one-half of the period. The data were taken after the reactor had reached stable periodic operation. Of particular interest is the rate overshoot in CO₂ production when the O₂ containing feedstream is introduced. This relatively high instantaneous rate, as compared with the steady-state rate for 10% CO, 10% O₂, is not as high a rate as is first observed when a similar feed stream is introduced to the reactor after the 250°C pretreatment in H₂. The slow transient seen during catalyst stabilization following pretreatment cannot be reproduced merely by reduction with CO at 147°C. Therefore, the slow transient seen reversibly under reaction conditions is likely due to a different process than that which occurs during initial stabilization. Also, when the 10% CO portion of the cycle was changed to pure He, no overshoot was observed when the CO, O₂ portion of the cycle was introduced.

Using only k_4 as an adjustable parameter, simulations of the cycling data were performed with the parameters determined from steady-state experiments and the value of n_s found from the step-response experiment. In these calculations, the fractional coverage of Oⁱ was evaluated by integrating Eq. (6). The best fit simulations resulting from minimizing an objective function based on the difference between the observed and calculated CO mole fraction response are shown in Figures 2(b) and 3(b) for periods corresponding to the experimental results in Figures 2(a) and 3(a). A value of $k_4 = 7.5 \times 10^{-8}$ mol/s was found to yield the optimal fit. Figures 2 and 3 show the excellent agreement between model and

data for two widely different periods. Using the estimated value of k_4 , simulation of the step-response experiment used for evaluating n_s gave the same result as was calculated when k_4 was unknown.

A more comprehensive comparison of the experimental data and model is presented in Figure 4, where the time-average reaction rate is shown for various symmetric cycling periods and feed streams of 10% CO, 10% O₂ and 10% CO. The average experimental reaction rate was calculated using the time-average CO effluent mole fraction. In these calculations, the assumption of constant exit molar flow rate was invoked yielding the equation

$$\bar{r} = \frac{F_T(\bar{x}_1^i - \bar{x}_1)}{(1 - 0.5\bar{x}_1)} \quad (9)$$

Because of the low conversion of CO and the high concentration of inert He, the assumption of constant F_o should be reasonable. The time-average reaction rate was calculated for the simulations using

$$\bar{r} = \frac{1}{\tau} \int_0^\tau k_2 x_1 \theta_1 dt, \quad (10)$$

where τ is the cyclic period. Both the experimental and simulated results indicate that as $\tau \rightarrow 0$, relaxed steady-state operation (Bailey and Horn, 1971), the average reaction rate increases. Thullie *et al.* (1986) have shown that Eley-Rideal surface kinetics will, in general, give the largest average reaction rate as the cycling period approaches zero.

The modeled relative rates of formation and consumption of Oⁱ on the surface can be tested with asymmetric cycled feed streams. Here, γ is the fraction of the period in which the feed is 10% CO. During the remainder of the period, $(1 - \gamma)\tau$, the feed contains 10% CO and $5/(1 - \gamma)\%$ O₂, so that the time-average mole fraction of O₂ in the reactant feed stream was 0.05 for all of the experiments. Figures 5 and 6 show a comparison between experiment and simulation for $\gamma = 0.25$ and $\gamma = 0.75$, respectively. The simulation for $\gamma = 0.25$ reproduces the experiment, but the simulation for $\gamma = 0.75$, while agreeing with the qualitative

shape of the experimental trajectories, gives a reduced reaction rate during the oxygen portion of the cycle. Summarized in Figure 7 are simulation and experimental time-average reaction rates for several values of γ . Shown are results for two different cycling periods, $\tau = 60$ s and 1800 s. As illustrated in Figure 7, the greatest disparity between model and experimental results are seen for $\gamma > 0.5$.

DISCUSSION

In agreement with past studies of oxidation reactions on silver, the experimental data presented here indicate the presence of at least two adsorbed oxygen forms on Ag/Al₂O₃ during CO oxidation at 147°C. An apparent inactive or negligibly active oxygen species is formed and consumed on a much slower time scale than is characteristic of the CO-O₂ reaction. While the exact chemical form of this inactive species has not been precisely determined, it is clear that this species can be removed only in a reducing environment and will not desorb at the reaction temperature. The presence of a contaminant in the oxygen feed stream causing the loss of activity seems unlikely because of the purity of the oxygen source and the ability of either CO or H₂ to restore the catalyst activity. These observations are consistent with the formation of an inert adsorbed oxygen species as was proposed in the reaction model.

Neither of the papers postulating reaction sequences for the CO-O₂ reaction over silver, Keulks and Chang (1970) nor Kobayashi (1982b), reports a comparably slow transient under their reaction conditions. There are two possible reasons for this disparity: (1) different reaction temperatures and (2) different experimental schemes. Reaction studies at temperatures comparable to those employed in those two works could not be performed in the present experimental apparatus because the resulting reaction rate was immeasurably small. Keulks and Chang

report data for CO introduced to an O₂ pre-exposed catalyst but not for O₂ introduction following CO reduction. An experiment similar to those presented here was reported by Kobayashi, using a step-change in the reactant feed from 5.5% CO, 94.5% He to 5.5% CO, 19.7% N₂O, 74.8% He. No overshoot was observed in CO₂ production at the reported reaction temperature of 20°C.

The model presented in Equations (1A-D) is similar to the reaction sequence proposed by Kobayashi (1982b) except that a monatomic oxygen species is taken as the active site for CO adsorption but as with the Kobayashi model, only one adsorbed oxygen form is assumed to be active. The vacant site in the proposed model is likely some type of silver oxide, which is not reduced by CO at 147°C but can be reduced at 250°C with H₂. This is corroborated by a comparison of the number of active sites for O₂ adsorption found from the chemisorption experiment and from fitting the experimental step-response data. The uptake of oxygen in the chemisorption experiment, which was performed on the catalyst used in the experimental reactor following the completion of the transient experiments, was more than three times the fitted value. Two characteristic time scales are suggested by the proposed model, one corresponding to the total number of active sites and one associated with the kinetics of the inert oxygen step. Experimental transients exhibited both fast and slow time scale responses attributed to the surface reaction, which could be reproduced by the model.

While the postulated reaction model reproduced a wide range of experimental cycling results, it was not as quantitatively accurate for asymmetric cycling with $\gamma > 0.5$. The difference between the simulated and experimental time-average reaction rates for $\gamma > 0.5$ implies that the activity of the catalyst can be regenerated more rapidly than is given by model simulations. As shown in Figure 6, though, the qualitative features of the CO and CO₂ responses for $\gamma = 0.75$ are reproduced by the simulation. For this large value of γ , any discrepancy between the experimental and simulated time-average reaction rate will be magnified because the

conversion of CO occurs only during 25% of the period.

CONCLUSIONS

The interaction of oxygen with silver is complex. Although oxygen adsorption experiments allow characterization of the possible forms of adsorbed oxygen species, the contribution of the various forms to oxidation kinetics is not clear. This complexity was manifested in long-time scale dynamics observed in the CO oxidation reaction on Ag/Al₂O₃ during step-response experiments. The transients were characterized using cycled feed stream experiments, where the cycle periods were varied for symmetric and asymmetric feed conditions. The overall reaction appeared to precede on two time scales that could be attributed to reactions occurring on the surface. These experiments could be explained with blockage of the active sites occurring because of some type of adsorbed oxygen species. A model was postulated with an inert adsorbed oxygen species that was able to give excellent reproduction of the experimental data.

NOTATION

F	flow rate (mol/s)
k_i	rate parameter (mol/s)
K_e	equilibrium parameter
n	reactor capacity (mol)
n_s	active sites on the catalyst (mol)
r	reaction rate (mol/s)
\bar{r}	time-average reaction rate (mol/s)
t	time (s)
x_i	gas-phase mole fraction
γ	fraction of the period with CO,He feed
τ	cyclic period (s)
θ_i	fractional surface coverage

subscripts

CO	carbon monoxide
o	outlet
O_2	oxygen
T	total

REFERENCES

- Bailey, J.E. and F. Horn, "Improvement of the Performance of a Fixed-Bed Catalytic Reactor by Relaxed Steady State Operation," *AIChE J.*, **17**, 550 (1971).
- Czanderna A.W., "The Adsorption of Oxygen on Silver," *J. Phys. Chem.*, **68**, 2765 (1964).
- Force, E.L. and A.T. Bell, "Infrared Spectra of Adsorbed Species Present During the Oxidation of Ethylene over Silver," *J. Catal.*, **38**, 440 (1975a).
- Force, E.L. and A.T. Bell, "The Relationship of Adsorbed Species Observed by Infrared Spectroscopy to the Mechanism of Ethylene Oxidation over Silver," *J. Catal.*, **40**, 356 (1975b).
- Keulks, G.W. and Chang C.C., "The Kinetics and Mechanism of Carbon Monoxide Oxidation," *J. Phys. Chem.*, **74**, 2590 (1970).
- Keulks, G.W. and J.F. Outlaw, "A Study of the Mechanism of Carbon Monoxide Oxidation over Silver: Interactions Between Carbon Monoxide and Preadsorbed Oxygen," *Proc. 5th Int. Congr. Catal.*, **2**, 959 (1972).
- Keulks, G.W. and A. Ravi, "Infrared Spectroscopic Study of Carbon Monoxide Adsorption on Hydrogen and Oxygen Treated Silver Surfaces," *J. Phys. Chem.*, **74**, 783 (1970).
- Kobayashi, M., "Characterization of the Adsorbed Layer of a Silver Catalyst in the Oxidation of Ethylene from Its Transient Adsorption Behavior," *Catalysis Under Transient Conditions*, ACS Symp. Ser., **178**, 209 (1982a).
- Kobayashi, M., "Rival Kinetic Models in the Oxidation of Carbon Monoxide over a Silver Catalysis by the Transient Response Method," *Chemical Reaction Engineering*, ACS Symp. Ser., **196**, 213 (1982b).
- Kobayashi, M. and H. Takegami, "Heterogeneity of a Silver Surface Used in the Oxidation of Carbon Monoxide," *Faraday Trans. 1*, **80**, 1221 (1984).

- Lawson, A., "Factors Influencing the Compensation Effect during Formic Acid Decomposition on Silver," *J. Catal.*, **11**, 295 (1968).
- Nowobilski, P.J., C. Takoudis, and M. Weaver, "Low Pressure Ethylene Epoxidation over Silver Catalysts," AIChE Annual Meeting, Miami Beach (1986).
- Prairie, M.R., B.H. Shanks, and J.E. Bailey, "Intentional Manipulation of Closed-Loop Time Delay for Model Validation Using Feedback-Induced Bifurcation Experiments," *Chem. Eng. Sci.* in press (1988).
- Sachtler, W.M.H., "The Mechanism of the Catalytic Oxidation of Some Organic Molecules," *Catal. Rev.-Sci. Eng.*, **4**, 27 (1970).
- Sachtler, W.M.H., C. Backx, and R.A. Van Santen, "On the Mechanism of Ethylene Epoxidation," *Catal. Rev.-Sci. Eng.*, **23**, 127 (1981).
- Seyedmonir, S.R., D.E. Strohmayer, G.L. Geoffroy, and M.A. Vannice, "Characterization of Supported Silver Catalysts II. Adsorption Studies of Well-Dispersed Ag on η -Al₂O₃," *Adsorp. Sci. Tech.*, **1**, 253 (1984).
- Shanks, B.H. and J.E. Bailey, "Experimental Investigations using Feedback-Induced Bifurcation: Carbon Monoxide Oxidation over Supported Silver," *Chem. Eng. Commun.*, **61**, 127 (1987).
- Thullie, J., L. Chiao, and R.G. Rinker, "Analysis of Concentration Forcing in Heterogeneous Catalysis," *Chem. Eng. Commun.*, **48**, 191 (1986).
- Temkin, M.I., "The Kinetics of Some Industrial Heterogeneous Catalytic Reactions," *Advan. Catal.*, **28**, 173 (1979).
- Verykios, X.E., F.P. Stein, and R.W. Coughlin, "Oxidation of Ethylene over Silver: Adsorption, Kinetics, Catalyst," *Catal. Rev.-Sci. Eng.*, **22**, 197 (1980).

TABLE 1: Parameters estimated from steady-state data.

k_1 (mol/s)	2.05×10^{-4}
k_2 (mol/s)	1.68×10^{-3}
k_3 (mol/s)	4.42×10^{-7}
k_{-3} (mol/s)	1.85×10^{-10}
K_e	9.74

FIGURE CAPTIONS

- Figure 1: Effluent trajectories of CO and CO₂ for a step-change of 1% CO, 10% O₂ to 10% CO, 10% O₂. Simulation results for $n_s = 7.5 \times 10^{-6}$ (solid), 3.0×10^{-5} (dashed), and 5.0×10^{-5} (dash-dot).
- Figure 2: Trajectories for symmetric cycling of 10% CO to 10% CO, 10% O₂ with $\tau = 60$ s; (a) experimental, (b) simulation.
- Figure 3: Trajectories for symmetric cycling of 10% CO to 10% CO, 10% O₂ with $\tau = 3600$ s; (a) experimental, (b) simulation.
- Figure 4: Time-average reaction rate experimental data points and simulations for different cycling periods using 10% CO to 10% CO, 10% O₂.
- Figure 5: Trajectories for asymmetric cycling with $\tau = 1800$ s, $\gamma = 0.25$; (a) experimental, (b) simulation.
- Figure 6: Trajectories for asymmetric cycling with $\tau = 1800$ s, $\gamma = 0.75$; (a) experimental, (b) simulation.
- Figure 7: Effect of γ on the time-average reaction rate for $\tau = 60$ s; experimental (circles), simulation (solid) and $\tau = 1800$ s; experimental (squares), simulation (dashed).

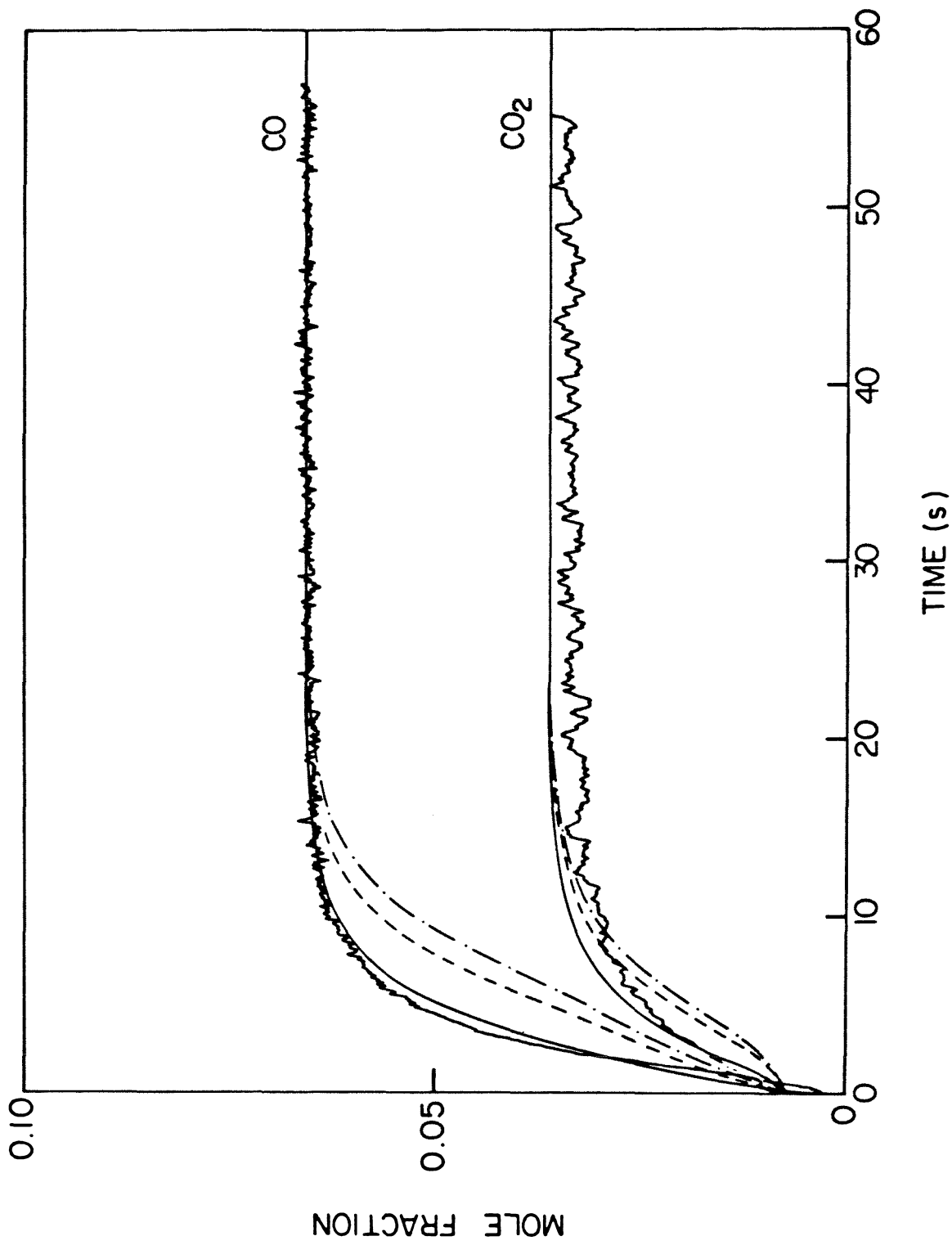


Figure 1

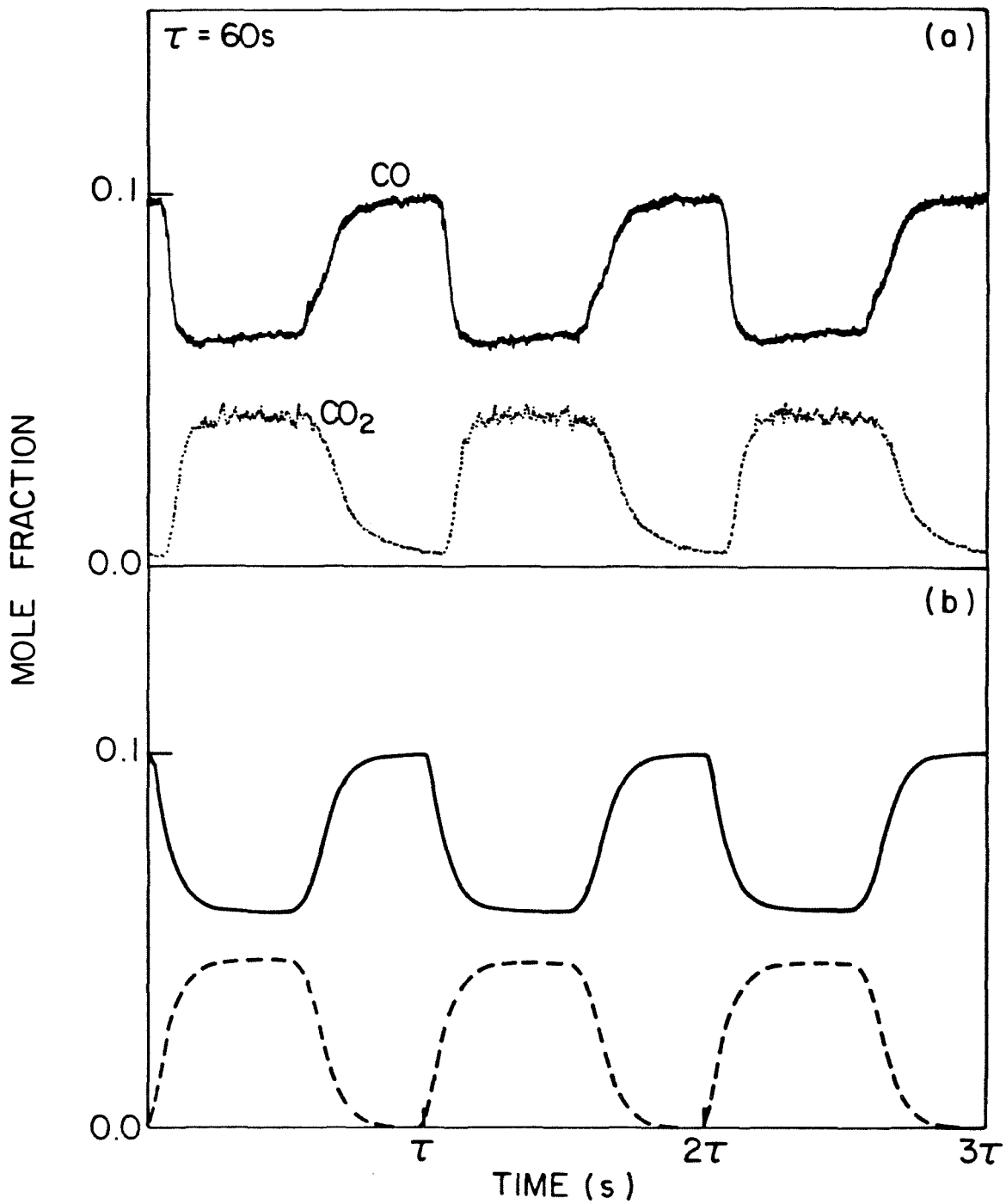


Figure 2

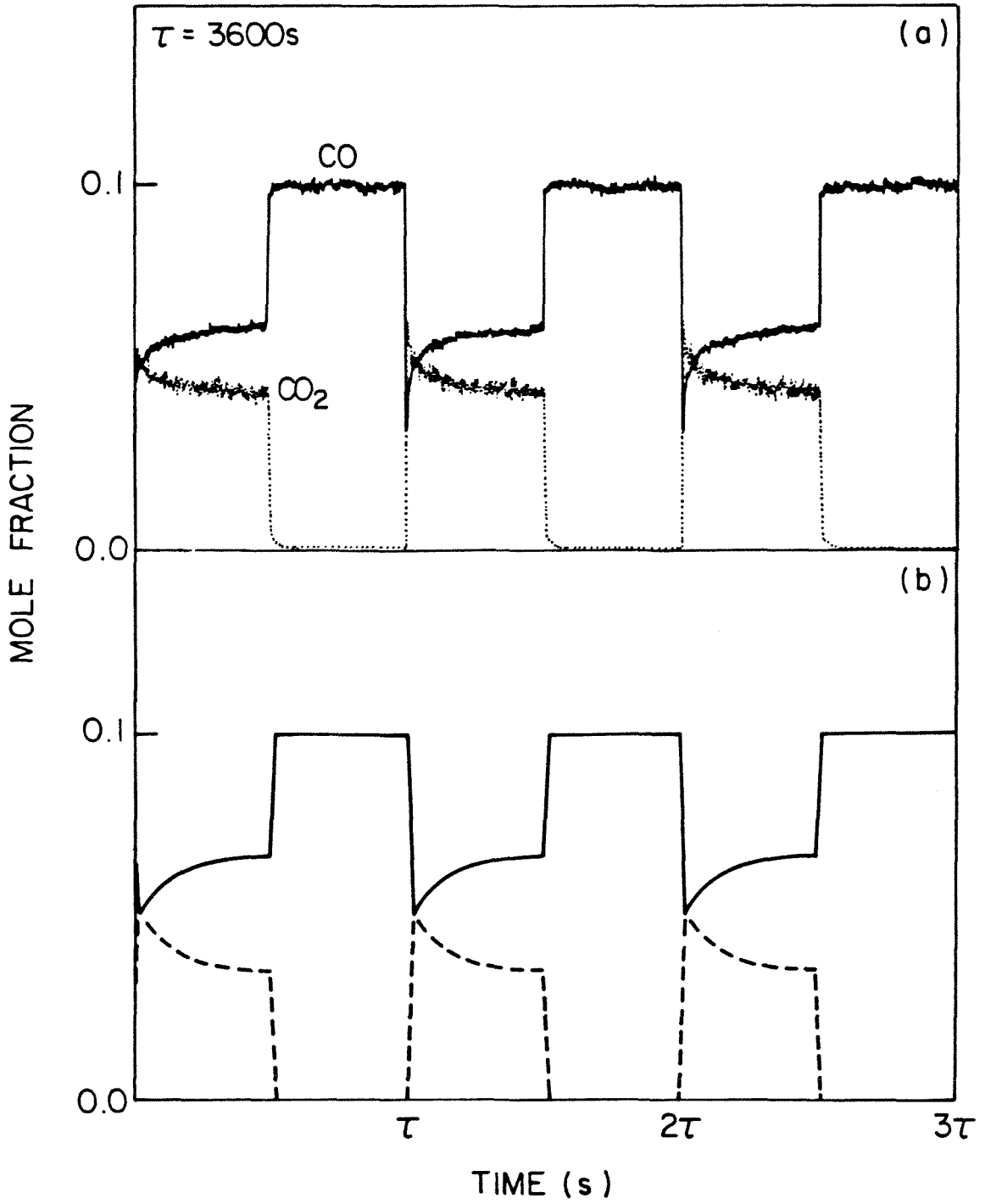


Figure 3

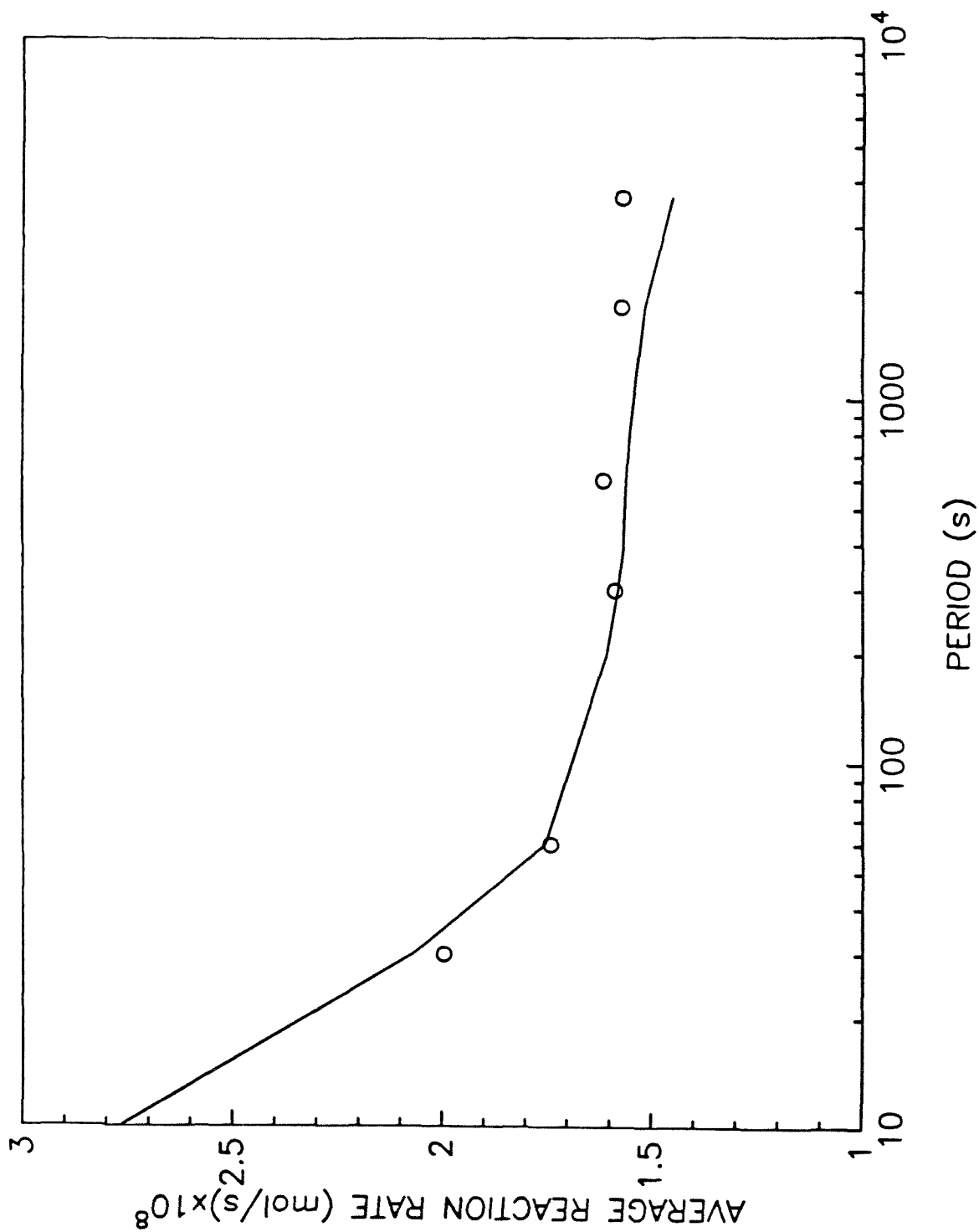


Figure 4

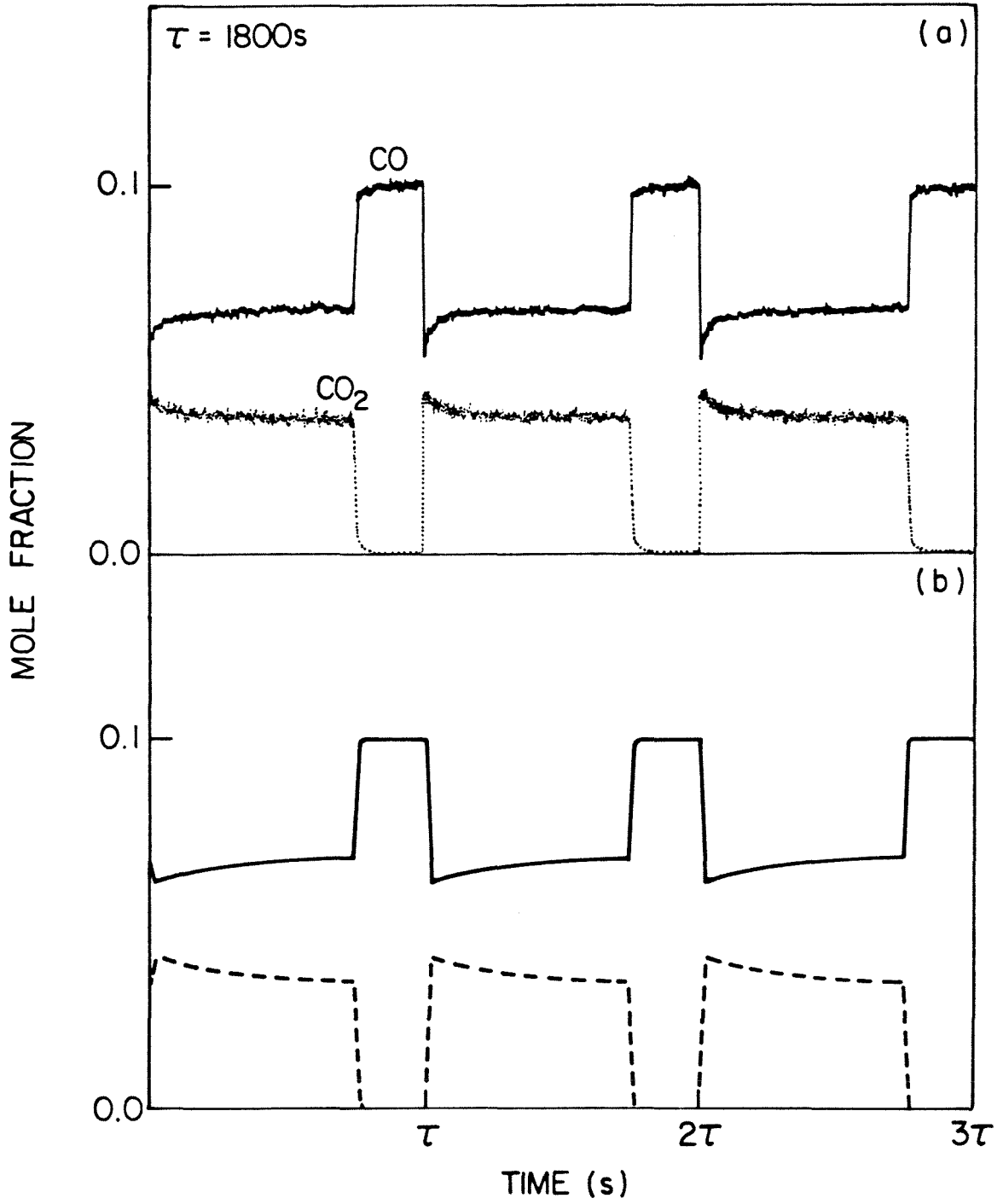


Figure 5

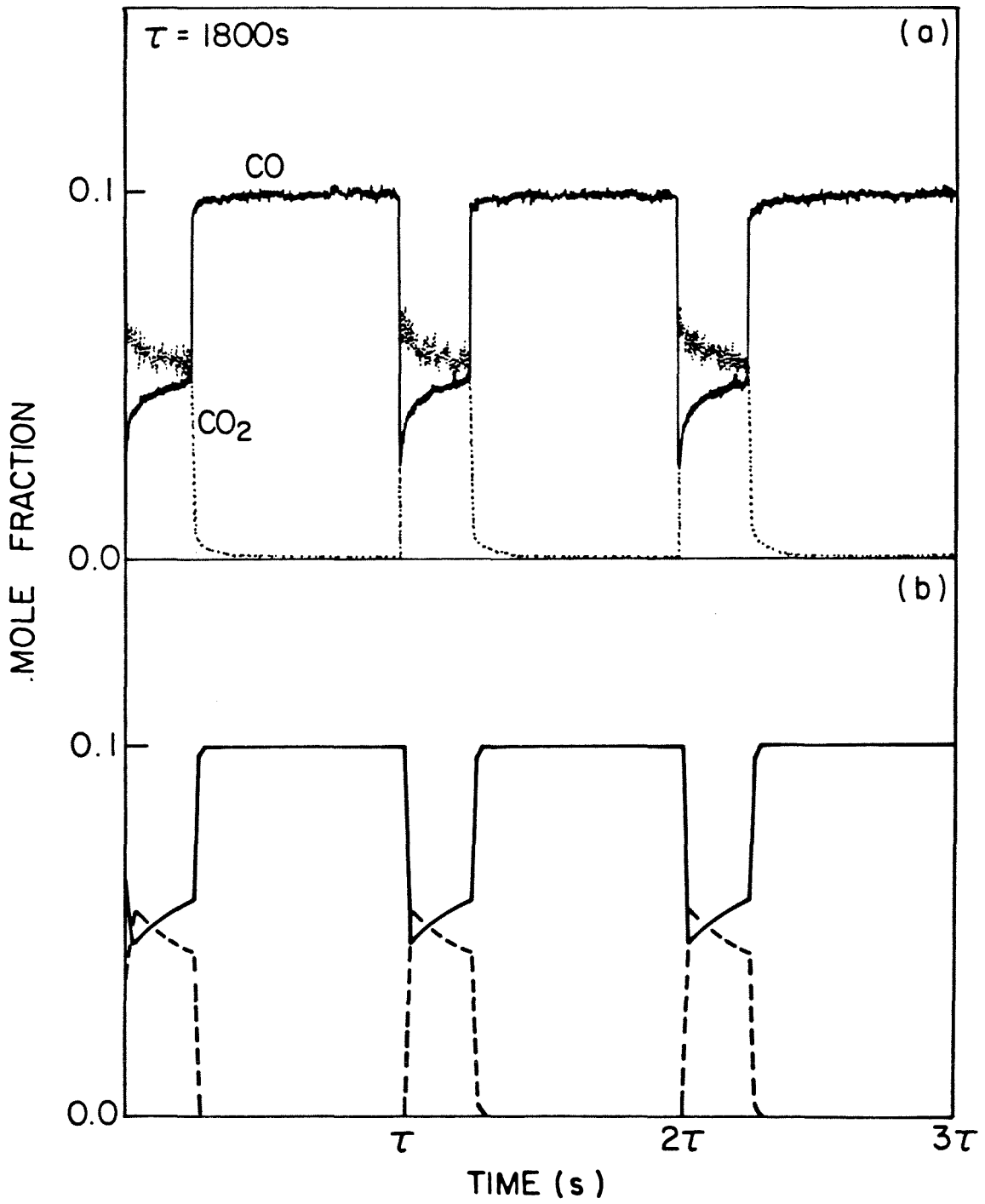


Figure 6

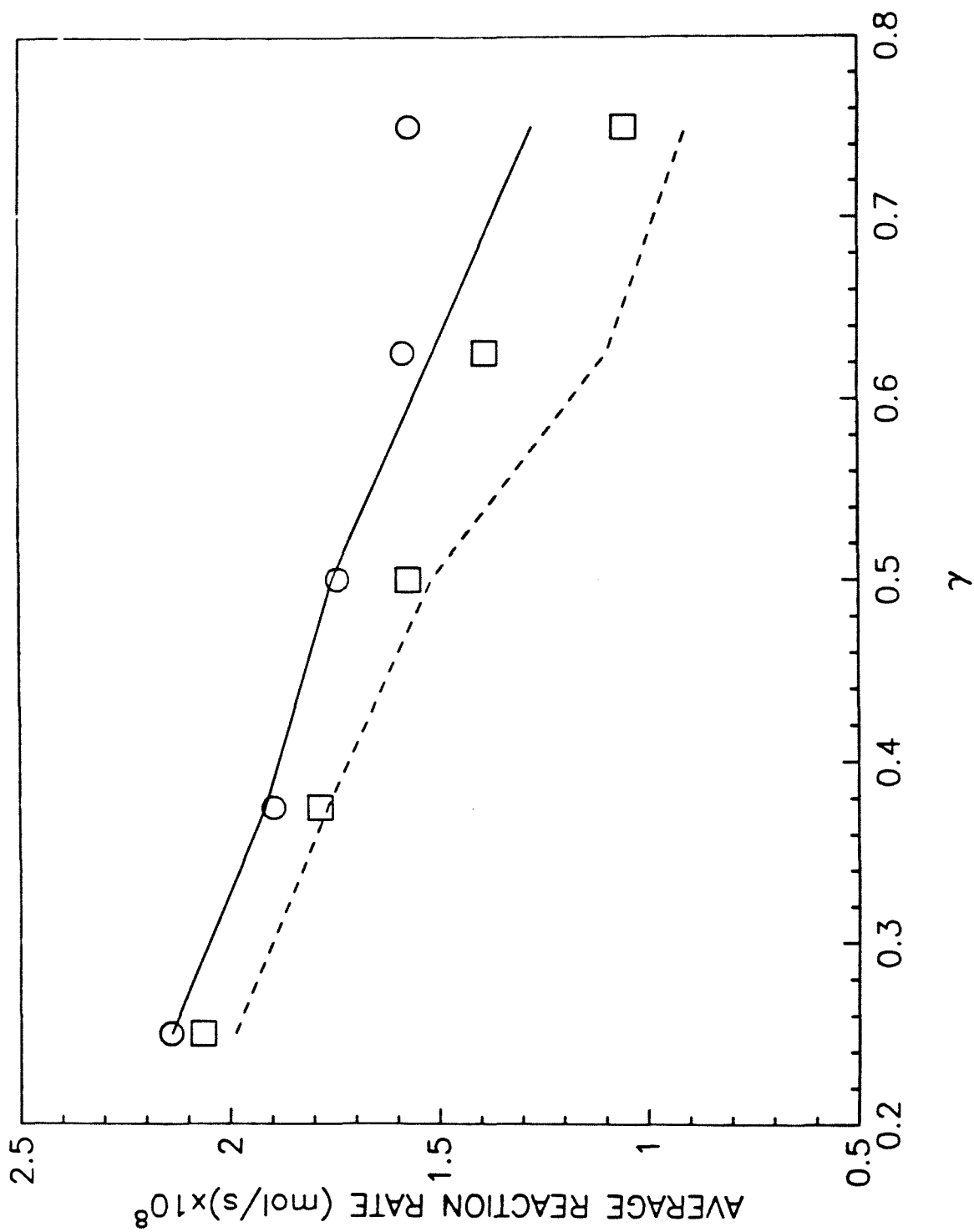


Figure 7

CHAPTER 5

APPLICATION OF THE FEEDBACK-INDUCED BIFURCATION

METHOD TO A CATALYTIC REACTION SYSTEM

INTRODUCTION

The use of feedback-induced bifurcations for nonlinear model evaluation and comparison was first introduced by Kuszta and Bailey (1982). The method is predicated on the availability of salient nonlinear model information exclusively when a system is close to bifurcation. Since most systems generally do not bifurcate autonomously at normal operating conditions, bifurcation information is frequently inaccessible for systems in conventional open-loop configuration. By introducing feedback control, a process can be systematically destabilized to obtain bifurcation information. This generalizes the type of systems that can employ bifurcation information for parameter estimation and model discrimination.

McDermott *et al.* (1985) used controller-induced bifurcations as well as steady-state and oscillation time trajectory data to estimate parameters in a dynamic model for a fixed-bed autothermal reactor. The reactor supported the water-gas shift reaction, the kinetics of which had been determined in previous experiments, so the bifurcation data were used to characterize the experimental apparatus. Feedback-stimulated instabilities were used by Prairie and Bailey (1986,1987) to estimate parameters in the ethylene hydrogenation reaction on supported Pt. There, the primary focus was to use the integration of bifurcation experiments with steady-state and transient experiments to estimate kinetic parameters in a well-characterized experimental system. An alternative application of the feedback-induced bifurcation method to heterogeneous catalytic reactions was examined in a simulation study by Lyberatos *et al.* (1984). Two models for the catalytic decomposition of N_2O that were indiscriminate in step-response simulations were found to yield quite different bifurcation behavior under feedback control. Shanks and Bailey (1987) found that two previously postulated reaction sequences for carbon monoxide oxidation on silver gave different closed-loop stability behavior, even in the presence of experimental time delay, which drastically

alters system stability. The two models were able to reproduce equally proficiently steady-state rate and feedback-induced steady-state bifurcation data, but both models failed to reproduce the experimental Hopf bifurcation data. The source of the breakdown of the models, *e.g.*, an incorrect reaction model, an inaccurate system model, or an inherent experimental problem, was not resolved.

The present work seeks to examine more critically the utility of applying the feedback-induced bifurcation method in the experimental study of heterogeneous catalytic reactions. A well studied reaction, CO oxidation on a supported Rh catalyst, is chosen as the model reaction, because the focus here is the experimental method rather than the reaction itself. Model parameters are primarily estimated independently from the bifurcation experiments. As in previous feedback-induced bifurcation work, the measurement of an effluent species is used in the control algorithm. However, by incorporating a reactor cell that can be used in conjunction with a transmission infrared detector, the measurement of a reaction intermediate is also used for feedback control. Finally, the usefulness of feedback-stimulated bifurcations to higher order instabilities is examined for discrimination between rival models.

EXPERIMENTAL SYSTEM

A reactor based on the reactor cell described by Oh and Hegedus (1982) was used in the experiments. The cell is constructed from two 4.4 cm dia. nonrotatable blank Conflat flanges supporting 20 mm dia. CaF₂ windows, which are mounted in the cell with silicon o-rings and threaded nuts. A stainless steel disc, suspended between the two flanges, is used to hold the catalyst wafer. The temperature in the reactor is measured with an exposed-tip thermocouple that has been bent to within approximately 0.1 mm of the catalyst surface. A variable transformer was

used to supply constant power to a heating element that was wrapped around the reactor cell. The experiments were performed at 160°C.

The gas handling system is described by Prairie *et al.* (1988). High purity gases, helium (99.995%), carbon monoxide (99.99%), oxygen (99.5%), and hydrogen (99.995%) are used with desiccant columns on the He and O₂ feed lines. A range of 0–20 sccm is possible with the CO, O₂, and H₂ mass flow controllers and 0–200 sccm with the He mass flow controllers. The accuracy of the mass flow controllers is ±2%. A total flow rate of 100 sccm was maintained in all of the experiments. The effluent concentration of CO was measured with a Wilkes Miran I infrared analyzer operating at 4.6 μm. Set-point control of the mass flow controllers and data acquisition were implemented with a HP9825 minicomputer.

A modified Beckman IR–8 infrared spectrophotometer was used to obtain the single-beam transmission infrared spectra of the catalyst surface. The modification consists of incorporating a HgCdTe detector (Santa Barbara Research, Model 40742), a high-speed chopper (Laser Precision, Model CTX–534), and a lock-in amplifier (Princeton Applied Research) into the spectrophotometer. By using the HgCdTe detector, the transmittance through the reactor cell can be monitored at a higher rate than is possible with a thermopile detector. Electronic smoothing of transmittance transients when operating with the high-speed detector are limited primarily to a 30 ms lock-in prefilter and a 0.1 s postfilter. Because of the small time constants associated with the electronic filters, dynamic effects that are due to electronic smoothing in the measurement of the transmittance are neglected in the model for the experimental apparatus. A monochromator slit width of 0.2 mm and a chopping speed of 400 Hz were used for all of the transmission IR spectra measurements.

The aqueous incipient wetness technique was used to prepare 5% Rh/Al₂O₃ catalyst from RhCl₃ and Alon fumed alumina. Following overnight drying, the catalyst powder was calcined at 500°C for five hours in flowing air. A catalyst

wafer, 44 mg and 0.012cm thick, was made by pressing the calcined powder at 500 psi in a 20 mm diameter die. Prior to mounting in the reactor cell, the wafer was reduced with 20% H₂ in He at 500°C for 3 hours. After cooling to room temperature in flowing He, the wafer was loaded into the cell and exposed *in situ* to 20% H₂ in He for 1 hour at 175°C. The reactor was then cooled to 160°C, where a baseline spectrum for the catalyst was obtained.

MODEL DEVELOPMENT

Oh *et al.* (1986) have postulated a reaction sequence for the CO–O₂ reaction over Rh, which has been shown to reproduce steady–state rate data from experiments with alumina–supported Rh catalysts as well as single crystal Rh(111). The sequence is given by



where S is a Rh surface site.

Reaction Model

The reactor used in the current work is similar to the reactor used by Kaul *et al.* (1987) to study CO oxidation on Pt/SiO₂. Therefore, the differential equations describing the reaction dynamics can be derived in an analogous manner to that employed by Kaul *et al.* Important assumptions in the model development are a well mixed gas phase and a negligible concentration gradient in the catalyst wafer. The equations describing the postulated reaction sequence in this reactor under isothermal operation and the imposed assumptions are

$$n \frac{dx_{g1}}{dt} = F_{CO} - x_{g1}F_o - A_s c_T k_g (x_{g1} - x_{c1}) \quad (4)$$

$$n \frac{dx_{g2}}{dt} = F_{O_2} - x_{g2}F_o - A_s c_T k_g (x_{g2} - x_{c2}) \quad (5)$$

$$n \frac{dx_{g3}}{dt} = -x_{g3}F_o - A_s c_T k_g (x_{g3} - x_{c3}) \quad (6)$$

$$\epsilon_s c_T \frac{dx_{c1}}{dt} = \frac{k_g c_T}{L} (x_{g1} - x_{c1}) - n_s (k_1 x_{c1} \theta_v - k_{-1} \theta_1) \quad (7)$$

$$\epsilon_s c_T \frac{dx_{c2}}{dt} = \frac{k_g c_T}{L} (x_{g2} - x_{c2}) - n_s k_2 x_{c2} \theta_v \quad (8)$$

$$\epsilon_s c_T \frac{dx_{c3}}{dt} = \frac{k_g c_T}{L} (x_{g3} - x_{c3}) + n_s k_3 \theta_1 \theta_2 \quad (9)$$

$$\frac{d\theta_1}{dt} = k_1 x_{c1} \theta_v - k_{-1} \theta_1 - k_3 \theta_1 \theta_2 \quad (10)$$

$$\frac{d\theta_2}{dt} = 2k_2 x_{c2} \theta_v - k_3 \theta_1 \theta_2, \quad (11)$$

where x_{g1} , x_{g2} , and x_{g3} are the mole fractions of CO, O₂, and CO₂, respectively, in the bulk gas phase; x_{c1} , x_{c2} , and x_{c3} are the mole fractions of CO, O₂, and CO₂, respectively, in the catalyst; and θ_1 and θ_2 are the fractional coverages of adsorbed CO and O, respectively. The Rh adsorption sites are assumed to be the same for CO and O, so the fraction of vacant sites, θ_v , is given by $1 - \theta_1 - \theta_2$. The effluent molar flow rate, F_o , can be related to the inlet molar flow rate, F_T , by the expression

$$F_o = F_T - A_s c_T k_g \sum_{i=1}^3 (x_{gi} - x_{ci}), \quad (12)$$

because the reactor is operated at constant temperature (160°C) and pressure (≈ 1 atm). Equation (12) can be substituted into Equations (4-6).

Estimation of Model Parameters

Steady-state rate experiments were performed to estimate the values of the rate parameters, k_i , and the mass transfer coefficient, k_g . Using inlet concentrations of 6-18% CO and 2-11% O₂, 50 different steady-state reaction rate measurements were obtained. The data were collected after 15 minutes of operation

at a given feed condition, which was sufficiently long to ensure a steady-state condition as measured by the effluent IR and reactor thermocouple. The rate of CO consumption was determined experimentally by monitoring the effluent mole fraction of CO. A temperature difference of $\pm 3^\circ\text{C}$ around the base 160°C temperature was observed between the high rates of reaction and the low rates. This effect probably contributed to scatter in the experimental data but was mitigated in the parameter estimation by fitting the models to a large number of steady-state rate measurements.

The theoretical steady-state rate of consumption for CO from the model is equivalent to

$$r = k_3\theta_1\theta_2. \quad (13)$$

The parameters were estimated by a minimization of the sum of squares of the difference between the experimental and theoretical consumption rates of CO. Since only the effluent mole fractions of CO, O₂, and CO₂ can be determined experimentally, the nonlinear, least-squares estimation requires simultaneous solution with Equations (7–11). A finite difference, Levenberg–Marquardt routine (IMSL routine ZXSSQ) was used in the estimation scheme. Summarized in Table 1 as Model A are the estimates of the rate parameters and of the mass transfer coefficient as were determined by allowing all five parameters to vary in the estimation algorithm. The parameter set listed for Model B are the rate parameters associated with the limit of no external mass transfer resistance ($k_g \rightarrow \infty$). The correlation coefficients for both of these models relative to all of the steady-state experimental rate data are quite similar.

With the exception of n_s , which will be discussed later, the values of the remaining model parameters were determined independently. A_s , L , and ϵ_s are physical properties of the catalyst and have been measured to be 6.28 cm^2 , 0.012 cm , and 0.78 , respectively. Since the temperature and pressure are known and constant, c_T can be calculated as $2.78 \times 10^{-5}\text{ mol/cm}^3$, assuming applicability of

the ideal gas law . The reactor operating at 160°C and an inlet flow rate of 100 sccm was found to yield an ideal CSTR response to a step-change in the inlet CO concentration with a time constant, τ , of 3.15 s. Using the relation $n = \tau F_T$, the value of n was computed.

Adsorbed CO Calibration

The transmission IR spectrophotometer was modified to include a high-speed detector so that transients in the adsorbed CO coverage on the catalyst surface can be monitored with rapid time resolution. This approach necessitates measuring the transmittance at only a single wavenumber during transient operation. Therefore, the fractional coverage of CO must be related to the transmittance at a specific wavenumber. Previous studies of CO adsorption on Rh (*e.g.*, Yang and Garland, 1957; Yates *et al.*, 1979) have identified three predominant adsorbed CO species: a linear CO form, a dicarbonyl form, and a bridged CO form. Clearly, a single wavenumber measurement would not be sufficient for characterizing the fractional coverage of CO when all three of these species are present. Rice *et al.* (1981) postulate that only the linear and bridged forms of adsorbed CO correspond to Rh in a zero oxidation state, while the dicarbonyl form is associated with Rh in a +1 oxidation state. High temperature reduction was employed in the current work in order to reduce the Rh completely.

Figure 1(a) shows the spectrum resulting after introducing 14% CO in He to the reduced catalyst at 160°C. The spectrum has been corrected for the baseline absorbance. Primarily, a single absorbance band at 2083 cm^{-1} is observed, which corresponds to CO adsorbed in a linear form. The small absorbance bands at higher wavenumbers are due to gas-phase CO. No absorbance band was resolved in the 1840–1880 cm^{-1} range that could be attributed to adsorption of CO in the bridged form. The absorbance bands for wavenumbers greater than 2100 cm^{-1} are due to the gas phase CO. Spectra (b) and (c) in Figure 1 result from feeds

of 5% O₂, 14% CO and 7% O₂, 14% CO, respectively. As the fractional coverage of CO decreases, the peak of the absorbance band shifts to lower wavenumbers, so the wavenumber chosen for monitoring transients in the CO coverage cannot always correspond to the wavenumber of maximum absorbance.

Calibration of the fractional coverage of CO with transmittance was performed at 2072 cm⁻¹. The steady-state transmittance at 2072 cm⁻¹ was determined for a feeds of 14% CO with 10 different concentrations of O₂, ranging from 3.5–8%. The fractional coverage of CO associated with the experimental transmittance was calculated from the steady-state model, using the same feed conditions. Shown in Figure 2 is the relationship between the transmittance at 2072 cm⁻¹ and the fractional coverage of CO determined from Model A. Also shown on this figure is the calibration curve resulting from a nonlinear regression fit to the data. The calibration curve is given by

$$T_{CO} = 0.419 - 0.282\theta_1 + 0.233\theta_1^2 - 0.593\theta_1^3, \quad (14)$$

where T_{CO} is the transmittance. Because this calibration scheme is model specific, each parameter set used has a corresponding calibration curve.

BIFURCATION RESULTS

Bifurcations from a stable reference steady state are induced in the reaction system by applying feedback control to the open-loop process. The reference steady state is established with fixed inlet flow rates of the reactants. Subsequently, an arctangent control function is superimposed on the inlet reactant flow rates. The control algorithms for the inlet flow rates have the general form

$$F_{CO} = F_{CO}^{ref} + \sum_{i=1}^8 \frac{2w_i}{\pi} \text{Tan}^{-1}[u_{CO_i}(x_i - x_i^{ref})] \quad (15)$$

$$F_{O_2} = F_{O_2}^{ref} + \sum_{i=1}^8 \frac{2w_i}{\pi} \text{Tan}^{-1}[u_{O_2_i}(x_i - x_i^{ref})], \quad (16)$$

where x_i is a state variable, x_i^{ref} is the value of the state variable at the reference steady-state condition, u_{CO_i} and $u_{O_2_i}$ are the gains to the CO and O₂ mass flow controllers, respectively, associated with the state variable, and w_i is the half-width of the arctangent function. Because the values of u_{CO_i} and $u_{O_2_i}$ can be independently manipulated, they are used as the bifurcation parameters. Prairie *et al.* (1988) have presented several reasons for choosing an arctangent control function. It should be noted that the arctangent control is equivalent to proportional control for small deviations from the reference steady state.

Because of the intrinsic presence of time delay (transport lag, measurement lag, *etc.*) in the experimental system, the local stability analysis for bifurcation points can be most readily performed in the frequency domain. Prairie *et al.* (1988) have presented a general block diagram for the experimental system. The resulting closed-loop transfer function matrix can be expressed by

$$\mathbf{G}_T = [\mathbf{I} + \mathbf{G}_P \mathbf{G}_{mfc} \mathbf{G}_c \mathbf{D}]^{-1} \mathbf{G}_P \mathbf{G}_{mfc} \mathbf{G}_c, \quad (17)$$

where the transfer function matrices for the individual components correspond to \mathbf{G}_P for the process being examined (here, the CO oxidation reaction in the reactor cell), \mathbf{G}_{mfc} for the mass flow controllers, \mathbf{G}_c for the control algorithm, and \mathbf{D} for the system time delay. To gain any insight into the bifurcation behavior of the process of interest, it is necessary to characterize accurately the three transfer function matrices, \mathbf{G}_{mfc} , \mathbf{G}_c , and \mathbf{D} that are inherent to the experimental method. The next section deals with the evaluation of these matrices and testing the resulting model for the case of no reaction in the reactor cell. This test will also provide a means for determining the accuracy of the assumption that the gas phase in the reactor cell is well mixed. Following the matrix characterization, a comparison of the experimental and simulated bifurcation behavior for the CO reaction on Rh/Al₂O₃ under feedback control can be initiated.

The zeros of the characteristic equation, which follows directly from Equation

(17),

$$p(s) = \det[\mathbf{I} + \mathbf{G}_p \mathbf{G}_{mfc} \mathbf{G}_c \mathbf{D}] \quad (18)$$

are used to determine the stability behavior of the model equations. When a single root of the characteristic equation has zero real and imaginary parts ($p(0)=0$) and the remaining roots all have a negative real component, the system is at a point of steady-state bifurcation. Previous studies (Prairie and Bailey, 1986; Shanks and Bailey, 1987) have shown that, because of the problem of obtaining a sufficiently precise value of x_i^{ref} for the control algorithm, imperfect steady-state bifurcation will inevitably occur, making the experimental determination of a steady-state bifurcation point from closed-loop operation very difficult. Therefore, no steady-state bifurcation experimental data will be presented. A Hopf bifurcation corresponds to two complex conjugate roots of the characteristic equation having zero real part ($p(i\omega)=0$), and the remaining roots all having a negative real component. The experimental manifestation of a Hopf bifurcation is the appearance of a harmonic limit cycle from a stable steady state, which is due to the perturbation of a bifurcation parameter. Eigenvalue structures necessary for higher order bifurcations have been presented by Lyberatos *et al.* (1985).

System Model Verification

The validity of the dynamic model for the experimental apparatus can be evaluated by comparing the bifurcation data from closed-loop operation of the reactor cell under nonreactive conditions at 160°C (*i.e.*, no oxygen in the feed stream) with the associated simulation results. For these conditions, the reactor cell simply becomes a mixing tank and the process transfer function is one-dimensional,

$$g_p = \frac{1}{\tau s + 1} \quad (19)$$

Only CO in He is fed to the cell with the control of the CO inlet flow rate based

on the measurement of the effluent CO mole fraction according to

$$F_{CO} = F_{CO}^{ref} + \frac{2w}{\pi} \text{Tan}^{-1}[u_{CO}(x_{g1} - x_{g1}^{ref})]. \quad (20)$$

For these experiments, $w = 3$ sccm and $F_{CO}^{ref} = 14$ sccm ($x_{g1}^{ref} = 0.14$). Despite the one-dimensional material balance for the reactor cell, the experimental closed-loop system can admit steady-state and Hopf bifurcations that are due to the presence of time delay. While the primary goal of these experiments is to test the accuracy of the experimental apparatus model, a byproduct of the comparison between the experiments and model analysis will be a check of the validity of the assumption of ideal mixing in the reactor cell. This is possible since the individual transfer functions, G_{mfc} , G_e , and D are evaluated independently from the bifurcation experiments

The most difficult component to characterize in the experimental apparatus is the transfer function matrix associated with the mass flow controllers. Although the mass flow controllers exhibit complicated dynamic behavior, particularly for high frequency set-point manipulation, G_{mfc} can be more readily approximated for the low frequency operation (< 1.5 rad/s) needed for the bifurcation experiments. The transfer functions for each the CO and O₂ mass flow controller were independently determined from open-loop frequency response experiments. A detailed description of the method used to evaluate the elements of G_{mfc} is presented elsewhere (Prairie *et al.*, 1988). Amplitude ratio and phase lag data for the CO and the O₂ mass flow controllers were found to be modeled adequately by a transfer function for a first order system with dead time in the frequency range of experimental interest. The two transfer functions are given empirically by

$$g_{CO} = \frac{1}{0.3s + 1} e^{-0.48s} \quad (21)$$

for the CO mass flow controller and

$$g_{O_2} = \frac{1}{0.2s + 1} e^{-0.41s} \quad (22)$$

for the O₂ mass flow controller. Because the effluent concentration of O₂ cannot be measured with this experimental apparatus, only the transfer function for the CO mass flow controller can be explicitly verified from the nonreactive bifurcation experiments. Therefore, it is assumed that if g_{CO} is found to be accurate, then g_{O_2} is also accurate since g_{CO} and g_{O_2} are evaluated by identical methods.

The evaluation of G_c and D is very direct. G_c is fixed by the choice of the control algorithm and from Equation (20) is

$$g_c = -cu_{CO} \quad (23),$$

where $c = 2w/\pi F_T$. The transfer function for the system time delay has the form

$$d = e^{-\tau_D s} \quad (24),$$

where τ_D is the time delay. The intrinsic value of τ_D is determined in the same step-response experiment that is used to evaluate n , where τ_D is the time lag between the implementation of the step-change in the inlet CO concentration and the appearance of a perturbation in the measurement of the effluent CO concentration. In this experiment, a sampling rate of 10 Hz was used, so τ_D has a 0.1 s resolution.

Substituting Equations (19,21,23,24) into Equation (18) yields the characteristic equation for the experimental system under nonreactive conditions

$$p(s) = 1 + \left(\frac{cu_{CO}}{0.3s + 1} \right) \left(\frac{1}{\tau s + 1} \right) e^{-(\tau_D + 0.48)s}. \quad (25)$$

The bifurcation parameters used in these experiments are u_{CO} and τ_D . At a Hopf bifurcation point, the equations for the bifurcation parameters are

$$u_{CO} = -\frac{1}{c} \sqrt{(0.3\tau\omega^2 - 1)^2 + (\tau + 0.3)^2\omega^2} \quad (26)$$

$$\tau_D = -0.48 - \frac{1}{\omega} \text{Tan}^{-1} \left[\frac{(\tau + 0.3)\omega}{1 - 0.3\tau\omega^2} \right] + \frac{\pi}{\omega}, \quad (27)$$

where ω is the frequency of the resulting limit cycle. Equations (26-27) describe the locus of the Hopf bifurcation points in the u_{CO} versus τ_D parameter space.

For the determination of an experimental Hopf bifurcation point, τ_D was fixed and the magnitude of u_{CO} was increased until the reference steady state bifurcated to a limit cycle. The manipulation of τ_D is accomplished by introducing a floating array into the control algorithm. The value of τ_D is set by the size of the array employed with the minimum delay limited by the intrinsic delay in the system, which is evaluated as previously discussed. Therefore, the computer-generated delay can only add to the intrinsic time delay.

Typical experimental data for a feedback-stimulated Hopf bifurcation of the mixed tank is shown in Figure 3(a) for $\tau_D = 8.2$ s. Plotted is the deviation of the effluent CO mole fraction from the reference effluent CO mole fraction for the final 90 s of 600 s total spent at each of six discrete values of u_{CO} . As described by Halbe and Poore (1981), the relationship between the amplitude of the limit cycle, ϵ , and the Hopf bifurcation point, u_{CO}^H , is a perturbation expansion given by

$$u_{CO} - u_{CO}^H = \epsilon^2 \delta'(0) + O(\epsilon^2), \quad (28)$$

where $\delta'(0)$ is a constant. Then, the experimental Hopf bifurcation point can be determined by measuring the amplitudes of the oscillations near the instability point as a function of u_{CO} and interpolating the squares of the resulting amplitudes to zero amplitude. Using this method, the Hopf bifurcation point in Figure 3(a) was found to occur for $u_{CO}^H = -58.8$. Figure 4(a) is a compilation of the experimentally determined gains required to induce Hopf instabilities for a range of time delays. The frequencies of the resulting oscillations are plotted in Figure 4(b).

Incorporating the value $\tau = 3.15$ s, determined from a step-response experiment, the bifurcation behavior of the model was calculated from Equations (26-27) and is represented by the curves in Figure 5. In a previous study, Prairie *et al.*

(1988) have used simulations in the time domain to determine that the Hopf bifurcation behavior of these types of experiments is relatively insensitive to system noise, to offset in the programmed reference state variable, and to discrete sampling for sampling frequencies of ≥ 4 Hz that are used in these experiments. The agreement between experimental and calculated results seen in Figure 4 indicate that the dynamic model for the experimental apparatus is reasonable and that the macromixing in the gas phase of the reactor cell closely approximates ideal CSTR behavior.

Gas-Phase Measurement

The first set of bifurcation experiments on the CO-O₂ reaction utilized feedback to the inlet flow rates of CO and O₂ based on the effluent CO mole fraction. For this control scheme, \mathbf{G}_c has two nonzero components, $g_{c,11}$ and $g_{c,21}$, each of the form of Equation (23). The element corresponding to the control algorithm for the CO inlet flow rate $g_{c,11}$, has $w = 3$ sccm and a gain u_{CO} , while the element for the O₂ inlet flow rate, $g_{c,21}$, has $w = 2$ sccm and a gain u_{O_2} . In these experiments, u_{CO} and u_{O_2} are the bifurcation parameters, and τ_D is held fixed at its minimum value. Using the method described in the previous section, the value of the intrinsic time delay was found to be 3.1 s. The delay matrix, \mathbf{D} , has two nonzero elements, d_{11} and d_{22} , that are each as given in Equation (24). Also, \mathbf{G}_{mfc} has two nonzero components, $g_{mfc,11}$ precisely as given in Equation (21) and $g_{mfc,22}$ from Equation (22).

The process transfer function, \mathbf{G}_p , is eight-dimensional and is derived by linearizing Equations (4-11) around the reference steady-state condition about which stability is being examined. After linearizing the equations and introducing deviation variables, $\bar{\mathbf{x}} = \mathbf{x} - \mathbf{x}^{ref}$ (\mathbf{x} is a vector of the state variables), the equations can be written in the general form

$$\tau \frac{d\bar{\mathbf{x}}}{dt} = \mathbf{A}\bar{\mathbf{x}} + \mathbf{B}u \quad (29)$$

$$\mathbf{y} = \mathbf{C}\bar{\mathbf{x}}, \quad (30)$$

where \mathbf{A} is the Jacobian of the system model evaluated at $\bar{\mathbf{x}} = 0$, \mathbf{u} is a vector of the manipulated variables, and \mathbf{y} is a vector of the observable variables. Taking the Laplace transform of Equations (29-30) and removing $\bar{\mathbf{x}}$ gives the process transfer function

$$\mathbf{G}_p(s) = \mathbf{C}(\mathbf{I}\tau s - \mathbf{A})^{-1}\mathbf{B}. \quad (31)$$

For a specific reference steady state, the resolvent of \mathbf{A} was determined numerically in the simulations using the QZ method (Golub and Van Loan, 1983). From Equation (18), the characteristic equation for the model analysis corresponding to these experiments becomes

$$p(s) = 1 + \left[\left(\frac{3g_{p,11}(s)u_{CO}}{50\pi(0.3s + 1)} \right) e^{-0.48s} + \left(\frac{g_{p,12}(s)u_{O_2}}{25\pi(0.2s + 1)} \right) e^{-0.41s} \right] e^{-3.1s}. \quad (32)$$

Experimental Hopf bifurcation points were determined analogously to those in the previous section except that now either u_{CO} or u_{O_2} was held fixed, while the other gain was manipulated until a Hopf bifurcation occurred. When forcing the system both directions across the bifurcation point, stabilizing or destabilizing the reaction system, no hysteresis was observed, indicating that the Hopf bifurcation is supercritical (Iooss and Joseph, 1980). Therefore, the relation between amplitude and gain in Equation (28) can be used to determine the gain necessary to induce a Hopf bifurcation from experimental data. The resulting Hopf bifurcation points are shown in Figure 6(a) for a steady state associated with a reference feed of 14% CO and 5.5% O₂. The frequencies of the feedback-stimulated limit cycles are shown in Figure 6(b) versus the CO gain value required for bifurcation.

One parameter, n_s , is left undetermined in the overall reaction system model after the steady-state parameter estimation and experimental apparatus characterization. This parameter was evaluated by a numerical fit to the experimental Hopf bifurcation gain and frequency gain data shown in Figure 5. A minimization of an objective function based on the sum of squares of the differences between

the observed and calculated bifurcation points and frequencies (Shanks and Bailey, 1987) was used to estimate n_s . The resulting value of n_s was 6.5×10^{-6} mol/cm³ for both of the models. Figure 5 shows the calculated stability diagram and bifurcation frequencies for the two models. The solid curve represents Model A and the dashed curve Model B. The straight line at the bottom of the envelope gives the locus of the steady-state bifurcation points. Passing through any other portion of the envelope will lead to a Hopf bifurcation. Using the method described by Shanks and Bailey (1988), the stability of the limit cycles near the Hopf bifurcation points was computed. As with the experiments, the Hopf bifurcations for the models were found to be supercritical. Using the Carleman approximation, Lyberatos and Tsiligiannis (1987) have shown that arctangent feedback can lead to stable limit cycles even when oscillations stimulated by a locally similar proportional feedback control were unstable.

The two points at which the locus of the Hopf bifurcation points intersect with the steady-state bifurcation line are neither Hopf nor steady-state bifurcation points. These two discrete points, following the classification of Lyberatos *et al.* (1985), are F_1 and F_2 bifurcation points as labeled on Figure 5(a) for Model A. The eigenvalue structure at a F_1 bifurcation point has two leading eigenvalues at the origin. Relaxation oscillations can exist near bifurcation for such a system. Toroidal oscillations are possible when a system passes through an F_2 bifurcation, at which the system has three leading eigenvalues on the imaginary axis, one at the origin and an imaginary conjugate pair. While these points theoretically exist, the experimental realization of either bifurcation with this feedback scheme is difficult. This is the result of the interaction of a Hopf bifurcation with an imperfect steady-state bifurcation such that the reaction system will move to a new steady-state prior to the bifurcation predicted by linear analysis. Once the system moves to a new steady state, because of the effect of imperfect steady-state bifurcation, the linear analysis is no longer valid. Therefore, the net effect

is that the F_1 and F_2 bifurcations as located in the model analysis will not exist experimentally unless the reference state variable is known to an accuracy greater than is possible with this experimental apparatus.

The primary result for the experiments with bifurcation stimulated by feedback from the measurement of the gas-phase CO is that both models are able to reproduce adequately the experimental stability diagram. Explicitly considering the relationship between the bifurcation frequency and the CO gain necessary to induce a Hopf instability, Model A more closely duplicates the experimental data than does Model B.

Surface Measurement

While the results of the previous section indicate some discrepancy between Model B and the experimental data, the evidence for elimination of Model B is not conclusive. Therefore, feedback-induced bifurcation experiments were performed, in which feedback to the inlet reactant flow rates was based on the transmittance at 2072 cm^{-1} . The control algorithms in this case are

$$F_{CO} = F_{CO}^{ref} + \frac{2w_1}{\pi} \text{Tan}^{-1}[u_{CO}(T_{CO} - T_{CO}^{ref})] \quad (33)$$

$$F_{O_2} = F_{O_2}^{ref} + \frac{2w_2}{\pi} \text{Tan}^{-1}[u_{O_2}(T_{CO} - T_{CO}^{ref})]. \quad (34)$$

Although the experiments use the deviation of the transmittance at 2072 cm^{-1} from the reference transmittance in the control algorithm, it is necessary to relate the transmittance to the fractional coverage of CO for the model analysis. This is done through the calibration curve as given in Equation (20) for Model A. For the calculations using Model A, the two nonzero elements of G_c become

$$g_{c,17} = c_1 u_{CO} (0.282 - 0.466\theta_1 + 1.78\theta_1^2) \quad (35)$$

$$g_{c,27} = c_2 u_{O_2} (0.282 - 0.466\theta_1 + 1.78\theta_1^2), \quad (36)$$

where $c_1 = 2w_1/\pi F_T$ with $w_1 = 3$ sccm, $c_2 = 2w_2/\pi F_T$ with $w_2 = 2$ sccm, and the value of θ_1 corresponds to its reference steady-state value. The precise forms of $g_{c,17}$ and $g_{c,27}$ are model specific according to the associated calibration curve for the relationship between the transmittance at 2072 cm^{-1} and θ_1 .

Both \mathbf{D} and \mathbf{G}_{mfc} have the same forms as in the previous section except $\tau_D = 0.7$ s, because the measurement of the transmittance occurs in the reactor rather than in the effluent stream. The reference steady state was again established with 14% CO and 5.5% O₂ in the reactor feed stream. \mathbf{G}_p is derived as previously where matrix \mathbf{C} must now reflect the use of the transmittance (*i.e.* θ_1) as the observable variable.

Shown in Figure 3(b) are typical experimental data that are used to determine a Hopf bifurcation point for the reaction system when feedback is based on the transmittance at 2072 cm^{-1} . The figure shows the deviation of the measured transmittance for the final 90 s of 600 s spent at each of 6 discrete values of u_{O_2} . The gain to the CO mass flow controller was held fixed at 40 throughout the experiment. A compilation of the experimentally determined Hopf bifurcation points is shown in Figure 6, along with the frequencies of the resulting oscillations. The higher frequency oscillations are at the limit of the applicability of Equations (21-22) for the CO and O₂ mass flow controllers. The experimental Hopf bifurcations were again found to be supercritical.

The calculated stability diagrams and bifurcation frequencies in Figure 6 are given by a solid curve for Model A and a dashed curve for Model B. The differences between the two models are much more pronounced in this case and clearly, Model A is much better at reproducing the experimental data than is Model B. The minor differences between the experimental data and Model A can be attributed at least partially to the method employed for correlating the transmittance and the fractional coverage of CO.

Several slight variants of Model A were also investigated. These include cov-

erage-dependent activation energy for the desorption of CO (Oh *et al.*, 1986), site exclusion by either adsorbed CO or O (Herz and Marin, 1980; Graham and Lynch, 1987), and island formation of the adsorbed species (Mukesh *et al.*, 1984). Parameters were determined for different models, each of which incorporated one of these variations, using exactly the same method as was used for Models A and B. External mass transfer was considered significant in the parameter estimations for all of the models. The calculated bifurcation behavior under feedback control from measured transmittance for each of the new models was indiscernible from that displayed by Model A.

Higher Order Bifurcations

A possible alternative approach for discriminating between the rival Models A and B, rather than feedback control based on θ_1 , is the determination of higher order bifurcations. As shown in Figure 5, F_1 and F_2 bifurcations are predicted to occur based on analysis of the model for the closed-loop system with reaction. These type of bifurcations were not experimentally realizable using the control scheme specified for the data in Figure 5. Shanks and Bailey (1987) show in a calculated stability diagram that higher order bifurcations can possibly be induced using similar closed-loop operation by increasing the time delay in the reaction system. Feedback-stimulated bifurcation experiments were performed under the same conditions employed to determine the bifurcation points in Figure 5 except that now, by using a floating array in the control algorithm, the system time delay was fixed at 20.1 s rather than at the $\tau_D = 3.1$ s used previously. With the larger time delay, oscillations near all of the bifurcation points were not harmonic. Only harmonic oscillations were observed near bifurcation in the experiments with smaller time delay.

The experimental behavior near two bifurcation points is shown in Figures 7 and 8. Plotted is the time trajectory of the deviation of the effluent CO mole

fraction from the reference effluent mole fraction corresponding to a feed of 14% CO, 5.5% O₂ for 6 sequential values of u_{CO} . The figures show the entire experiments for two fixed u_{O_2} values, -120 (Figure 7) and 190 (Figure 8). When u_{CO} was changed to a new value, the time was reset to zero with the initial conditions in the time delay array set by operation at the previous u_{CO} , so each experiment required 1 hr total. As seen in Figure 7, the dynamic response near the bifurcation point for $u_{O_2} = -120$ is characterized by relaxation oscillations. The dynamic behavior near $u_{O_2} = 190$ has irregular high frequency features dissolving into low frequency oscillations as u_{CO} is decreased. This behavior is particularly clear for the final 240 s at $u_{CO} = 180$ and is similar to that seen from the interaction of two different frequency oscillations (Kevrekidis *et al.*, 1986). For O₂ gains between -100 and 150, the system displayed harmonic oscillations near the bifurcation points. The experimental bifurcation points and resulting oscillation frequencies are shown in Figure 9.

Using $p(s)$ from Equation (32) with $\tau_D = 20.1$ s, the calculated stability diagrams for Models A and B are given by the solid line and dashed line, respectively, in Figure 9(a). The locus of the Hopf bifurcation points is now more complicated than in the bifurcation diagram in Figures 5 and 6, where the Hopf bifurcation portion of the stability envelope represents a continuum of oscillation frequencies starting at a frequency of zero (F₁ bifurcation point) and ending at the F₂ bifurcation point. As shown in Figure 9(b), the frequencies of the oscillations induced by passing through a Hopf bifurcation point have discontinuities along the Hopf bifurcation portion of the envelope. These points of discontinuity correspond to F₃ bifurcation points (Lyberatos *et al.*, 1985), where there are 4 leading eigenvalues, 2 imaginary conjugate pairs with different magnitude imaginary components. The F₃ bifurcation points calculated for Model A are labeled in Figure 9(a).

The bifurcations in Figures 7 and 8 are located near the F₃ bifurcation points in the model analysis using Model A. The dynamic responses in these figures are

clearly different from the limit cycles observed previously near Hopf bifurcations, but the exact classification of the bifurcation based on experimental observation is difficult. A Hopf instability is defined by a local condition and therefore, dynamic behavior insufficiently close to a bifurcation point cannot be used to characterize the type of bifurcation. Bifurcations close to a F_3 bifurcation point are affected by the F_3 point, so the ability to determine experimentally a precise F_3 point in these types of experiments is unlikely. The region in the calculated stability diagrams corresponding to CO gains of greater than 200 displays the largest discrepancy between the two models. Model B predicts a larger stable area in this region. When imposing $u_{CO} > 200$ in the experiments, the results were difficult to analyze for a precise bifurcation. This behavior would be more likely reproduced by Model A, as the model analysis using Model A gives a very small region of stable operation for $u_{CO} > 200$, which includes several F_3 bifurcation points.

DISCUSSION AND CONCLUSIONS

The use of the feedback-induced bifurcation method for model identification relies on a comparison of the bifurcation or stability diagrams determined experimentally and through model analysis. For the catalytic reactions that have been studied, the calculated stability diagrams consist of the loci of steady-state and Hopf bifurcation points and two higher order F_1 and F_2 bifurcation points. The exception to this is the model prediction of isolated F_3 bifurcation points for systems in which time delay has been artificially increased. While the model analysis indicates the existence of higher order bifurcations, only Hopf and steady-state bifurcations have been observed experimentally, using the feedback-induced bifurcation method. Higher order dynamics have been observed, but the exact point at which a higher order bifurcation occurs has not been experimentally isolated. A discussion of the stability diagram resulting from applying the feedback-induced

bifurcation method can be structured according to three classes of bifurcations that are calculated from model analysis, steady-state, Hopf, and higher order bifurcations.

The steady-state bifurcation points can be readily calculated for system models, but measurement restrictions affect the experimental determination of steady-state bifurcation points. Because of limited experimental precision of the state variable value at the reference condition used in the control algorithms, imperfect steady-state bifurcations are observed experimentally, which obscures the steady-state bifurcation points. Therefore, the locus of static bifurcation points in an experimental stability diagram is difficult to determine. Shanks and Bailey (1987) show that the calculated locus of steady-state bifurcation points for two reaction models for CO oxidation on Ag are different. However, when simulating the experimental conditions that necessarily produce imperfect steady-state bifurcation, both models reproduce the experimental data equally proficiently. Static bifurcation data were used by Prairie and Bailey (1986) to discriminate between rival parameter sets for ethylene hydrogenation. The discrimination resulted from a comparison of the behavior of the reaction system and model in an operating region, where the reference steady-state was unstable and was not a result of actually comparing the static bifurcation points for the two parameter sets. Even if the point of steady-state bifurcation could be determined experimentally, model analysis for the two models as shown in Figures 5, 6, and 9 indicates that the same gain values are required to induce static bifurcation. The results from these studies indicate that the feedback-induced steady-state bifurcations are of limited use in model identification.

Hopf bifurcation points are more readily determined experimentally than are static bifurcation points and have been shown in simulations of feedback experiments (Prairie *et al.*, 1988) to be insensitive to small deviations in the state variable value at reference condition employed in the control algorithms. The

usefulness of Hopf bifurcation data for model development is strongly dependent on the state variable measurement used for feedback control. Figures 5 and 6 clearly demonstrate the advantage for this reaction of feedback based on a reaction intermediate, adsorbed CO, rather than on the gas-phase CO mole fraction. This advantage in differentiating between the calculated Hopf loci for the two models occurs despite the model-dependent method employed to calibrate transmittance with fractional surface coverage. The applicability of Hopf bifurcation data generated by feedback control for model development, in reaction systems in which reaction intermediates are not monitored, has been addressed by Prairie and Bailey (1987) and Shanks and Bailey (1987). Those studies showed that model development in the form of parameter estimation or model discrimination was possible from comparison of experimental and calculated Hopf bifurcation points when feedback was based on reactant species. However, even when a measurement of a reaction intermediate is used in the control algorithms, small variations in a model, as described earlier with coverage dependent activation energy, site exclusion by adsorbed species, and adsorbate island formation, will not necessarily alter the location of the calculated Hopf bifurcation points in the stability diagram. Thus, bifurcation behavior resulting from closed-loop operation may be insensitive to some aspects of a process model.

The existence of higher order bifurcations from model analysis appears to be strongly influenced by the value of the system time delay. It is clear, though, that the time delay does not completely dominate the bifurcation behavior of a reaction system, since the calculated stability diagrams at relatively large time delay values differ for different parameter sets and models. If the experimental points at which higher order bifurcations resulting from feedback control could be determined in the bifurcation diagram, these points might be successfully exploited for model identification. Unfortunately, these bifurcation points are isolated from each other and are located adjacent to Hopf bifurcation points and therefore, the interaction

of these effects renders the experimental resolution of an F_1 or higher bifurcation point difficult.

From an experimental viewpoint, it is apparent that the most useful form of feedback-induced bifurcation for application in model identification is a Hopf bifurcation. This work, as well as several previous experimental studies using the feedback-induced bifurcation method in heterogeneous catalytic reaction systems, indicates that the gains required to induce Hopf instabilities can be systematically determined. The limitations on the method are primarily imposed by the ability to monitor only a subset of the species participating in a reaction. As demonstrated in a simulation study of continuous microbial growth systems by O'Neil and Lyberatos (1986), the scope of processes that can be examined by the feedback-induced bifurcation method is not restricted to heterogeneous catalytic reaction systems.

NOTATION

A	Jacobian matrix
A_s	catalyst wafer area (cm^2)
B	coefficient matrix of manipulated variables
c	scale factor for the arctangent function
c_T	gas concentration (mol/cm^3)
C	coefficient matrix of the process observables
d_{ii}	element of the delay matrix
D	delay matrix
F	flow rate (mol/s)
g_{ii}	element of transfer function matrix
G	transfer function matrix
k_g	external mass transfer coefficient (cm/s)

k_i	rate parameter (s^{-1})
L	catalyst wafer thickness (cm)
n	reactor capacity (mol)
n_s	active sites on the catalyst/volume (mol/cm^3)
$p(s)$	characteristic function
r	reaction rate (mol/s)
t	time (s)
T_{CO}	transmittance
u	controller gain
\mathbf{u}	vector of manipulated variables
w	half-width of the arctangent function (sccm)
x_i	state variable
\mathbf{x}	vector of the state variables
\mathbf{y}	vector of the observables
θ_i	fractional surface coverage
ϵ	oscillation amplitude
ϵ_s	catalyst wafer porosity
τ	reactor residence time (s)
τ_D	system time delay (s)
ω	bifurcation frequency (rad/s)

subscripts

c	controller
CO	carbon monoxide
mfc	mass flow controller
o	outlet
O_2	oxygen
p	process
T	total

superscripts

H Hopf

ref reference condition

REFERENCES

- Golub, G.H. and C.F. Van Loan, *Matrix Computations*, Johns Hopkins University Press, Baltimore, Md. (1983).
- Graham, W.R.C. and D.T. Lynch, "CO Oxidation on Pt: Model Discrimination Using Experimental Bifurcation Behavior," *AIChE J.*, **33**, 792 (1987).
- Halbe, D.C. and A.B. Poore, "Dynamics of the Continuous Stirred Tank Reactor with Reactions $A \rightarrow B \rightarrow C$," *Chem. Eng. J.*, **21**, 241 (1981).
- Herz, R.K. and S.P. Marin, "Surface Chemistry Models of Carbon Monoxide Oxidation on Supported Platinum Catalysts," *J. Catal.*, **65**, 281 (1980).
- Iooss, G. and D.D. Joseph, *Elementary Stability and Bifurcation Theory*, Springer-Verlag, New York (1980).
- Kaul, D.J., R. Sant, and E.E. Wolf, "Integrated Kinetic Modelling and Transient FTIR Studies of CO Oxidation on Pt/SiO₂," *Chem. Eng. Sci.*, **42**, 1399 (1987).
- Kevrekidis, I.G., L.D. Schmidt, and R. Aris, "Some Common Features of Periodically Forced Reacting Systems," *Chem. Eng. Sci.*, **41**, 1263 (1986).
- Kuszta, B. and J.E. Bailey, "Nonlinear Model Identification By Analysis of Feedback-Stimulated Bifurcation," *IEEE Trans. Autom. Control*, **AC-27**, 227 (1982).
- Lyberatos, G., B. Kuszta, and J.E. Bailey, "Discrimination and Identification of Dynamic Models via Introduction of Feedback," *Chem. Eng. Sci.*, **39**, 739 (1984).
- Lyberatos, G., B. Kuszta, and J.E. Bailey, "Versal Families, Normal Forms, and Higher Order Bifurcations in Dynamic Chemical Systems," *Chem. Eng. Sci.*, **40**, 1177 (1985).
- Lyberatos, G. and C.A. Tsiligiannis, "Analysis of Feedback Induced Hopf Bifurcations via the Carleman Approximation," *Chem. Eng. Commun.*, **57**, 1 (1987).

- McDermott, P.E., H.-C. Chang, and R.G. Rinker, "Experimental Investigation of Controller-Induced Bifurcation in a Fixed-Bed Autothermal Reactor," *Chem. Eng. Sci.*, **40**, 1355 (1985).
- Mukesh, D., W. Morten, C.N. Kenney, and M.B. Cutlip, "Island Models and the Catalytic Oxidation of Carbon Monoxide and Carbon Monoxide-Olefin Mixtures," *Surf. Sci.*, **138**, 237 (1984).
- Oh, S.H. and L.L. Hegedus, "Dynamics of High-Temperature Carbon Monoxide Chemisorption on Platinum-Alumina by Fast-Response IR Spectroscopy," *Catalysis Under Transient Conditions*, (A.T. Bell and L.L. Hegedus, Eds.), ACS Symp. Ser., **178**, 79 (1982).
- Oh, S.H., G.B. Fisher, J.E. Carpenter, and D.W. Goodman, "Comparative Kinetic Studies of CO-O₂ and CO-NO Reactions over Single Crystal and Supported Rhodium Catalysts," *J. Catal.*, **100**, 360 (1986).
- O'Neil, D.G. and G. Lyberatos, "Feedback Identification of Continuous Microbial Growth Systems," *Biotechnol. Bioeng.*, **28**, 1323 (1986).
- Prairie, M.R. and J.E. Bailey, "Application of Feedback-Induced Bifurcation for Evaluating Steady-State and Transient Heterogeneous Catalysis Kinetic Models," *Chem. Eng. Sci.*, **41**, 937 (1986).
- Prairie, M.R. and J.E. Bailey, "Experimental and Modeling Investigations of Steady-State and Dynamic Characteristics of Ethylene Hydrogenation on Pt/Al₂O₃," *Chem. Eng. Sci.*, **42**, 2085 (1987).
- Prairie, M.R., B.H. Shanks, and J.E. Bailey, "Intentional Manipulation of Closed-Loop Time Delay for Model Validation Using Feedback-Induced Bifurcation Experiments," *Chem. Eng. Sci.* in press (1988).
- Rice, C.A., S.D. Worley, C.W. Curtis, J.A. Guin, and A.R. Tarrer, "The Oxidation State of Dispersed Rh on Al₂O₃," *J. Chem. Phys.*, **74**, 6487 (1981).
- Shanks, B.H. and J.E. Bailey, "Experimental Investigations using Feedback-Induced Bifurcation: Carbon Monoxide Oxidation over Supported Silver," *Chem. Eng. Commun.*, **61**, 127 (1987).

Yang, A.C. and C.W. Garland, "Infrared Studies of Carbon Monoxide Chemisorbed on Rhodium," *J. Phys. Chem.*, **61**, 1504 (1957).

Yates, J.T., T.M. Duncan, S.D. Worley, and R.W. Vaughan, "Infrared Spectra of Chemisorbed CO on Rh," *J. Chem. Phys.*, **70**, 1219 (1979).

TABLE 1: Parameters estimated from steady-state data.
(r^2 is the correlation coefficient for the model relative to all of the steady-state experimental data)

Parameters	Model A	Model B
k_1 (s^{-1})	5.3×10^3	1.2×10^3
k_{-1} (s^{-1})	1.9×10^2	4.5×10^1
k_2 (s^{-1})	1.0×10^2	8.9×10^1
k_3 (s^{-1})	1.1×10^3	4.5×10^1
k_g (cm/s)	6.5	$\rightarrow \infty$
r^2	0.876	0.836

FIGURE CAPTIONS

- Figure 1: IR spectra of CO adsorbed on Rh/Al₂O₃ at 160°C. (a) 14% CO, (b) 5% O₂, 14% CO, (c) 7% O₂, 14% CO.
- Figure 2: Calibration curve relating the transmittance at 2072 cm⁻¹ and the fractional coverage of adsorbed CO estimated from Model A.
- Figure 3: Experimental Hopf bifurcation data. (a) Mixing cell with $\tau_D = 8.2$ s. (b) Feedback based on transmittance with $u_{CO} = 40$.
- Figure 4: Experimental (points) and calculated (line) bifurcation behavior under nonreactive conditions. (a) The locus of time delay and CO gain, u_{CO} , values at which Hopf bifurcation occurs. (b) Frequencies at the Hopf bifurcation points.
- Figure 5: Experimental (points) and calculated bifurcation behavior (Model A (solid) and Model B (dashed)) with feedback based on the gas-phase CO mole fraction for a reference feed of 14% CO, 5.5% O₂. (a) The locus of gain values at which bifurcation occur with the F₁ and F₂ bifurcation points labeled for Model A. (b) Frequencies of the Hopf bifurcation portion of the stability diagram.
- Figure 6: Experimental and calculated bifurcations stimulated by feedback based on the transmittance at 2072 cm⁻¹ for a reference feed of 14% CO, 5.5% O₂. (a) Stability diagrams for the experimental data (points), Model A (solid), and Model B (dashed) in the feedback gain space. (b) Frequencies at the Hopf bifurcation points.
- Figure 7: Time trajectories of the CO deviation variable under feedback control for increasing magnitude of u_{CO} , $u_{O_2} = -120$, and $\tau_D = 20.1$ s. Larger magnitude u_{CO} values lead to relaxation oscillations.
- Figure 8: Time trajectories of the CO deviation variable under feedback control with $u_{O_2} = 190$, $\tau_D = 20.1$ s, and reference feed of 14% CO, 5.5% O₂.

Figure 9: Experimental (points) and calculated bifurcation behavior (Model A (solid) and Model B (dashed)) for $\tau_D = 20.1$ s and a reference feed of 14% CO, 5.5% O₂. The end sections of the stability envelope have been magnified (x2) for clarification. (a) Bifurcation diagrams with the F₃ bifurcation points labeled for Model A. (b) Hopf bifurcation frequencies where the jump discontinuities in frequency correspond to F₃ points. The small blackened circles in (a) and (b) give the endpoints of the frequency trace around the stability envelope.

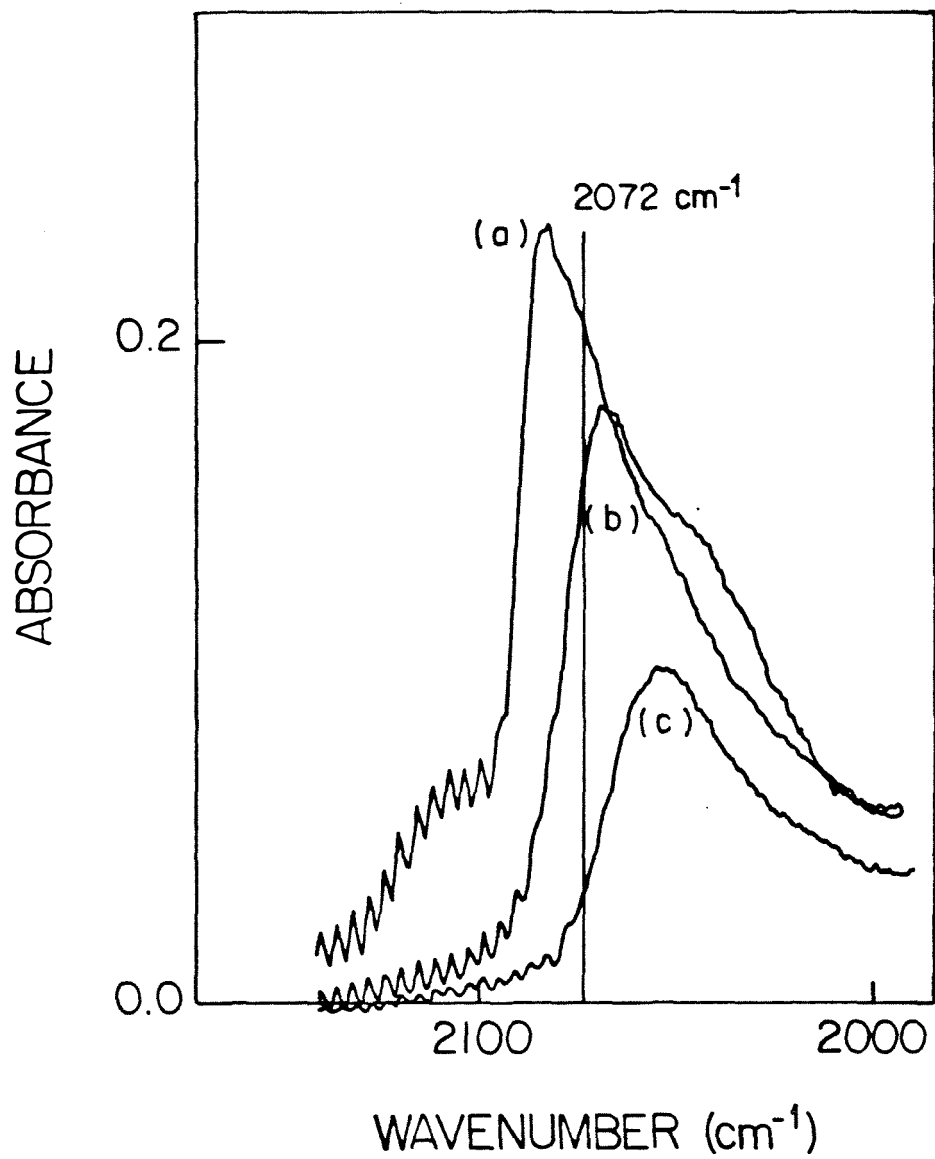


Figure 1

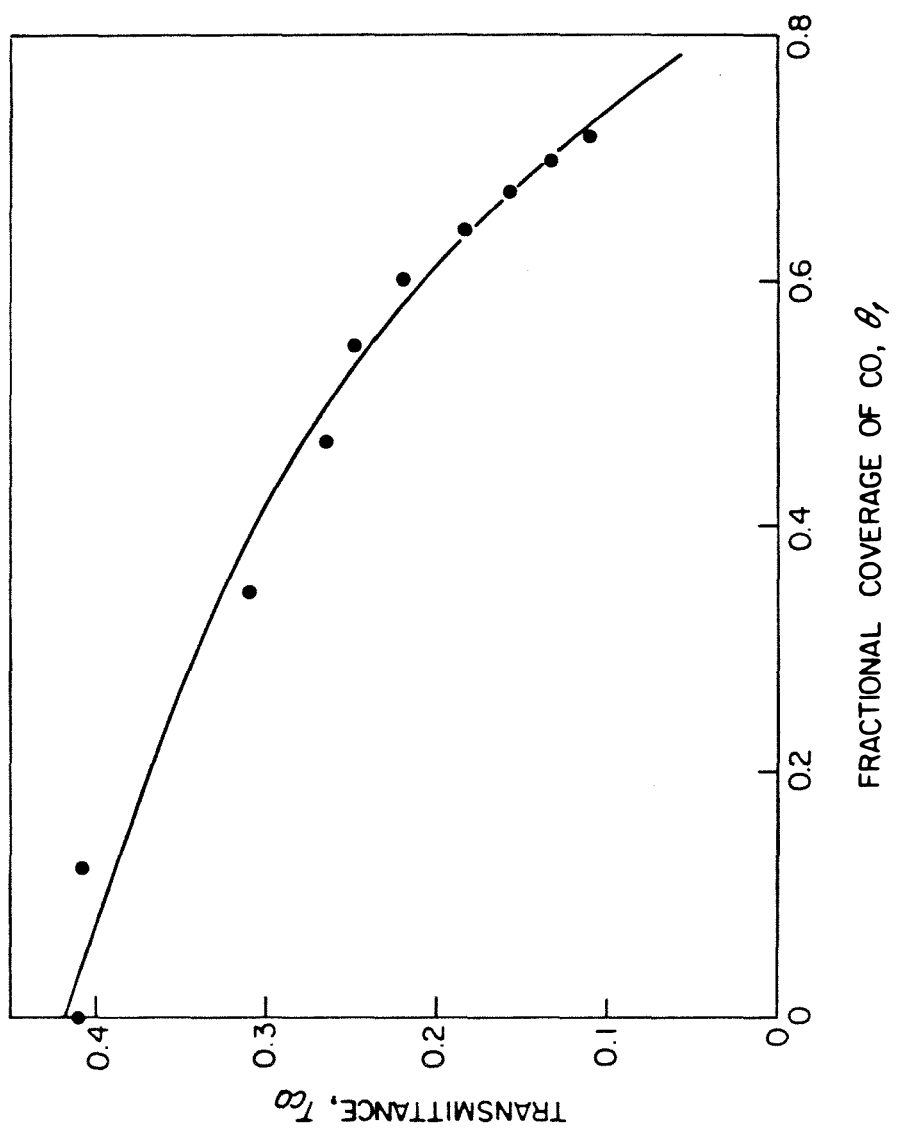


Figure 2

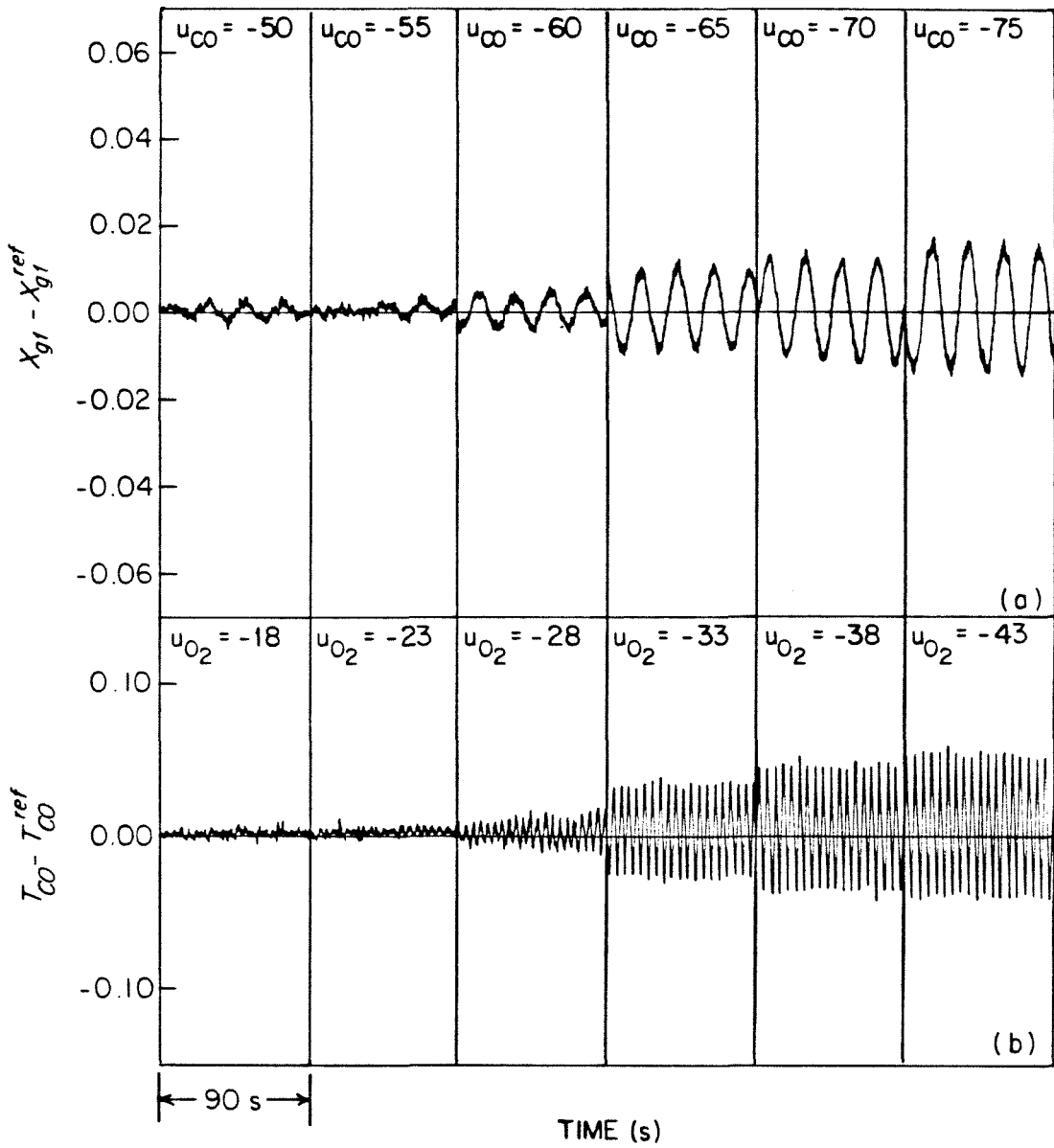


Figure 3

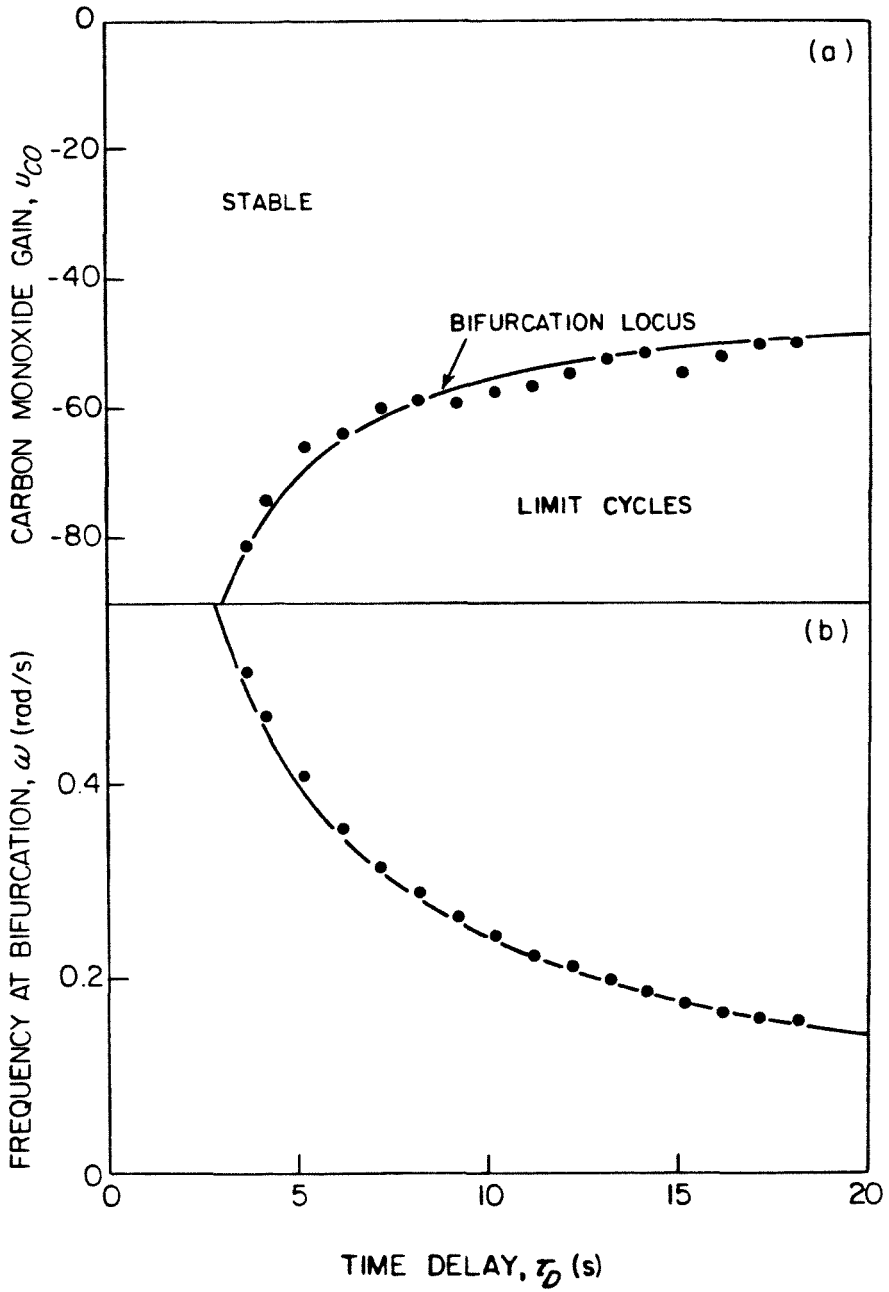


Figure 4

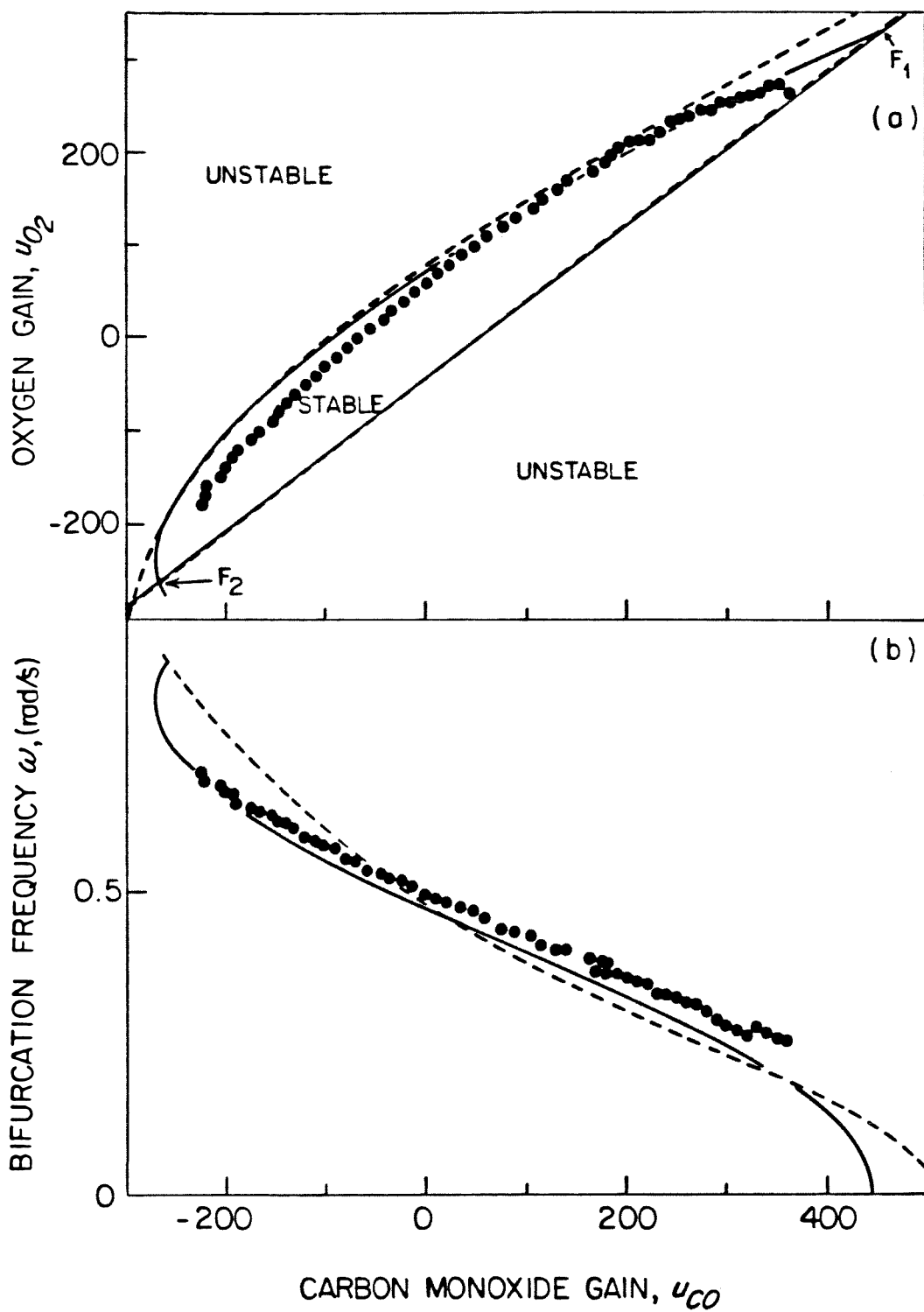


Figure 5

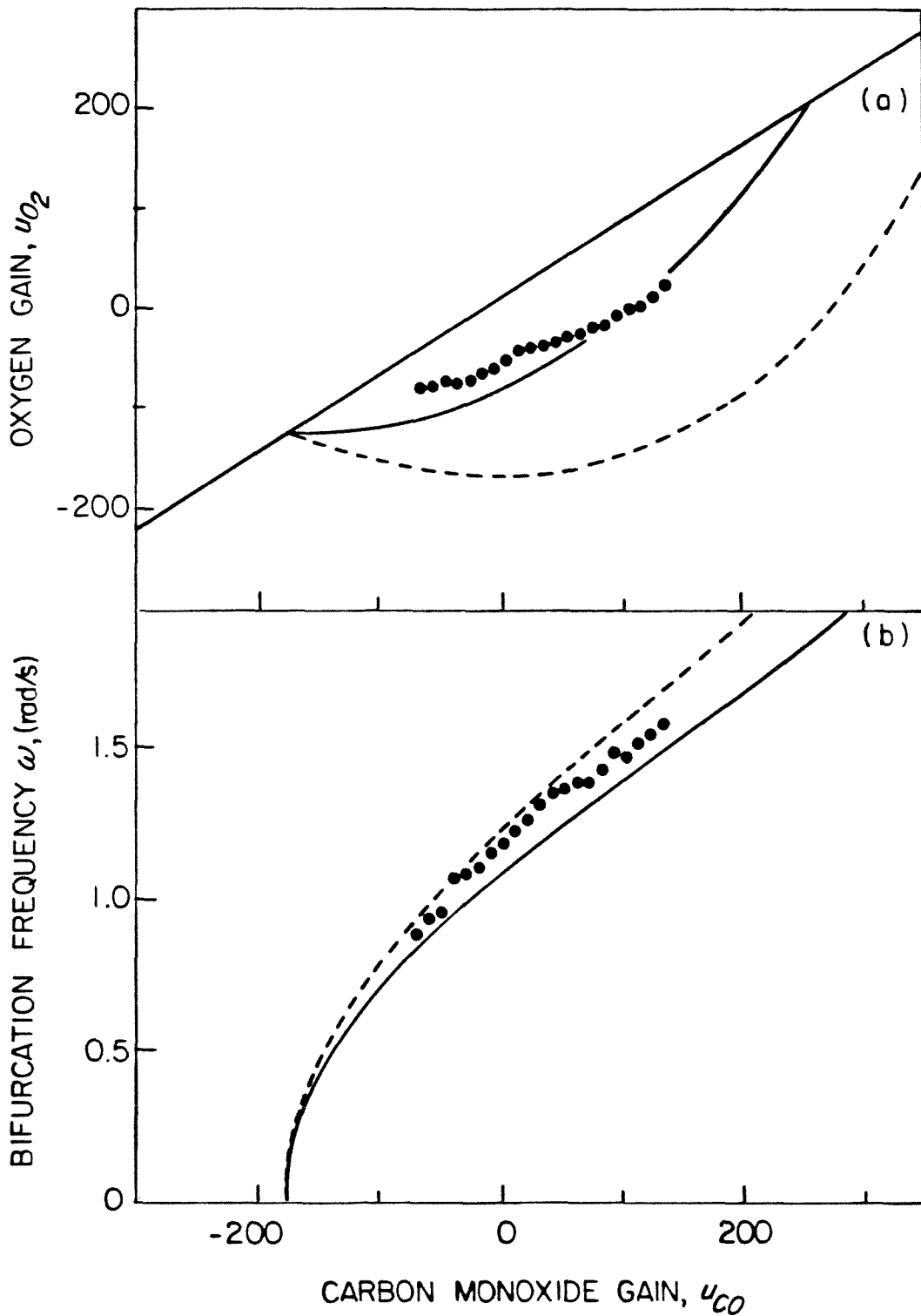


Figure 6

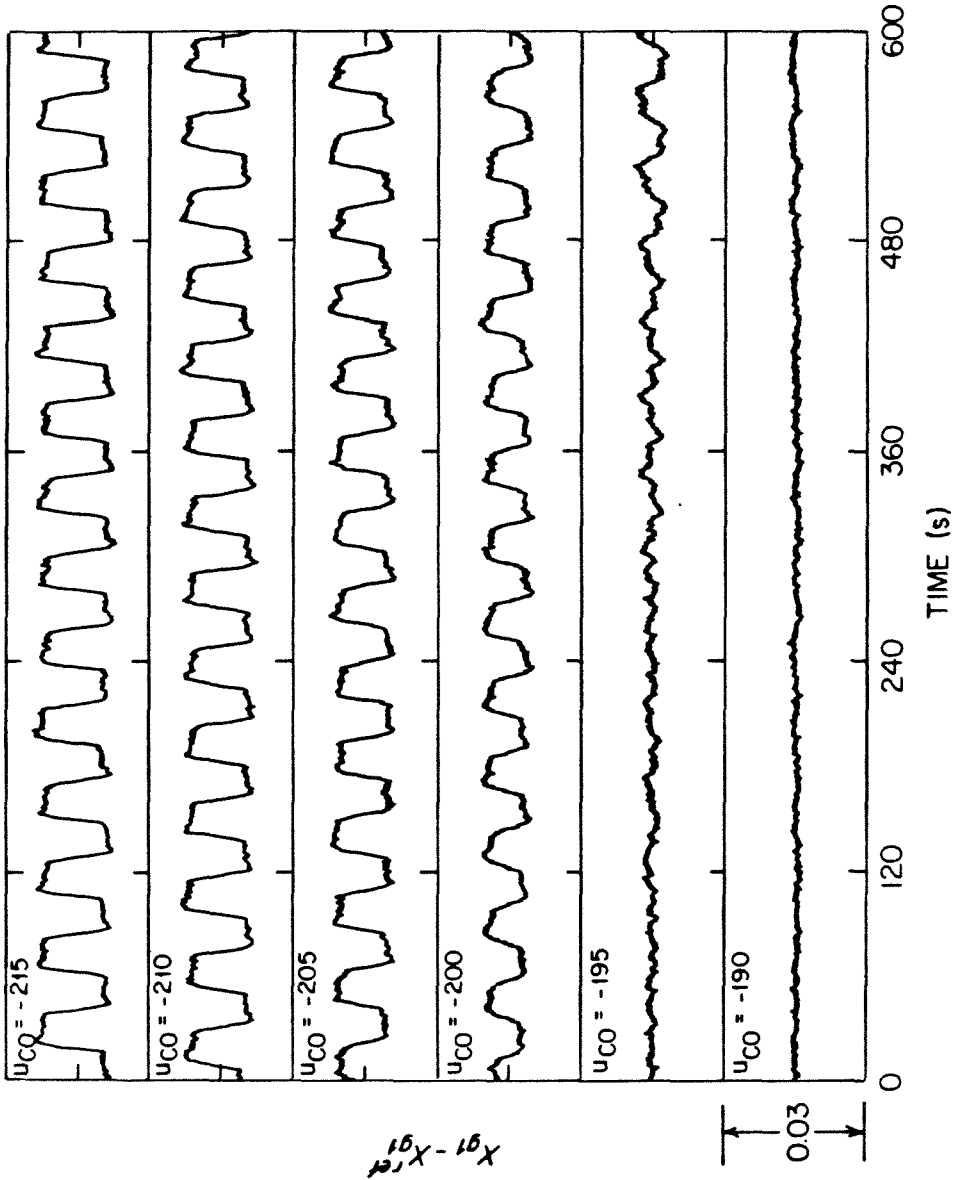


Figure 7

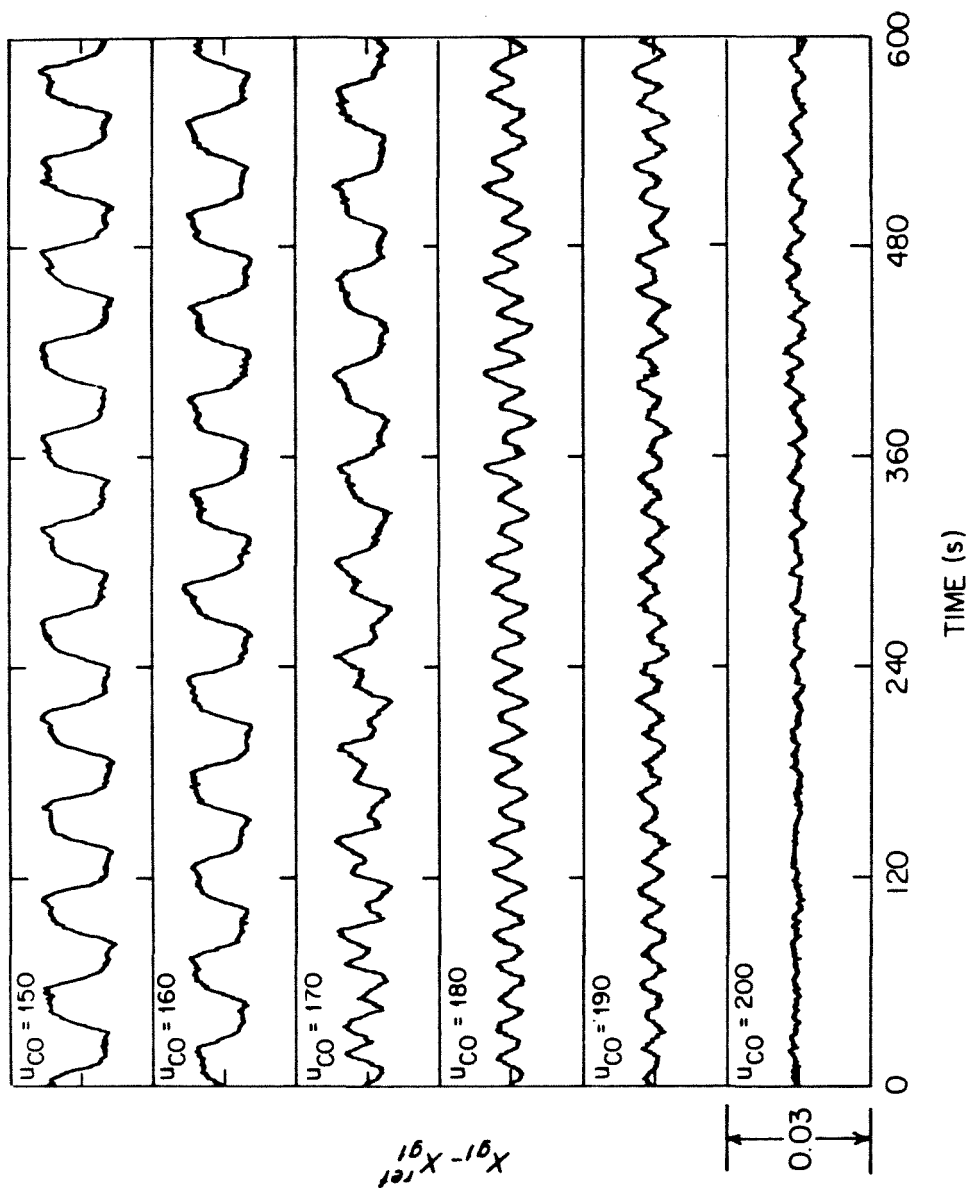


Figure 8

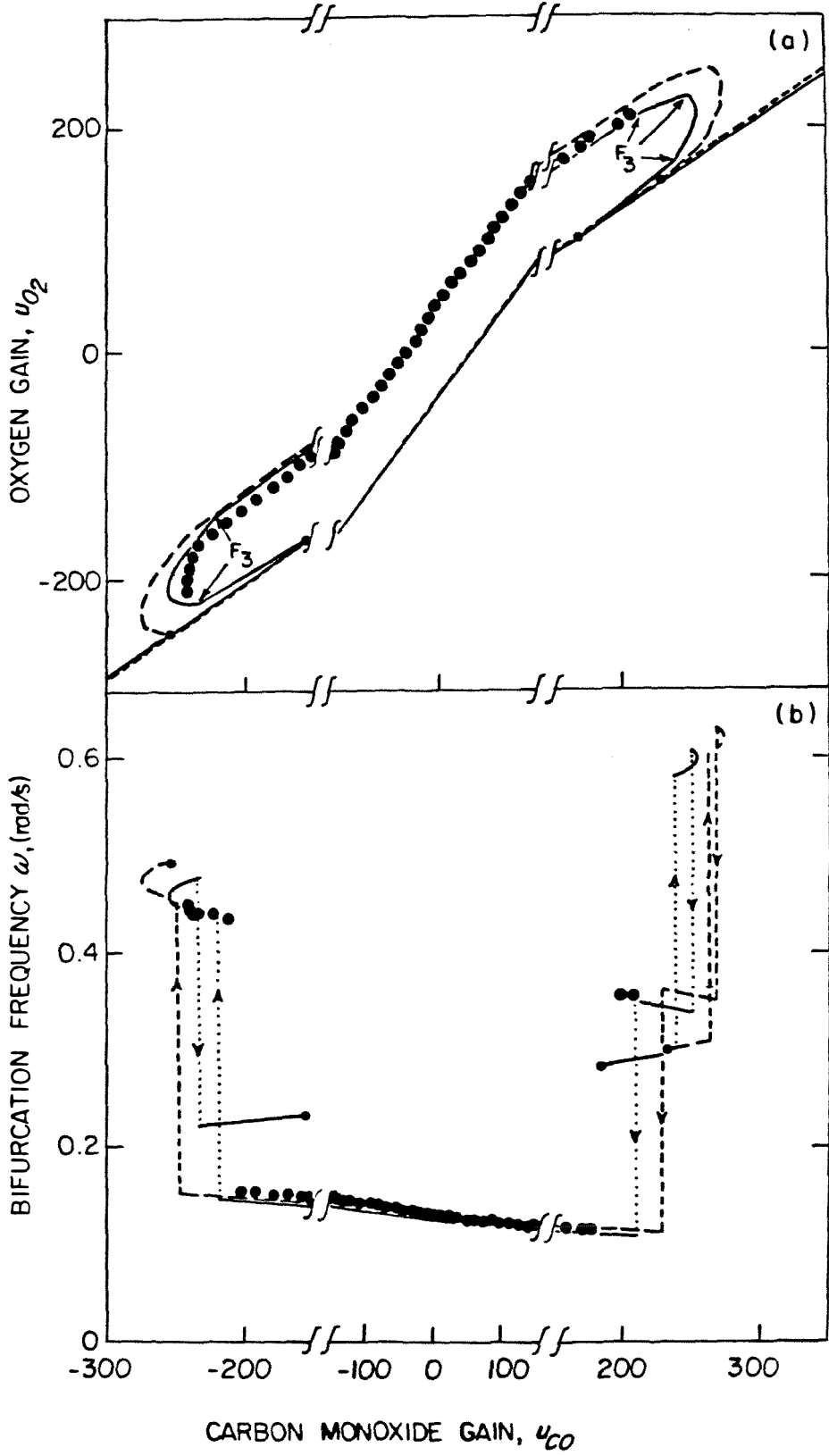


Figure 9

CHAPTER 6

EXPERIMENTAL INVESTIGATION OF ENTRAINMENT

PHENOMENA IN A PERIODICALLY FORCED,

AUTONOMOUSLY OSCILLATING PROCESS

INTRODUCTION

Recently there has been increased interest in studying the dynamic response of self-oscillatory systems subjected to periodic forcing. Rehmus and Ross (1985) have presented a review of periodically perturbed oscillatory chemical systems that exhibit behavior including entrainment as well as quasi-periodic and chaotic responses. Numerical work on the cyclic forcing of the Brusselator model has been reviewed by Tomita (1982), where the phenomena of period doubling cascades leading to chaos and periodic and quasi-periodic limit cycles were simulated. While relatively high-amplitude forcing has been used to study period doubling bifurcations and chaos, low-amplitude forcing can be utilized to observe the behavior of quasi-periodicity and frequency locking.

Specifically considering low-amplitude forcing, Kevrekidis *et al.* (1984,1986a, 1986b) developed a general theoretical framework for the behavior of periodically forced oscillatory systems, which was applied to three examples: an autocatalytic homogeneous Brusselator, a bimolecular surface reaction, and a nonisothermal CSTR with a single reaction. A rigorous structure for the classification of expected behavior was presented, which includes subharmonic, harmonic, and quasi-periodic oscillations. Kevrekidis *et al.* employed an entrainment diagram to provide a concise summary of these dynamic phenomena associated with the periodic forcing of a particular oscillatory system. The entrainment diagram is a parametric mapping of categories of system output responses in the forcing amplitude versus the forcing frequency plane.

Entrainment diagrams have been experimentally determined for a few systems. Using the oscillatory Belousov-Zhabotinskii reaction, Buchholz *et al.* (1985) observed the dynamic response that are due to sinusoidal flow rate changes, and Hudson *et al.* (1986) subjected the reaction to periodic forcing of the reactant feed concentration in a CSTR. Dulos and DeKepper (1983) used periodic light irra-

diation of the autonomously oscillating Briggs-Rauscher reaction to demonstrate entrainment phenomena experimentally.

While there exists a strong mathematical foundation for the study of dynamic behavior in periodically forced oscillating systems, the sparse experimental data have been limited to few systems. The primary hurdles in the experimental work in this area are the difficulty in obtaining an autonomous oscillatory system and, once found, in maintaining a stable and reproducible limit cycle in the system (see, for example, the review of CO-O₂ oscillations on Pt by Razon and Schmitz, 1986). This problem can be surmounted by applying the method of feedback-induced bifurcation in which stable periodic oscillations are stimulated by forcing the system through a Hopf bifurcation point. Kuszta and Bailey (1982) first introduced the idea of feedback-induced bifurcation as a means of nonlinear model identification. This idea has been amplified and applied in several theoretical and experimental papers (Lyberatos *et al.* 1984,1985; Prairie and Bailey, 1986,1987).

The purpose of the present work is to introduce the use of feedback-induced bifurcation for providing stable limit cycles in systems that do not oscillate naturally. These feedback-induced limit cycles can then be used with periodic forcing to demonstrate experimentally the behavior that has been analyzed by Kevrekidis *et al.*, and to evaluate a dynamic process model, comparing model and experimental behavior. This enlarges the set of dynamic conditions and bifurcation phenomena that can be used to test and to improve transient models of chemical processes. While the goal of studying entrainment behavior is to probe system dynamics, the system chosen for this study is a CSTR without reaction. This system provides a simple example of the dynamic behavior resulting from periodic forcing of a feedback stimulated limit cycle. The extension of this idea to examining more complex systems requires only introducing the system to be studied into the closed-loop configuration.

As has been shown elsewhere (Prairie *et al.* 1988), measurement lag is an

essential ingredient for creating a limit cycle in a continuous stirred tank with feedback control based on the measurement of an effluent concentration. By utilizing the closed-loop operation of a continuous stirred tank, an autonomously oscillating system is provided, which is here analyzed with periodic forcing.

EXPERIMENTAL METHOD

A detailed description of the experimental system is provided elsewhere (Prairie *et al.* 1988), but a brief explanation of the experimental conditions is necessary. Ethylene and helium were fed to the reactor through Tylan mass flow controllers at a constant total flow rate of 100 sccm, of which the ethylene feed rate contributed 10 sccm, for steady-state or reference operation. The stainless steel fixed-bed, internal recycle reactor behaved as an ideal CSTR, with a residence time of 4.7 seconds for this flow rate. A Wilkes Miran I variable filter infrared analyzer operating at $10.4 \mu\text{m}$ was used to monitor the ethylene concentration in the reactor effluent. The effluent ethylene concentration measurement was input to a Hewlett-Packard 9825B microcomputer, which in turn used the measurement to adjust the set points of the mass flow controllers.

Figure 1 shows a schematic of the experimental system. Central to this work is the existence of a process in an autonomous oscillatory base state. This state is produced by introducing feedback control of the continuous stirred tank. Once the oscillatory base is established, sinusoidal forcing is input to the closed-loop system.

An arctangent feedback control of the ethylene feed stream with the form

$$u_i(t) = u_{ref} + \frac{2c}{\pi} \text{Tan}^{-1} [K(x(t - \tau_D) - x_{ref})] \quad (1)$$

was implemented on the computer. Here u_i is the flow rate set point, K is the controller gain, x is the effluent ethylene mole fraction, and c is the half-width of

the arctangent function. The dynamic behavior of the experimental system for this control scheme has been characterized by Prairie *et al.* (1988). In that work, it was shown that flow lags in the apparatus contribute a time delay τ_D in the loop which must be included for description of the Hopf bifurcation properties of the closed-loop system.

The state-space representation of the closed-loop process must also include the dynamic contribution from the mass flow controller. This is a complicated dynamic element of the closed-loop process in its own right, including measurement, control, and valve actuation functions. The inlet ethylene feed rate may be written as

$$F_i(t) = F_{ref} + \int_0^t u(p)g(t-p)dp, \quad (2)$$

where $g(t)$ is the impulse response function associated with the ethylene mass flow controller. Prairie *et al.* (1988) have shown that, for the region of operation used in this study, this function has the approximate form

$$g(t) = \delta(t - \tau_C), \quad (3)$$

where $\tau_C = 0.39$ s. The transfer function for the mass flow controller was determined from open-loop frequency response experiments. In this work, the validity of Equation (3) will be evaluated by comparing the experiments and simulations performed using this model under forced, closed-loop conditions.

The forced cycling experiments were performed by superimposing a sinusoidal forcing function on the feedback control, with the overall result

$$u_i(t) = u_{ref} + \frac{2c}{\pi} \text{Tan}^{-1} [K(x(t - \tau_D) - x_{ref})] + \alpha \sin(\omega t) \quad (4)$$

as the programmed inlet flow rate. The base oscillatory state to which the periodic forcing was applied was established, using $K = -55$ and $\tau_D = 10$ s. For these conditions, the natural frequency of the system is 0.239 rad/s. Data were collected for 10 minutes at each prescribed forcing amplitude and frequency.

ENTRAINMENT DIAGRAM

When an oscillatory system is subjected to periodic forcing, the inputs that can be most readily manipulated are the forcing amplitude, α , and frequency, ω . Therefore, a useful representation for the behavior of the system is a parametric or "entrainment" diagram in the $\alpha, \omega/\omega_o$ plane, where ω_o is the frequency of the autonomous oscillation. In the limit as $\alpha \rightarrow 0$, periodic trajectories will occur when the ratio of ω to ω_o is equal to the ratio of prime numbers, k/l ; otherwise, quasi-periodic trajectories will result. The periodic oscillations will have a period of k times the forcing period. The value of the forcing frequency, where $\omega/\omega_o = k/l$ as $\alpha \rightarrow 0$, is the converging point of an entrainment region (or entrainment or resonance horn) within which frequency locking occurs, leading to forced periodic oscillations with frequency $\omega_o k/l$. For sufficiently small α , the resonance horns, in which frequency locking is equal to k/l , widen in the entrainment diagram with increasing forcing amplitude. The forms of the resonance horns become more complex as α increases to the extent that the entrained regions interact.

RESULTS

Figure 2 shows experimental trajectories for several periodic limit cycles using a forcing amplitude of 1.2 sccm and six forcing frequencies: $1/2$, $2/3$, $1/1$, $4/3$, $3/2$, and $2/1$ times the natural frequency. While the fundamental resonance is seen at $k/l = 1$, subharmonic oscillations are shown for $k/l = 1/2$, $2/3$, $4/3$, and $3/2$. The limit cycles with subharmonic resonances have multi-peaked oscillations with l peaks. By incrementally increasing ω for a fixed α and recording the resulting time trajectories, the entrainment diagram for the system can be defined experimentally. The data points in Figure 3 show the experimentally determined parametric mapping. Only the entrainment horns for $\omega/\omega_o = 1/2$, $2/3$, and 1

are shown; however, entrainment horns will emanate from the $\alpha=0$ axis whenever $\omega/\omega_o = k/l$. As can be seen from the figure, the experimental data outline a much larger entrainment region for the fundamental resonance than for the subharmonic resonances. Outside the entrainment horns, quasi-periodic behavior is observed.

Simulations were also performed to see if the experimental results could be reproduced by a mathematical model of the system. The unsteady-state ethylene material balance for the closed-loop apparatus is given by the equation

$$\tau \frac{dx(t)}{dt} = x_{ref} + \frac{2c}{\pi F_t} \text{Tan}^{-1} [K(x(t - \tau_D - \tau_C) - x_{ref})] + \alpha \sin(\omega t) - x(t), \quad (5)$$

where τ is the reactor residence time. The equation was solved using the IMSL subroutine DGEAR with parameters identical to those employed in the experiments. Time delay was simulated by using a floating array that was initialized to the reference conditions.

Presented in Figure 3 is a comparison of the simulated and experimental resonance horn boundaries for the system. Figure 4 shows the simulated trajectories for the same ω/ω_o ratios used in Figure 2. As can be seen from these figures, the simulated entrainment diagram as well as the form of the effluent concentration trajectories correspond closely with the experimentally observed behavior. This result is not surprising, since the principal source of ambiguity in the system model is the transfer function for the mass flow controller. While it is expected that the simulated and experimental behavior will coincide for a simple mixing tank and control system, the ability to characterize the dynamic responses for this system yields a basis from which more complicated systems can be readily incorporated into the closed-loop structure and studied.

CONCLUSIONS

Reproducible autonomous limit cycles are a necessary basis for forced cycling of an oscillatory system to be an effective tool in model evaluation. This problem has been addressed by applying the method of feedback-induced sustained oscillations to generate the basis, "unforced" oscillation. The system with superposed feedback and sinusoidal forcing was shown to yield an experimental entrainment diagram that was calculated for a continuous stirred tank model with time delay. By stimulating an oscillatory state in a system, the introduction of feedback with superimposed periodic cycling can be used to examine nonlinearities in systems that do not readily produce a wide variety of interesting dynamic behavior at normal operating conditions. Feedback can be applied to generate oscillations in much more complicated systems such as reactors with heterogeneous catalytic reactions (Prairie and Bailey, 1986,1987; Shanks and Bailey, 1987). This characteristic obviates the need to search extensively the parameter space of a reaction system for a region of autonomous oscillatory operation necessary to study the periodic forcing of an oscillatory system. Also, the feedback configuration allows generation of the basis autonomous oscillation for systems that do not exhibit an autonomous oscillation for any open-loop operation.

NOTATION

c	half-width of arctangent feedback function (sccm)
F_i	inlet ethylene flow rate (sccm)
F_t	total flow rate (sccm)
K	controller gain
u	flow rate set point

x	ethylene mole fraction
α	forcing amplitude (sccm)
τ	reactor residence time (s)
τ_C	controller time delay (s)
τ_D	system time delay (s)
ω	forcing frequency (rad/s)

Subscript

<i>ref</i>	at reference steady-state conditions
------------	--------------------------------------

REFERENCES

- Buchholz F., A. Freund, and F.W. Schneider, "Periodic Perturbation of the BZ-Reaction in a CSTR: Chemical Resonance, Entrainment and Quasi-Periodic Behavior," *Temporal Order*, L. Rensing and N.I. Jaeger, Eds., Springer-Verlag, New York, 116 (1985).
- Dulos, E. and P. DeKepper, "Experimental Study of Synchronization Phenomena under Periodic Light Irradiation of a Nonlinear Chemical System," *Biophys. Chem.*, **18**, 211 (1983).
- Hudson, J.L., P. Lamba, and J.C. Mankin, "Experiments on Low-Amplitude Forcing of a Chemical Oscillator," *J. Phys. Chem.*, **90**, 3430 (1986).
- Kevrekidis, I.G., L.D. Schmidt, and R. Aris, "On the Dynamics of Periodically Forced Chemical Reactors," *Chem. Eng. Commun.*, **30**, 323 (1984).
- Kevrekidis, I.G., L.D. Schmidt, and R. Aris, "Some Common Features of Periodically Forced Reacting Systems," *Chem. Eng. Sci.*, **41**, 1263 (1986).
- Kevrekidis, I.G., L.D. Schmidt, and R. Aris, "Resonance in Periodically Forced Processes," *Chem. Eng. Sci.*, **41**, 670 (1986).
- Kuszta, B. and J.E. Bailey, "Nonlinear Model Identification By Analysis of Feedback-Stimulated Bifurcation," *IEEE Trans. Autom. Control*, **AC-27**, 227 (1982).
- Lyberatos, G., B. Kuszta, and J.E. Bailey, "Discrimination and Identification of Dynamic Models via Introduction of Feedback," *Chem. Eng. Sci.*, **39**, 739 (1984).
- Lyberatos, G., B. Kuszta, and J.E. Bailey, "Versal Families, Normal Forms, and Higher Order Bifurcations in Dynamic Chemical Systems," *Chem. Eng. Sci.*, **40**, 1177 (1985).
- Prairie, M.R. and J.E. Bailey, "Application of Feedback-Induced Bifurcation for Evaluating Steady-State and Transient Heterogeneous Catalysis Kinetic Models," *Chem. Eng. Sci.*, **41**, 937 (1986).

- Prairie, M.R. and J.E. Bailey, "Experimental and Modeling Investigations of Steady-State and Dynamic Characteristics of Ethylene Hydrogenation on Pt/Al₂O₃," *Chem. Eng. Sci.*, **42**, 2085 (1987).
- Prairie, M.R., B.H. Shanks, and J.E. Bailey, "Intentional Manipulation of Closed-Loop Time Delay for Model Validation Using Feedback-Induced Bifurcation Experiments," *Chem. Eng. Sci.* in press (1988).
- Razon, L.F. and R.A. Schmitz, "Intrinsically Unstable Behavior during the Oxidation of Carbon Monoxide on Platinum," *Catal. Rev.-Sci. Eng.*, **28**, 89 (1986).
- Rehms, P. and J. Ross, "Periodically Perturbed Chemical Systems," *Oscillations and Traveling Waves in Chemical Systems*, R.J. Field and M. Burger, Eds., John Wiley and Sons, New York, 287 (1985).
- Shanks, B.H. and J.E. Bailey, "Experimental Investigations using Feedback-Induced Bifurcation: Carbon Monoxide Oxidation over Supported Silver" *Chem. Eng. Commun.*, **61**, 127 (1988).
- Tomita, K., "Chaotic Response of Nonlinear Oscillators," *Physics Reports*, **86**, 113 (1982).

FIGURE CAPTIONS

- Figure 1: The upper portion of this schematic diagram shows the closed-loop configuration which can be applied to generate an autonomous closed-loop oscillation which includes the process of interest (here a continuous stirred tank). As indicated in the lower portion of the figure, sinusoidal input forcing may then be applied to study the response of the autonomous oscillation to periodic forcing.
- Figure 2: Experimental ethylene effluent trajectories for six forcing frequencies with a forcing amplitude of 1.2 sccm.
- Figure 3: Entrainment diagram with experimental data points and simulated resonance horn boundaries (lines) for $\omega/\omega_o=1/2, 2/3,$ and 1.
- Figure 4: Simulated ethylene effluent trajectories for the same conditions presented in Figure 1.

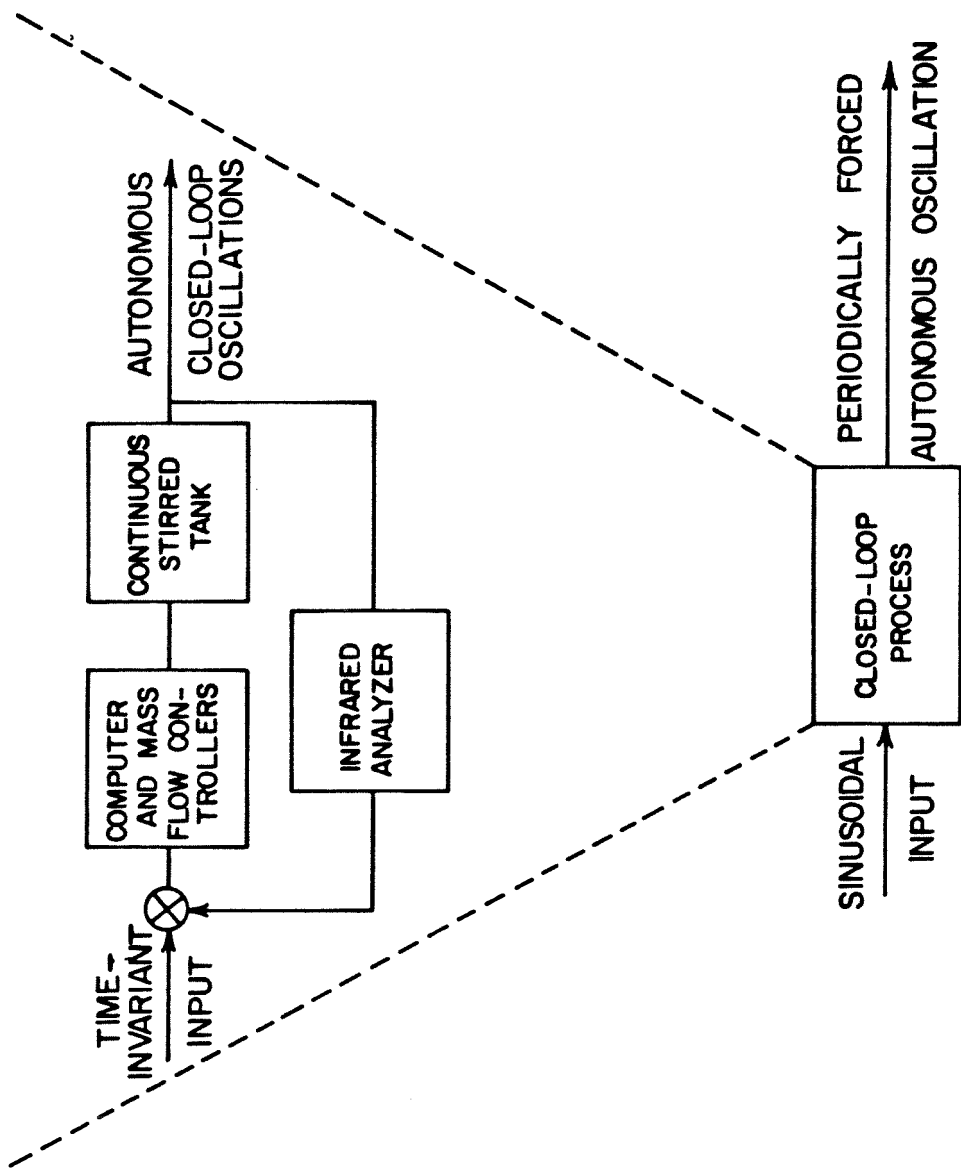


Figure 1

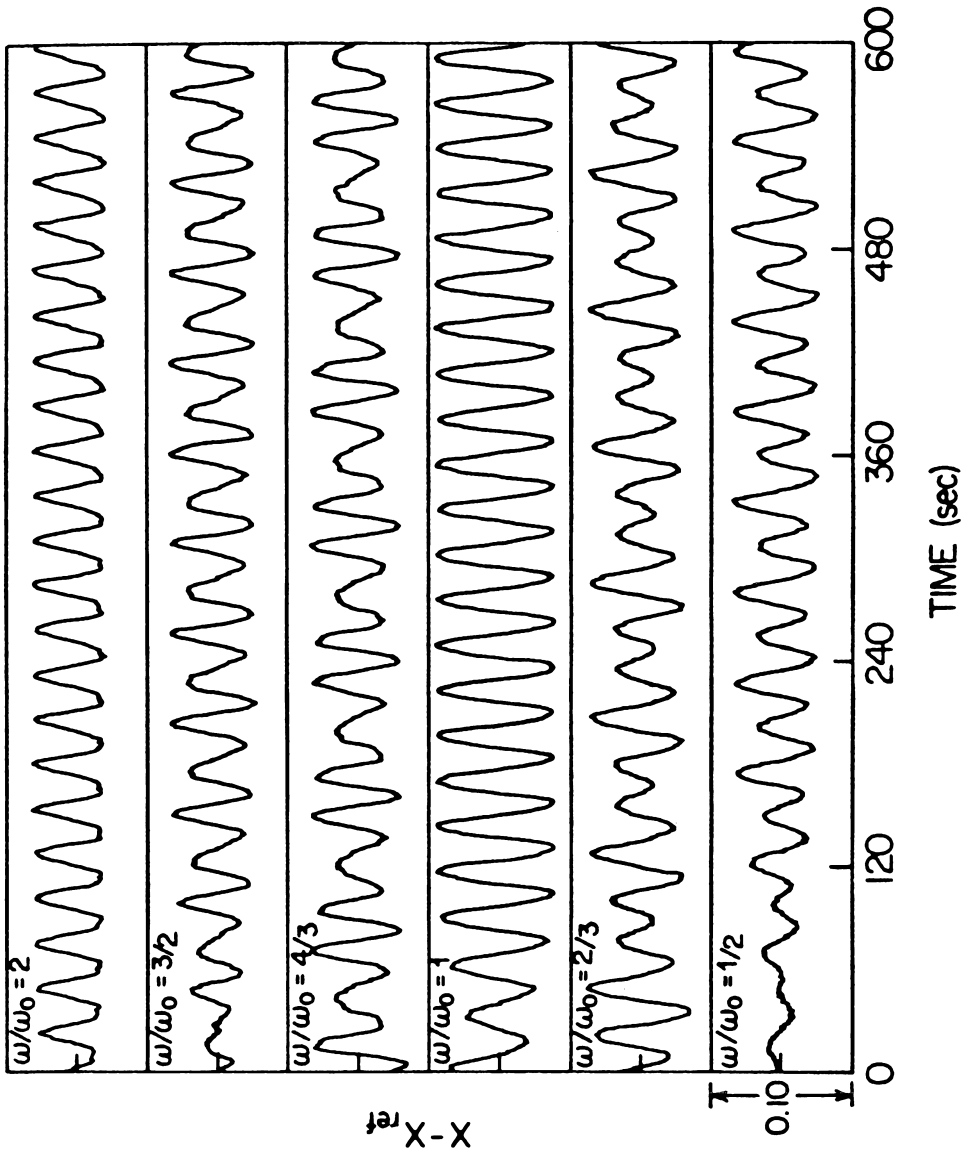


Figure 2

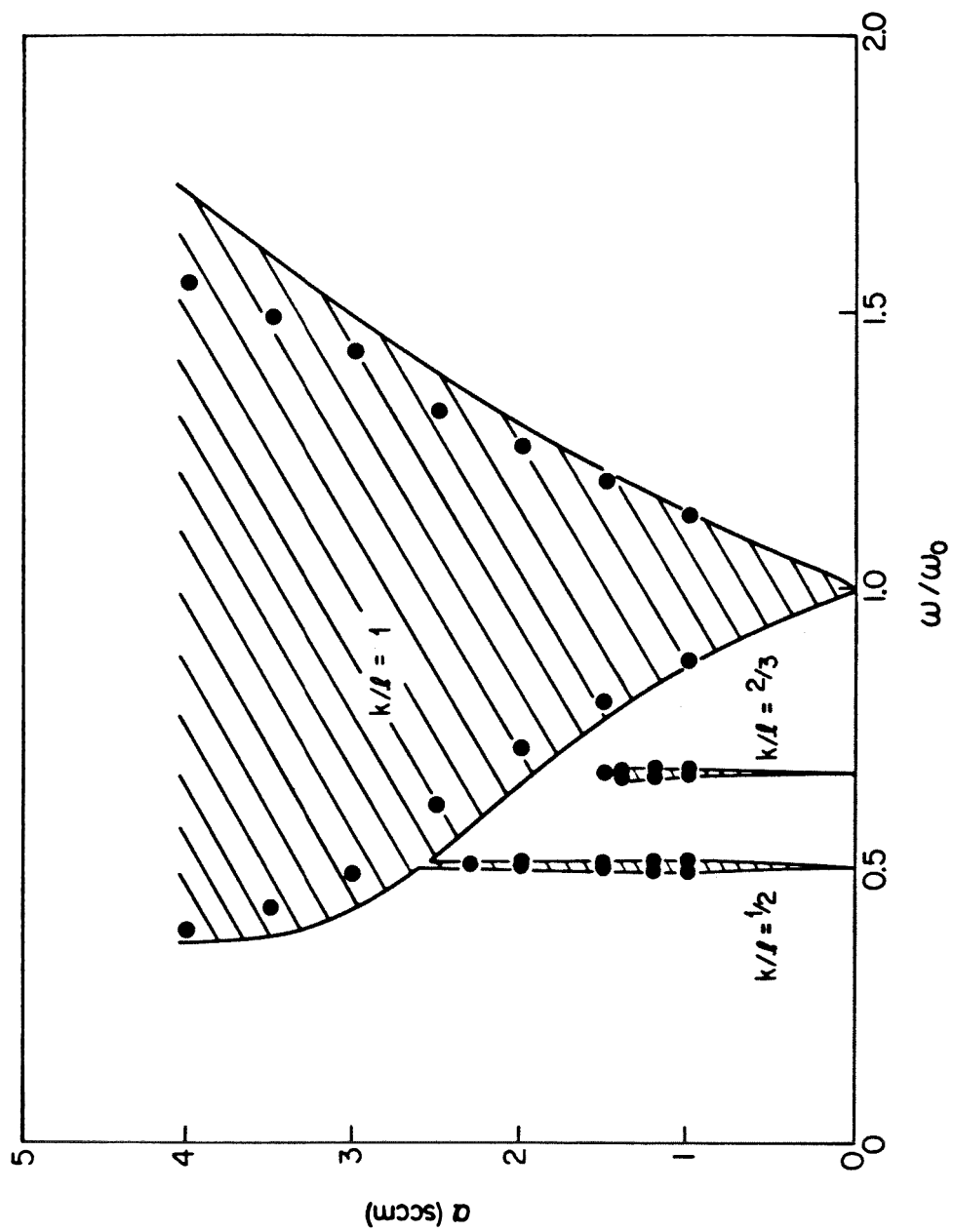


Figure 3

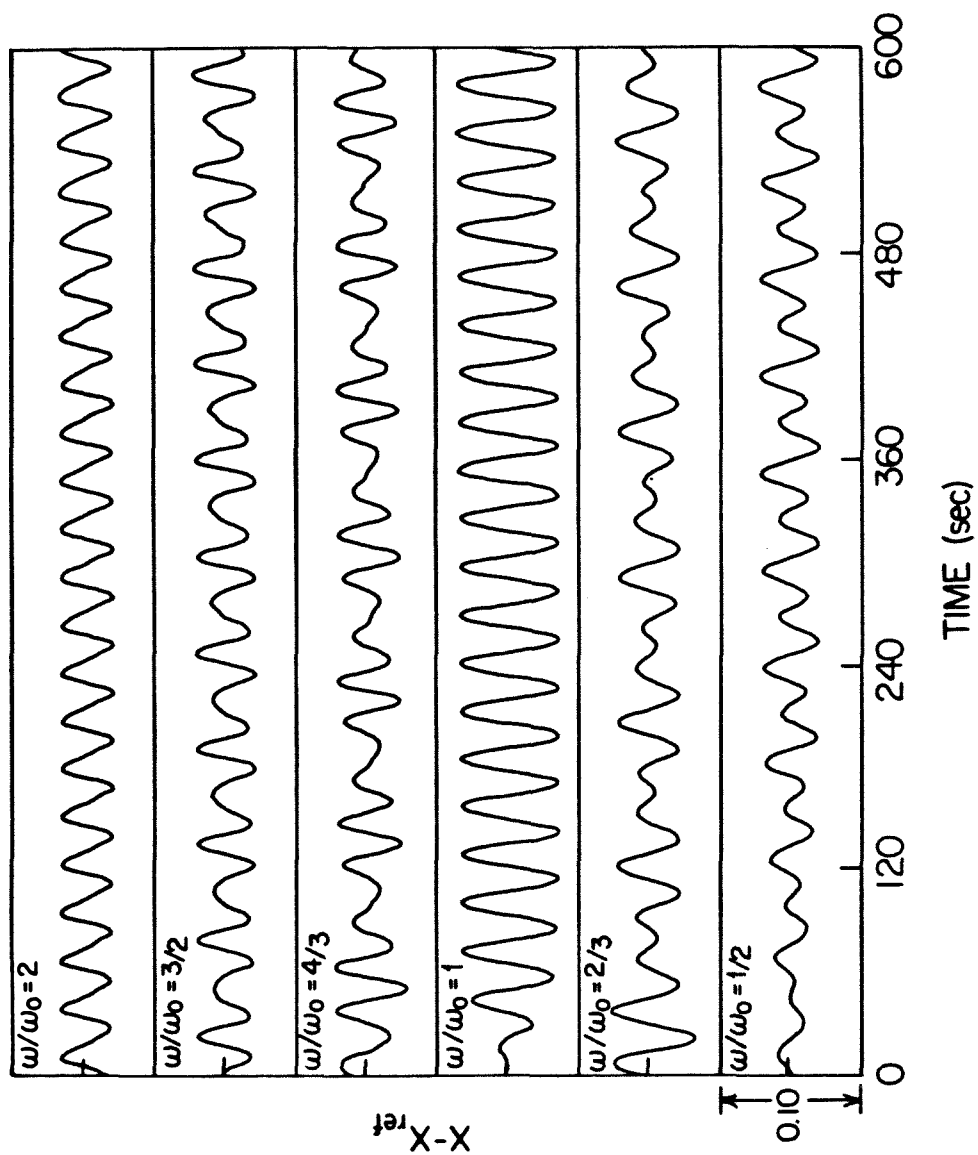


Figure 4

CHAPTER 7

CONCLUSIONS

Data from static and dynamic experiments and the corresponding model simulations and calculations have been presented for two reaction systems, CO oxidation on supported Ag and Rh. The experimental data were used for kinetic mechanism development, parameter estimation, and model discrimination. The complementary information available from the various experimental techniques highlights the advantage of implementing an integrated experimental program in order to optimally approach model development in heterogeneous catalytic reactions from a phenomenological perspective. Strongly emphasized in the work was the feedback-induced bifurcation method, because it represents a novel approach for examining and exploiting nonlinear behavior. Although the feedback-induced bifurcation method had been previously proposed and studied numerically, the experimental implementation of the method had been of limited scope. Unlike previous studies with controller-induced instabilities, this work based feedback control on the concentration of an adsorbed reaction intermediate as well as of gas-phase species and considered the feedback stimulation of higher order bifurcations.

The feedback-induced bifurcation method was found to be sensitive to some mechanistic differences in the models postulated for CO oxidation on silver that were indiscriminate in steady-state and step-response simulations. However, the calculated controller-induced instabilities were insensitive to slight variations such as surface coverage-dependent desorption activation energies in the kinetic model for CO oxidation on Rh. This insensitivity to model variants occurred despite the use of fractional coverage of adsorbed CO as the measurement on which feedback was based. Still, the potential usefulness of the feedback-induced bifurcation method for model development seems to be analogous to the usefulness of more conventional open-loop experimental techniques in that the more reaction species that can be monitored, the more effective is the method.

Although it has been demonstrated that the feedback-induced bifurcation

data can provide information about heterogeneous catalytic reactions, which is unavailable from steady-state and step-response experiments, the sensitivity of the closed-loop stability behavior to the characterization of the intrinsic properties of the experimental apparatus is a major drawback in the analysis of the bifurcation experiments. This sensitivity is particularly evident in the strong correlation of the modeled dynamics of the mass flow controllers and the value of the system time delay with the calculated closed-loop bifurcation behavior. An advantage of using open-loop experiments is that mass flow controller and time delay effects do not need to be precisely evaluated. Bifurcation data from closed-loop experiments, though, can frequently be more readily analyzed than open-loop bifurcation data. An example is illustrated in the observation of autonomous oscillations in the CO oxidation reaction on Rh. In those experiments, the oscillations were postulated to be driven by thermal fluctuations on the catalyst surface that could not be measured and characterized with the experimental system. In contrast, the feedback-induced bifurcations for the same reaction system could be modeled, assuming an isothermal condition on the catalyst surface, because the bifurcation data result from using feedback to destabilize a steady-state operating condition. Thermal fluctuations that occur after the bifurcation are of no consequence in the analysis of the closed-loop experiments.

Bifurcation data obtained from closed-loop operation of a reaction system can be used to test a proposed reaction model, but mechanistic information about the reaction cannot be extracted from this type of data. As demonstrated for both reaction systems, stimulus-response experiments can give insight into the underlying kinetic mechanism. The relative reactivities of two adsorbed carbonyl species on Rh were readily resolved by step-response experiments and stimulus-response experiments were also used to postulate an alternative reaction sequence for the oxidation of CO on Ag.

Clearly, each experimental technique that has been employed in this work

for model development in catalytic reaction systems has advantages and limitations. Therefore, it is best to integrate several different techniques to identify a representative reaction model. The use of experiments in which reactor inputs are manipulated greatly expands the scope and sensitivity of the experimental tools that can be applied to the development of heterogeneous catalytic reaction models.